The Effect of Convective Currents on the Drying of Reconstituted Alberta Oil Sands Gangue

By

Annie Kuang

A thesis submitted in partial fulfillment of the requirements for the degree of

Master of Science

in

Chemical Engineering

Department of Chemical and Materials Engineering

University of Alberta

Abstract

Oil sands account for over 98% of Canada's oil reserves and current commercial extraction methods have several shortcomings, including significant water and energy consumption, accumulation of tailings ponds, being impractical for low grade ores, and substantial greenhouse gas emissions. Non-aqueous or solvent extraction has the potential to replace the current hot-water process, thus also addressing these concerns. In non-aqueous extraction, bitumen is recovered from the ore using an organic solvent and the resulting solid mixture, also called "gangue", consists of residual bitumen, solvent, and any water initially in the ore. Despite the many advantages, non-aqueous extraction methods have not been implemented on a commercial scale due to the difficulty of removing solvent from the extracted gangue while maintaining high bitumen recovery.

In this study the effects of an induced convective current on the recovery of solvent was examined for samples of varying bitumen and water content. The horizontal air velocity over the samples were 0.9, 2.3, 3.0, and 3.5 m/s. Reconstituted gangue samples were prepared with known bitumen, water, and cyclohexane fractions to eliminate the variability associated between batches of real gangue. To investigate the effect of current velocity on samples of varying bitumen, reconstituted gangue samples with 0, 0.5, 1.0, 1.5, and 2.0 wt.% bitumen carbon, 3.7 wt.% water and 12 wt.% cyclohexane were prepared. To determine the role of air velocity on gangue samples of varying water, samples with 0, 3.7, 6, and 8 wt.% water, 1 wt.% bitumen carbon, and 12 wt.% cyclohexane were prepared. Samples were dried under a fume hood at the various air velocities and at ambient temperature and pressure for two hours.

The drying curve of all samples exhibited two stages, a faster initial stage and a slower final stage separated by a breakpoint. The initial stage is dominated by cyclohexane liquid films that maintain connectivity between the bulk solution and the external surface. The final stage is characterized by water evaporation, where the flux is limited by diffusion within the gangue. Any increase in the initial flux corresponds to increased solvent removal.

Increasing air velocity was observed to increase initial flux but only to a certain extent, after which the initial flux becomes independent of flow velocity. The optimal flow velocity for samples with less than 1.5% bitumen carbon was observed to be 3 m/s. The relative increase in initial flux was more prominent for samples with less residual bitumen given the same flow velocity increase. For samples with higher amounts of residual bitumen, higher flow rates are required to maximize initial flux. The positive effect of increased flow velocity on solvent removal is not diminished as long as the fraction of water remains between 4 – 7 wt.%. In the absence of water, cyclohexane liquid film formation is suppressed, resulting in significantly lower initial fluxes at all flow velocities. Shorter transition times were observed when the initial flux increases. Despite comparable increases in the initial flux, the transition time decease for samples with 6 wt.% water was smaller than for samples with 8 wt.% water.

This study provides new insight on the factors governing cyclohexane removal from gangue, but also acknowledges that additional work is required to develop a comprehensive model that accurately accounts for all parameters and mechanisms of the drying gangue.

Acknowledgements

Throughout this thesis I am fortunate to have received assistance, guidance, and motivation from many individuals, all which I am grateful to.

I would like to thank my supervisor, Dr. Phillip Choi, for his continued support, guidance, and teaching. I am grateful for his insightful advice and admire his meticulous and investigative approach to research and problem solving.

I would like to thank the lab technicians at IOSI, Lisa Brandt and Brittany Mackinnon, led by Research Associate Dr. Xiaoli Tan for all the lab equipment setups, trainings and assistance provided.

I would like to thank Syncrude Canada for providing the oil sands samples.

Finally, I would like to acknowledge Future Energy Systems and thank them for funding this project.

Table of Contents

List of Figures

List of Tables

1. Introduction

1.1. Background

With over 166 billion barrels, Canada has the world's third largest proven oil reserves, most of which is found in Alberta [1]. The oil sands of Alberta lie under 142,200 km^2 of land and are primarily found in three regions: Athabasca, Cold Lake, and Peace River [2]. Oil sands are a mixture of bitumen, water, and sand. Oil deposits with higher amounts of fine solids tend to have lower bitumen content. Depending on the amount of connate water and the properties of the mineral solids, oil sand deposits can be classified as water-wetted (e.g., Canadian oil sands) or oil-wetted (e.g., Venezuelan or United States oil sands) [3]. Separation of bitumen from water-wetted oil deposits can be achieved using water-based gravity separation, while oil-wetted deposits require the use of solvents and chemicals [4].

Alberta's oil sands were formed millions of years ago through bacterial degradation of light crude oil trapped in rock pores in oil reservoirs, leaving behind thick, viscous bitumen [5]. Crude oil is categorized by their density and sulfur content. Oil with a lower API gravity are considered heavier and will require more processing or result in a higher fraction of lower valued by-products, such a heavy fuel oil [6].

In 2019, Alberta produced over 3 million barrels of bitumen per day, with surface mining and in-situ operations accounting for 45% and 55% of production, respectively [7]. Alberta's oil and natural gas sector provides immense economic opportunities for both Alberta and Canada, generating over $100 billion towards Canada's gross domestic product (GDP) in 2018 [8].

Continued sustainable development of Canadian oil sands will help secure Canada's energy future and maintain energy security.

1.2. Current Commercial Extraction Methods

Currently there are two methods utilized commercially for bitumen extraction in the Alberta oil sands: in-situ and surface mining. The method used to extract the bitumen will depend on the depth of the oil deposit. Deposits located less than 75 m below ground can be surface mined, while deposits located deeper than 75 m must be recovered through in-situ methods [4]. It is estimated that 20% of the Canadian oil reserves can be recovered through mining operations, while recovery of the remaining 80% requires in-situ technologies [4]. Currently, in situ methods account for ~53% of current production, with the remaining ~47% extraction via surface mining [9].

For surface or open pit mining operations, vegetation and surface coverings are removed before the ore is mined, crushed, and mixed with hot water and caustic soda to form a slurry. In the conditioning phase, the slurry travels through the hydro-transport pipeline and bitumen is liberated from the solids through attachment to air bubbles [5]. High temperatures reduce the viscosity of the bitumen and facilitate engulfment of the bitumen by air bubbles. During the extraction phase, the aerated bitumen is lower in density and will float to the top of the gravity separation vessel where it will be collected from the top as bitumen froth and sent for froth treatment [5]. Froth treatment involves the addition of either a naphtha-based hydrocarbon or a paraffinic solvent, with only the latter producing a marketable product stream [10]. Coarse solids collected during the extraction and froth treatment phases are sent to tailing ponds. The first hot

water extraction process was patented by Dr. Karl Clark, and such aqueous extraction methods have been commercially utilized since 1967 [11].

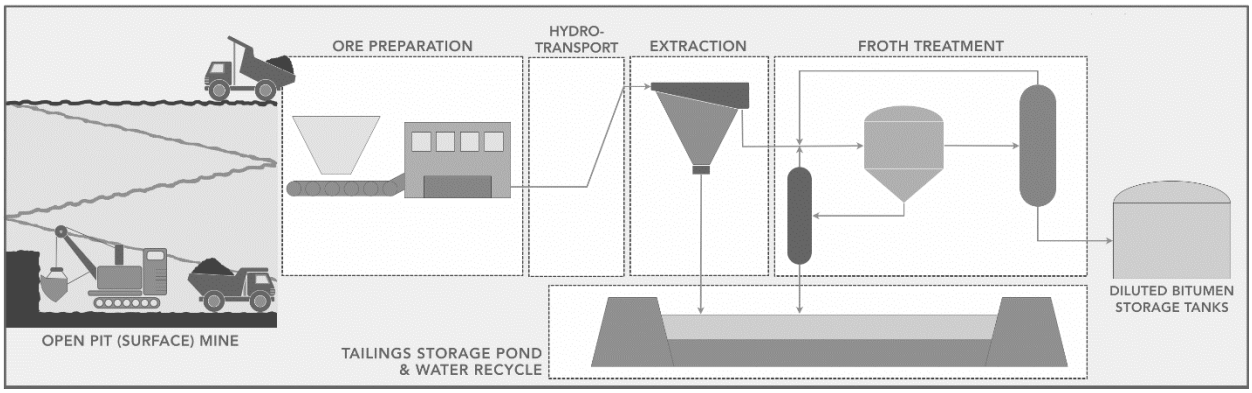

Figure 1. Process overview of bitumen extraction from mined oil sands [12]

There are several in-situ extraction methods that can be utilized for bitumen deposits too deep to be mined. The two most common in-situ methods employed are Cyclic Steam Simulation (CSS) and Steam-Assisted Gravity Drainage (SAGD). In CSS, a single vertical well is drilled and steam is injected to heat the bitumen [5]. Steam injection continues for several weeks until the reservoir is fully saturated [13]. In the soaking phase, the bitumen stays in the hot pressurized reservoir for several days or weeks and becomes more fluid and less viscous [13]. The bitumen/steam mixture is then pumped to the surface in the same well during the production phase [13]. In SAGD, two wells are drilled and high-pressure steam is injected into the top injection well. As the bitumen heats up, it liquefies and flows into the lower producing well. The bitumen/steam emulsion is then pumped to the surface and sent for separation and further processing. Water is recovered and recycled back in both CSS and SAGD operations. Other in-situ extraction methods include Toe to Heel Air Injection (THAI) and Vapour Extraction Process (VAPEX), where ignited air and solvents are used, respectively [13].

Advantages to in-situ methods include a smaller footprint, more efficient water usage, the elimination of tailings ponds, and lower costs to build, maintain and operate [13]. Disadvantages to in-situ operations are lower bitumen recoveries, higher degrees of uncertainty, more greenhouse gas (GHG) emissions, and an increased difficulty to stop and start [13]. Bitumen recovery rates for in-situ operations can vary between 40% - 60%, while typical recovery rates for mining operations are over 90% and can be as high as 95% [13].

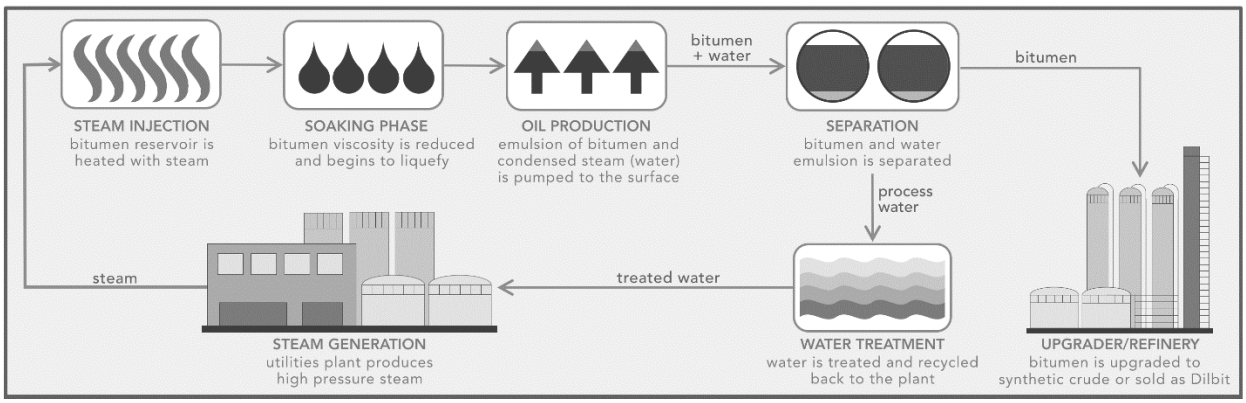

Figure 2. Process overview of bitumen extraction via in-situ methods **[13]**

1.3. Disadvantages of Aqueous Extraction Methods

Challenges with conventional aqueous-extraction methods include high water consumption, expansion of tailings ponds, high energy use, high greenhouse gas emissions, and difficulty recovering bitumen from low grade and oil-wetted ores.

1.3.1. Water Consumption

Commercial aqueous extraction methods are possible because of the hydrophilic nature of the oil sand mineral solids. Hot water extraction techniques for surface mining operations use roughly 2.5 barrels of fresh water for every barrel of bitumen produced, while in-situ methods require an

average of 0.2 barrels of fresh water per barrel of bitumen [9]. Although 80 – 95% of water used in established mines and 85–95% for in situ operations are recycled, some water is inevitably lost or discharged as wastewater [9]. In Alberta, water utilized by energy companies can be classified as non-saline or alternative water; sources of non-saline water include lakes and rivers, surface runoff water and groundwater, while alternative water sources include saline groundwater, wastewater and recycled water [14]. In Alberta, over 140 billion m^3 of non-saline water is available and in 2018 approximately 7% (9.6 billion m^3) was permitted for industrial use [15]. Out of this 7%, roughly 12% (1.1 billion m^3) was allocated to the energy sector. Withdrawal of fresh surface water from rivers, especially during low flow seasons, may have detrimental effects on the surrounding ecosystem and threaten aquatic life [3].

1.3.2. Tailings Ponds

Oil sand tailings, a by-product of hot water extraction processes, are a mixture of water, clay, residual bitumen, and chemicals. The production of one barrel of bitumen yields roughly 3.3 m^3 of discharged tailings sludge [5]. Although coarse sand solids settle quickly, the fine clay solids remain suspended for significantly longer. This suspension contains roughly 30 wt.% fine solids and 70 wt.% water and is referred to as mature fine tailings (MFT) [5]. Due to the repulsive forces between fine solid particles, this suspension may take decades to de-water if left unprocessed. The volume of MFT is dependent on the rate of bitumen production and is accumulating at a rapid pace; if bitumen production continues as projected, Syncrude and Suncor will amass an estimated 1 billion and 800 million m^3 of fine tailings by 2025 and 2033, respectively [5].

Tailings contain an array of toxic materials including bitumen, naphthenic acids, cyanide, phenols, arsenic, cadmium, chromium, copper, lead, and zinc [16]. These substances are released during the processing of oil sands and become increasingly concentrated in tailings ponds over time. Volatilization of components in tailings and biodegradation of hydrocarbons by resident microbes also leads to air-borne emissions of pollutants, such as volatile organic compounds (VOCs), CO_2, and CH_4 [3]. There is also evidence that pollutants from oil sands development, such as polycyclic aromatic hydrocarbons and heavy metals, are being found up to 50 kms away [17], [18].

Tailings ponds are also a risk for wildlife. Despite implementing methods to deter wildlife from tailings, there have been multiple incidents involving avian deaths [19]. Tailings can also leach into groundwater and the Athabasca River, and introduce acute toxins to aquatic life [20].

Companies are actively investigating new remediation technologies for tailings, such as Suncor's holistic Tailings Reduction Operations (TRO™) and permanent aquatic storage structure (PASS), and Canadian Natural Resources' (CNRL) Non-Segregating Tailings (NST) process and Atmospheric Fines Drying (AFD) technique [21], [22]. Although there are various remediation techniques, the rate of tailings accumulation is significantly greater than reclamation efforts [5].

1.3.3. Energy Intensity

Hot water based or aqueous extraction methods are energy intensive as large amounts of thermal energy are required to heat water to adequate bitumen liberation temperatures. To achieve slurry temperatures of 40–50°C during surface mining operations for bitumen liberation, water must be heated to 70–90°C, expending the energy equivalent of 20% of a barrel of bitumen [5]. At times

it is also possible to generate electricity via steam through the combustion of waste coke or through reusing waste heat from the upgraders on site [3]. Compared to other energy sources such as hydroelectric energy and conventional oil, the energy return on energy invested (ERoEI) of minable oil sands is significantly lower [23].

Table 1. ERoEI of Various Energy Sources [23]

Energy Source	ERoEI Value
Hydroelectric energy*	11 – 267
Conventional oil	19 – 100
Coal	50
Wind	18
Athabasca minable oil sands (naphthenic froth treatment)	14
Athabasca minable oil sands (paraffinic froth treatment)	8.5
In-situ oil sands (SAGD)	5.5

* The high variance of the ERoEI value for hydroelectric energy and conventional oil is due to the variability of the local geography and resource reserve.

1.3.4. Green House Gas (GHG) Emissions

GHGs are produced during the combustion of hydrocarbons, and trap heat in the atmosphere causing temperatures to rise. In fact, 97% of climate scientists agree anthropogenic activity is responsible for most temperature increases over the last 250 years [24]. GHG emissions also have vast environmental, human health and economic impacts.

Canada's total GHG emissions in 2018 were 729 Mt CO_2 eq, with the oil and gas sector accounting for 26% of emissions at 193 Mt CO_2 eq [25]. Oil sands account for roughly 10% of Canada's total GHG emissions, and mining and in-situ operations have an average emission intensity of 48 and 78 kg of CO_2 eq per barrel of bitumen, respectively [26]. These intensity indicators are dependant on a variety of factors, such as the quality of the ore and the extraction process. Carbon emissions from oil sands are the fastest growing source of emissions in Canada, with its upward trajectory impeding the country's ability to meet emission reduction commitments and plan to become carbon neutral [27].

Recent air sampling measurements using aircrafts over the Canadian oil sands revealed that CO_2 emission intensities for oil sands facilities are significantly larger than those reported by industry [26]. Results of a top-down approach leads to 64% higher GHG emission from surface mining facilities and 30% higher overall GHG emission than values disclosed by industry using bottom-up approaches [26].

1.3.5. Low-Grade and Oil-Wetted Ores

Bitumen recovery via aqueous extraction techniques can exceed 90% for most water-wetted ores. Lower grade ores contain a lower bitumen content and larger amounts of fines/clays. Fine solids are defined as those < 45μm. Higher fines/clays content decreases bitumen attachment to air bubbles and reduces froth quality and bitumen recovery; bitumen recovery rates for low grade ores can be below 60% [3]. According to the Alberta oil sands royalty guidelines, high, medium, and low-grade ores contain roughly 13%, 10% and 8% bitumen, respectively [28]. With the inevitable depletion of high-grade ores, a blend of medium and lower grade ores will require

processing in the future. In Alberta, for ores with 11 wt.% bitumen or greater, the minimum recovery required is 90 wt.%, as established by provincial guidelines.

Bitumen from oil-wetted ores found in Utah or Indonesia cannot be recovered using conventional aqueous techniques and must rely on non-aqueous extraction methods. In Utah, Petroteq Energy has developed a solvent composed of hydrophilic, hydrophobic, and polycyclic hydrocarbons that claims to extract up to 99% of all hydrocarbons [29].

1.4. Non-Aqueous Extraction Methods

Non-aqueous extractions (NAEs), also known as solvent extractions, have the potential to drastically reduce freshwater intake, eliminate tailings ponds, improve energy efficiency and decrease GHG emissions, while maintaining high bitumen recovery. Figure 3 is a schematic flow diagram of a basic solvent extraction process; the process can be adapted depending on specific requirements.

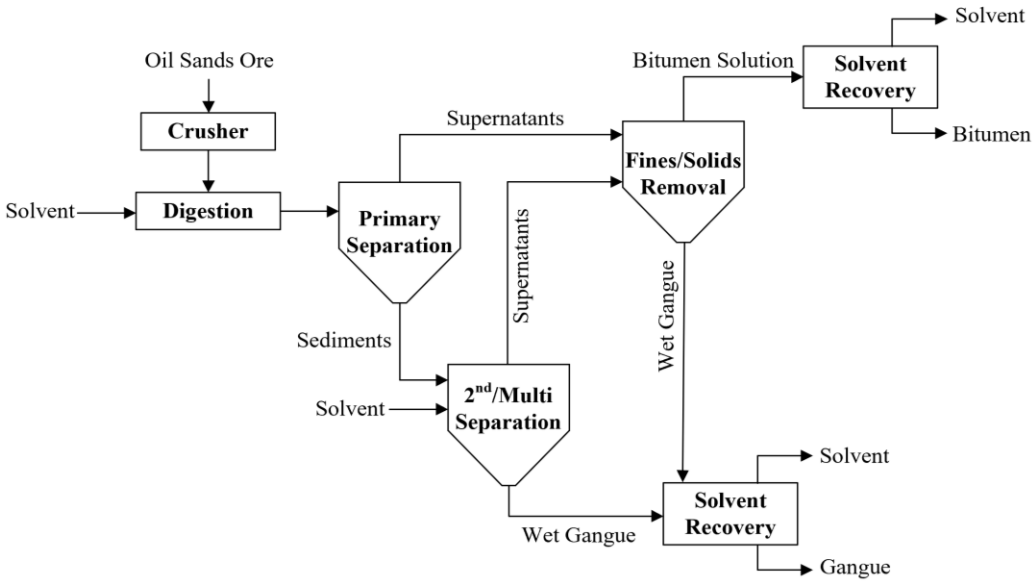

Figure 3. Schematic flow diagram of basic solvent extraction process [3].

Selection of a suitable solvent for NAEs is critical in its implementation. A good solvent should result in high bitumen recoveries, minimize the transfer of fine solids to the final product and be easily removed and recovered post extraction [30].

Coulson used both low-boiling organic solvents (benzene, toluene, and xylene) and high-boiling organic solvents (kerosene, coal tar naphtha and petroleum naphtha) as diluents to facilitate bitumen separation though decreasing the viscosity of bitumen within the oil sands prior to aqueous extraction [31]. Although both types of solvents were successful in reducing bitumen viscosity, higher boiling petroleum fractions were recommended to minimize overall solvent loss; aromatic or olefinic solvents were preferred over paraffinic solvents due to their increased solubility of bitumen [31].

Gantz and Hellwege use trichloroethylene as the solvent in combination with a small amount of a surfactant at 150°C and 3.4 x 10^5 Pa to achieve a bitumen yield of 99% with a solvent loss of less than 0.5% [32]. Cormack et al. demonstrated that highly aromatic solvents such as toluene and benzene are 3 to 5 times faster at dissolving bitumen than aliphatic solvents such kerosine, but also acknowledged there are parameters beyond aromaticity that are also important [33]. Meadus et al. evaluated solvent extraction using naphtha and kerosene preloaded with bitumen as the solvent [34]. Results indicated an improved solvency attributed to an enhanced aromatic content resulting from the addition of bitumen [34]. Leung and Philips investigated the effectiveness of bitumen extraction with benzene, toluene and kerosine in stirred tanks, and concluded that solvents with high aromatic content or low boiling points tend to be good solvents [35].

Painter at al. performed bitumen extraction using toluene and an ionic liquid [36]. The ionic liquid was attracted to the sand and clay surfaces via electrostatic forces to enable to release of

bitumen, resulting in recoveries of over 90% with no detectable ionic liquid in the residue sand and clays, and no ionic liquids or fine solids in the bitumen product [36]. Although no water was required for bitumen extraction, it was required to recover the ionic liquid, and the introduction of water also adds most problems associated with aqueous extraction processes [37]

Hooshiar et al. studied NAE of high and medium grade oil sands ores using mixtures of heptane and toluene, resulting in total bitumen recoveries of over 96% for both ores [38]. For high grade ores, they found bitumen recovery to be unaffected by the toluene to heptane ratio, while for the medium grade, high fines, poor processing ore, the bitumen recovery decreased when the amount of toluene decreased.

Wu and Dabros studied bitumen extraction with light hydrocarbons as the solvent, followed by centrifuge filtration or regular pressure filtration [39]. Of all the solvents tested (toluene, n-pentane, hexane, cyclopentane, and a mixture of n-pentane and cyclopentane), cyclopentane was found to be the best given its high bitumen recovery and low boiling point. Bitumen recoveries for both high and low grade ores were comparable to the conventional aqueous based process.

Noorjahan et al. concluded cycloalkanes are advantageous in NAEs because of their high solvent power, high vapour pressure and low odour [40]. Nikakhtari et al. compared various light hydrocarbon solvents, including aromatics, cycloalkanes, biologically derived solvents, and mixtures of solvent for bitumen extraction from Alberta oil sands at ambient temperature and pressure [30]. By comparing bitumen recovery, amount of residual solvent in the extracted gangue and content of fine solids in the extracted bitumen, they deemed cyclohexane to be most promising, with 94.4% bitumen recovery, 5 mg of residual solvent per kg of gangue, and 1.4 wt.% fines in the recovered bitumen. Wang et al. also concluded cyclohexane is a good solvent

for bitumen extraction because of high bitumen recovery combined with low solvent and energy consumption [37].

An important factor to consider for solvent-based bitumen extractions is the solvation power or solubility parameter of a solvent. The solubility parameter describes the dissolving capability of a solvent and its miscibility [3]. Thermodynamically, bitumen extraction via solvents can be viewed as a mixing/dissolving process between solvent and solute [3], [37].

The solubility parameter described by Hildebrand [41], [42] was derived from the cohesive energy density of the solvent and given as

$$\delta_T = (e_{coh})^{1/2} = \left(\frac{\Delta H^{vap} - RT}{V}\right)^{1/2} \quad (1)$$

In Equation (1), δ_T is the Hildebrand (or total) solubility parameter, e_{coh} is the cohesive energy density, ΔH^{vap} is the enthalpy of vaporization, R is the gas constant, T is the absolute temperature, and V is the molar volume. When the solubility parameter between two liquids is small, they will be miscible with each other because the resulting enthalpy of mixing will be small, as given by

$$\Delta H^{mix} = V_m \varphi_s \varphi_a (\delta_s - \delta_a)^2 \quad (2)$$

In the previous equation, ΔH^{mix} is the enthalpy of mixing, V_m is the molar volume of the solution, φ_s and φ_a are the volume fractions of the solvent and solute, respectively, and δ_s and δ_a are the solubility parameters of the solvent and solute, respectively.

Pal et al. observed that bitumen recovery did not follow a simple relationship with the Hildebrand solubility parameter of various solvent blends (cycloalkanes and n-alkanes) [43]. When solvents were blended to yield the same solubility parameter, the cyclohexane/hexane mixture resulted in a higher bitumen recovery than cyclohexane/pentane and cyclohexane/heptane mixtures. The migration of fine solids into the bitumen product was less sensitive to the solubility parameter of a solvent than the recovery of bitumen [43].

Rahimian and Zenke screened 76 liquid solvents to predict the solubility of bitumen and concluded all good solvents for bitumen possessed a solubility parameter between 15.3 and 23 $MPa^{1/2}$ [44]. However, not all liquids in that range are good bitumen solvents because dispersive interactions alone cannot fully explain the solubility behaviour of bitumen as there are other interactions, such as polar interactions and hydrogen bonding, that are important [44]. Solvents that dissolve bitumen without asphaltene precipitation has a solubility parameter close to that of asphaltene [35].

The Hildebrand solubility parameter is impractical for systems with molecular interactions other than dispersion forces. The Hansen solubility parameter is a more appropriate measure given that it describes the cohesive energy as the sum of three interactions: dispersion (δ_D), polarity (δ_P), and hydrogen bonding (δ_H) [45].

$$\delta_T{}^2 = \delta_D{}^2 + \delta_P{}^2 + \delta_H{}^2 \quad (3)$$

Redelius demonstrated that the Hansen solubility parameter is fairly accurate at predicting the solubility of bitumen in different solvents and all good solvents have a low δ_P and a high δ_H value [46]. He also showed that polar interactions and hydrogen bonding are important for the solubility properties and stability of bitumen and therefore also its mechanical properties.

Despite promising results from solvent extraction, none have been implemented on a commercial scale due to the difficulty in removing solvents from the extracted gangue while maintaining high bitumen recoveries [30]. The Alberta government has set the limit on permissible solvent loss as 4 volumes of solvent per 1000 volumes of bitumen produced for current commercial bitumen extractions using aqueous techniques.

1.5. Drying of Porous Media

To understand the removal of solvent from non-aqueous extracted oil sands gangue, an understanding of the drying mechanisms in porous media must be developed. After NAE, the gangue consists of porous clay/sand solids, a small amount of water, and residual bitumen and solvent. Although there is limited literature for the drying of two immiscible liquids, such as an organic solvent and water in a porous matrix, there are studies on the drying of water in a porous medium that provides insight on the two-liquid system.

1.5.1. Liquid Films on Drying of Porous Media

A porous media can be viewed as a network of pores connected by throats [47] . Throats are narrower and have higher capillary forces compared to pores [48]. To visualize the matrix in 3D, pores can be viewed as spheres and throats as cylinders [47]. Drying within the porous media involves the displacement of the evaporating fluid by air [49], [50]. When capillary forces are dominant over viscous and gravitational forces the displacement process of the subsiding liquid can be described by percolation theory [48], [50]. Invasion percolation theory describes the displacement process where the path taken is the one of least capillary resistance, i.e., the next pore to be invaded by gas is the one with the largest diameter [47]. If there are significant viscous and gravitational effects, the drying pattern will depart from invasion percolation and the displacement is then described as invasion percolation in a stabilizing agent [51]. The simplest and most intuitive drying model for porous media is evaporation of the liquid within the pore followed by diffusion of the evaporated gas towards the exposed, open region. A more comprehensive understanding of this drying process came with studies on viscous effects [52], gravitational effects [53], and temperature gradients [54]. However, none of these effects account for the significantly higher drying rates observed experimentally by Laurindo and Prat [53]. The high experimental drying rate is attributed to liquid film formation that maintains hydraulic connectivity to the evaporating surface, and these liquid films are formed on the porous media wall as liquid-gas menisci recedes [55].

Early studies on the drying of porous media neglected liquid films. Yiotis et al. modeled the porous medium as a 2-D network of pores where all but one boundary is impermeable to mass and flow transfer, as shown in Figure 4 [56].

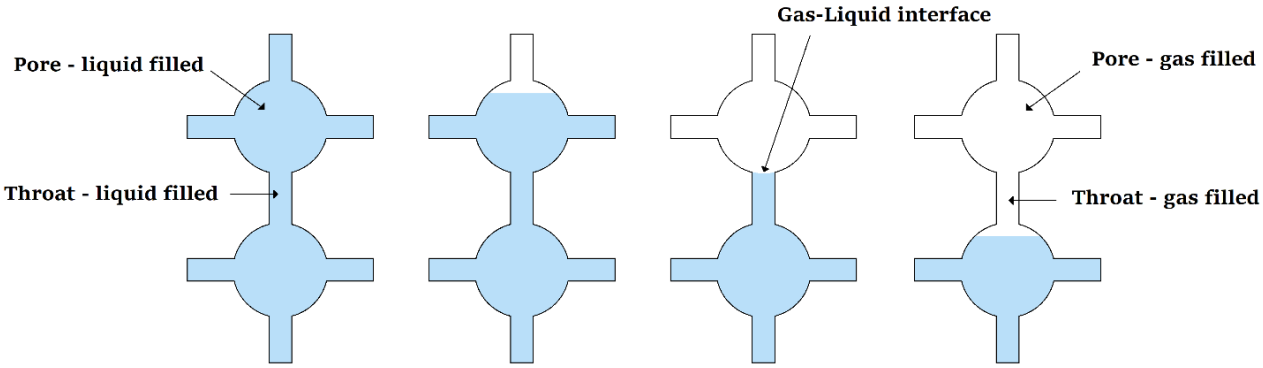

Figure 4. 2-D network pore structure with the invasion of the liquid-filled pores by gas.

In the model established by Yiotis et al., the pore bodies are depositories for liquid and gas, and assumed to be without flow or capillary resistance, while throats are the barriers that hinder flow and mass transfer, and assumed to be of negligible volume. An interfacial pressure difference is established at the interface between the stationary gas and liquid at the opening of a throat. When the pressure difference between two pores reaches the threshold capillary pressure, the liquid-gas interface recedes instantaneously.

Another possible drying mechanism involves the formation of liquid films along the wall of the porous media when the liquid-gas meniscus recedes, as shown in Figure 5. Studies on the effects of thick films demonstrated film flow as a major transport mechanism during the drying of porous media [50], [57].

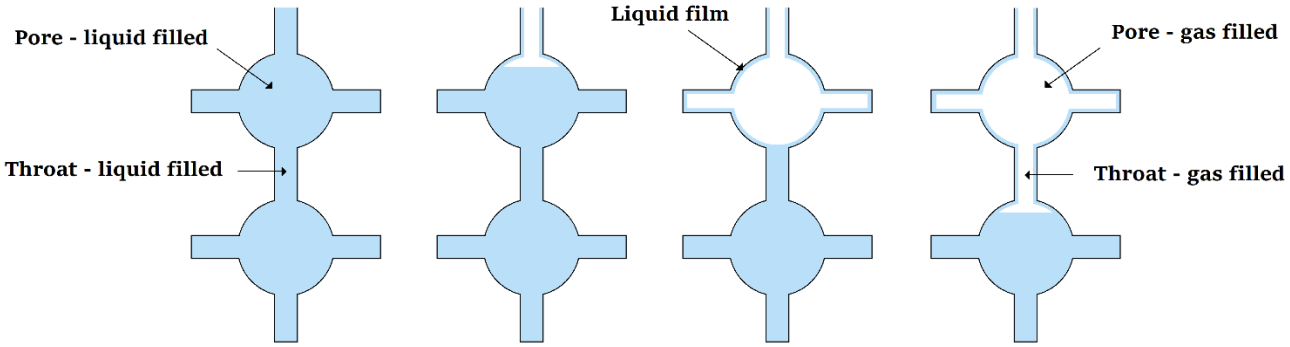

Figure 5. 2-D pore structure with formation of liquid films as the liquid-gas interface recedes

Liquid films are formed due to capillary forces within the porous matrix. To understand the effects of capillary forces, a simple cylindrical geometry is utilized. Capillary pressure is the pressure difference between the liquid and gas phase. This pressure difference (ΔP) can be calculated with the Young-Laplace equation for a curved liquid surface.

$$\Delta P = \gamma\left(\frac{1}{R_1} + \frac{1}{R_2}\right) \tag{4}$$

As shown by Equation (4), the pressure difference is proportional to the interfacial or surface tension, γ, and inversely proportional to the principle radii of curvature, R_1 and R_2. For a cylindrical capillary, the meniscus formed is spherical, as shown in Figure 6. Capillary action results from a combination of cohesive forces within the liquid and adhesive forces between the liquid and solid wall.

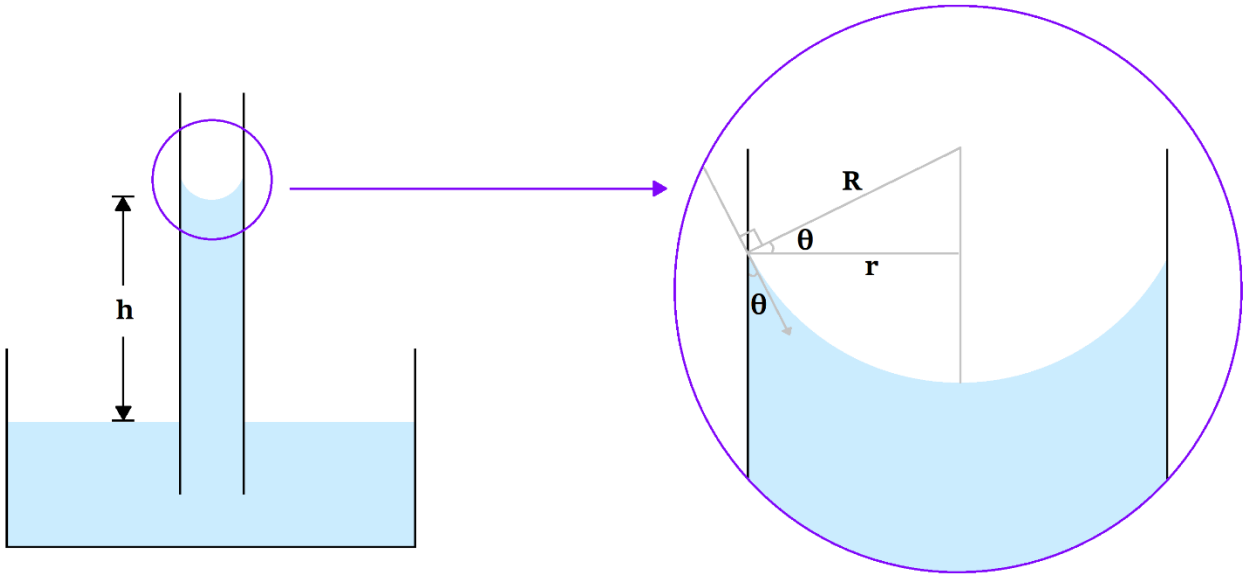

Figure 6. Capillary action in a cylindrical tube and formation of a liquid-gas meniscus.

For capillaries like those in Figure 6, the pressure difference can also be estimated as

$$\Delta P = \rho g h \tag{5}$$

As evident in Figure 6, the radius of curvature, R, is equal to $\frac{r}{\cos(\theta)}$, where r is the capillary radius and θ is the contact angle between the wetting liquid and capillary wall. The resulting capillary pressure, P_c, equation is

$$P_c = P_{gas} - P_{liquid} = \frac{2\gamma\cos(\theta)}{r} \tag{6}$$

Combining Equations (5) and (6), the height of the capillary rise, h, can be calculated as

$$h = \frac{2\,\gamma \cos(\theta)}{\rho g r} \tag{7}$$

Liquid films will only wet the capillary walls if the contact angle is between 0° and 90° - i.e., the liquid has a higher affinity for the solid surface than air [58]. Wettability describes the tendency of a fluid to adhere to a solid surface in the presence of other immiscible fluids and is quantified using the contact angle. Capillary suction causes the liquid to rise in the capillary and occurs as the liquid wets the capillary wall and forms a meniscus [58]. As evident in Equation (7), a smaller capillary radius results in a higher capillary pressure.

The drying process with liquid film formation consists of three distinct regions, as shown in Figure 7. The open boundary region is the only side that is exposed to free-flowing air at ambient conditions. The gas region consists of pores filled by the invading, diffusive gas; the film region contains pores filled with gas, but also wetted by liquid films; and the liquid region initially spans the entire domain and contains only liquid-filled pores. It is important to note Figures 4, 5 and 7 only illustrate the concept of pores, throats and liquid films and are not representative of reality where pores, particles and throats will have varying shapes and sizes.

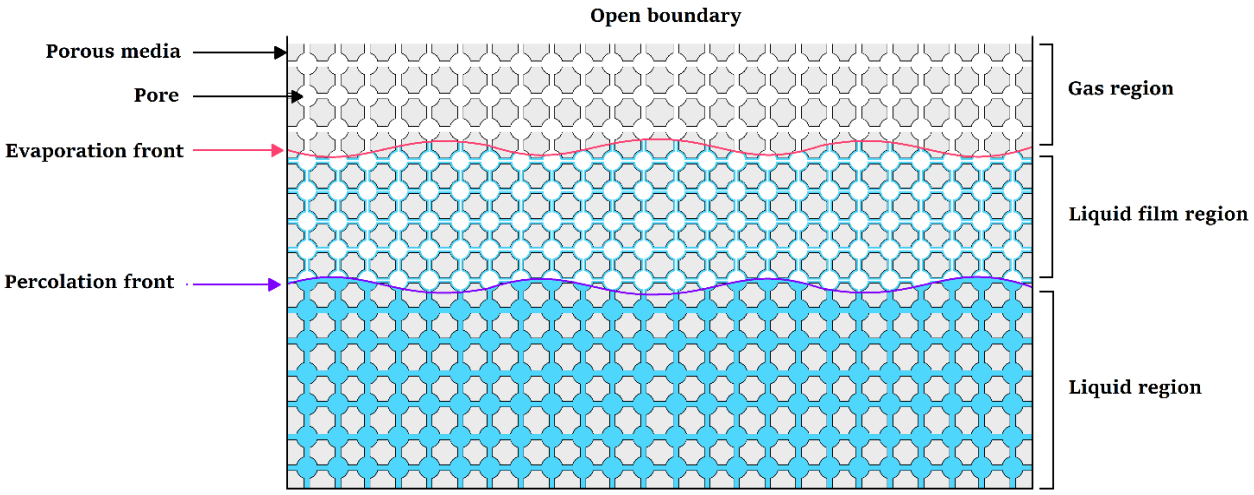

Figure 7. Regions during the drying of porous media with formation of liquid films.

The drying process of a porous media can be divided into stages; the first stage of drying is the constant rate period (CRP) or stage 1 evaporation. Initially, the porous media is entirely saturated with liquid. As the liquid evaporates into the open region, liquid films are formed due to capillary action and stage 1 drying is maintained as long as liquid films provide hydraulic connectivity to the open boundary. At the open boundary, the surface remains saturated with the evaporating species if the thickness of the external mass transfer boundary layer is significantly larger than the characteristic pore size [59]. The rate of drying during this stage is comparable to that of a free liquid surface and is controlled by external mass transfer [60].

A critical film length (critical average distance between percolation front and open region) is reached when capillary effects are overcome by viscous and gravitational effects, at which the liquid film will detach from the open region [61]. The film tips, now acting as the evaporative front, recedes deeper into the porous medium, leaving behind an increasing dry region below the open surface. The effective diffusivity within the matrix is significantly lower than that of the

external surface, and as the evaporation front recedes the resistance to mass transfer within the matrix increases. As a result, the rate of drying continuously decreases and is controlled by diffusive mass transfer through the dry region; this period of drying is called the falling rate period (FRP) or stage 2 drying.

Lehmann et al. proposed the concept of a characteristic length that marks the depth of the drying front at the end of stage 1 drying and indicates the maximum hydraulically connected distance between the evaporation front and percolation front; this length can be determined from the pore size distribution [62]. As long as the liquid film length is less than the characteristic length, drying remains at the CRP.

As aforementioned, the formation of liquid films is determined by the balance between capillary forces and viscous and gravitational effects. The capillary number, *Ca*, the ratio of viscous forces to capillary forces, can be evaluated according to Yiotis et al. [51] as

$$Ca = \frac{\mu_l V}{\gamma} = \frac{\pi D C_e \mu_l}{2\alpha \rho_L r_0 \gamma} \tag{8}$$

Where μ_l is the liquid viscosity, V is the average liquid velocity, D is a measure of the gas diffusivity, C_e is the equilibrium concentration of the vapour, α is a dimensionless geometric factor, ρ_l is the liquid density, and r_0 is the capillary size. For viscous effects to have a noticeable effect on the drying rate, Ca must be of *order 1* [51].

The Bond number, *Bo*, the ratio of gravity to capillary forces, can be calculated as

$$Bo = \frac{g\rho_L r_o^2}{\gamma} \tag{9}$$

where g is the acceleration due to gravity. Higher values of Bo correspond to increased gravitation effects and results in a shorter CRP or stage 1 drying [59].

The Sherwood number, Sh, is the ratio of convective to diffusive mass transfer and describes the mas transfer mechanism at the surface or open region of a porous media. As defined by Yiotis et al. [59], it can be calculated as

$$Sh = \frac{hr_0}{D_{eff}} \tag{10}$$

where h is the convective mass transfer film coefficient, r_0 is the pore length and D_{eff} is the effective internal diffusivity. The Sherwood number increases as the external boundary layer becomes thinner, and smaller Sh values lead to longer liquid films [59].

Although cylindrical capillaries were assumed in early derivations, solids will form uneven pores, and spherical pores are inadequate at representing the true pore geometry. In reality, film formation will occur at the corners of polygonal shaped pores, with the film thickness decreasing as it moves away from the bulk liquid, as depicted in Figure 8 [57].

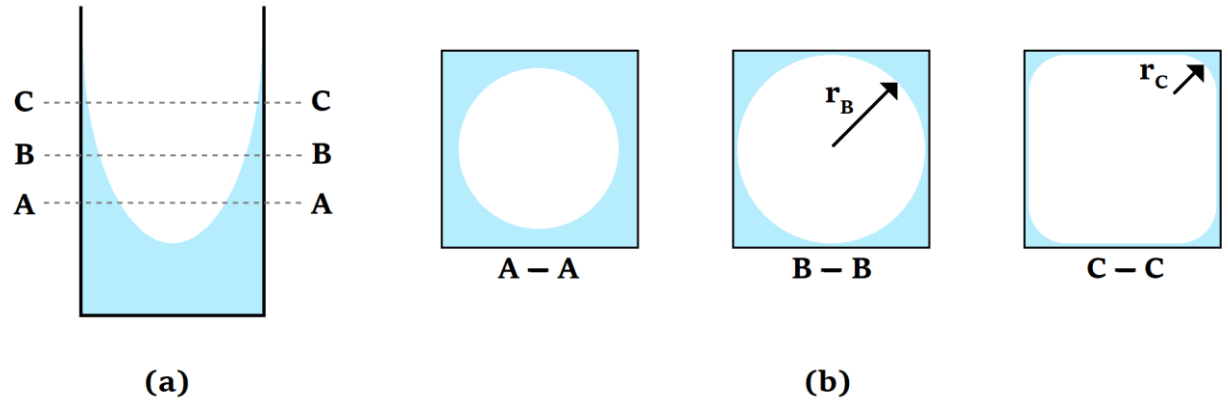

Figure 8. Liquid film formation. (a) Liquid films formed due to capillary action with decreasing film thickness as it moves away from the bulk liquid and (b) cross sectional view of liquid films in the corners of a simple square pore.

Evaporation rate in channels of polygonal geometry is significantly faster than circular geometries due to liquid film formation along the channel corners [57]. When the contact angle is lower than a critical value, liquid films are trapped by capillarity at the corners. The critical contact angle depends on the shape of the pore and can be estimated as $\theta_C = \pi/N$ where N is the number of sides – e.g. N = 3 for triangular pores. Existence of these corner films significantly increases the overall rate of drying in capillaries though decreasing the need for transport via diffusion. Pore shape has a significant effect on both drying rate and time, and for a given contact angle, the drying time increases significantly with N.

Varying the boundary layer at the open region of the porous matrix will only affect the CRP or the capillary regime, the duration when liquid films extend to the open boundary and provide continuity between the expose region and saturated liquid region [57]. If liquid films are connected to the open region for extended periods, the drying process is sensitive to external

drying conditions. Other mechanisms that affect the CRP include capillary effects associated with the distribution of throat size, invasion percolation in a gradient and film flow [57].

In a porous medium with mixed hydrophobic and hydrophilic particles, waters to form liquid films along the hydrophilic particles while air particles will invade the space around hydrophobic particles [63]. Results from drying experiments performed by Shokri et al. with water and varying fractions of hydrophobic particles showed shortening CRPs with increased hydrophobic fractions [64]. Liquid films are not formed if the evaporating fluid does not wet the porous surface, and evaporation from porous media with partial wettability is supressed relative to a fully wettable media [65]. The suppression of evaporation and therefore reduction of the drying rate is due to the loss of hydraulic connectivity and increased transport through diffusion. Evidence suggests that wettability is significant in the drying process because the introduction of hydrophobic/hydrophilic particles can strengthen or weaken capillarity depending on the properties of the evaporating liquid.

1.5.2. Drying of Oil Sand Gangues

Renaud studied the effects of temperature and pressure on the recovery of cyclohexane from solvent extracted gangue of both rich-grade and low-grade ores [58]. Tests were conducted between 25°C and 95°C at increments of 10°C, with pressures of 300, 500, 700 mbar. Mass flux for all stages of the cyclohexane removal process was higher for gangue from rich grade oil sands ore. During the final drying stages, this observation was attributed to lower fines content in rich-grade ores. Fine particles are hydrophilic and form clumps held together by water. These hydrophilic formations on the evaporating surface reduced cyclohexane saturation and lowered the evaporative flux of gangue from low grade ores. Fine particles also result in smaller pores

that supressed vapour pressure according to the Kelvin effect and a more tortuous path for diffusion. Increasing temperature and decreasing pressure both resulted in an increased evaporative flux for cyclohexane, and the total time required to reach a residue cyclohexane concentration of 260 ppm for both increasing temperature and decreasing pressure followed a power law relationship. The input of energy through heating or creation of a vacuum lost significance at higher temperatures.

Panda explored the effects of residue bitumen and initial cyclohexane content on cyclohexane removal from Alberta oil sands gangue [66]. A protocol was developed to make reconstituted gangue, a gangue sample with a known and controllable composition. Samples with varying residue bitumen and cyclohexane content were dried for 2 hours at ambient conditions at several bed heights. During the drying process, residue bitumen in the gangue migrated to the top of the sample and formed a dark, bitumen rich layer. Results showed that a higher residual bitumen content led to slower cyclohexane removal; this was due to decreased sorptivity because viscosity increased when bitumen is dissolved in the cyclohexane. Sorptivity is a measure of a medium's capacity to absorb or desorb liquid by capillarity. Lower bitumen migration was observed for the 8 wt.% initial cyclohexane sample compared to 12 wt.% sample due to the reduced capillary connectivity to the top of the packed bed. Panda concluded to achieve < 260 ppm of residue cyclohexane after 2 hours of drying at ambient conditions, the residue bitumen content should be < 1.8 wt.% and the bed height should be < 1 cm.

Ejike investigated the role of fine solids in solvent recovery of reconstituted Alberta oil sands gangue using the process outline by Panda [67]. Drying experiments were conducted at ambient conditions for 2 hours with reconstituted gangue samples prepared using rich-grade solids (10%

fines) or low-grade solids (~20% fines) in combination with 12 wt.% cyclohexane or 12 wt.% cyclohexane and 3.7 wt.% water. Samples with only cyclohexane showed two types of distinct drying stages. The first drying stage corresponded to stage 1 evaporation where cyclohexane liquid films maintained hydraulic connectivity to the external surface. The second stage occurs when capillary connectivity is lost and mass transfer is limited by diffusion of cyclohexane through the porous media. For samples with water, a third drying stage type dominated by water diffusion followed the solvent dominated stage. Particle size distribution and wettability of the gangue depended on the fraction of fine solids and results showed an increase in fines content resulted in the reduction of solvent recovery and increased solvent retention.

Nikakhtari et al. examined the effects of relative humidity, temperature, and water on the removal of cyclohexane of the extracted gangue [68]. Two distinct drying stages were found, with the initial stage mainly removing cyclohexane and the second stage mainly removing water. Relative humidity had insignificant effects on the first stage of drying but reduced the rate of the second stage because it decreased the rate of evaporation for water. The final residual cyclohexane concentration was unaffected by relative humidity, except at 90% relative humidity where residual cyclohexane increased more than 200%. Increasing the temperature from 24°C to 60°C increased the first and second drying stage by 97% and 100%, respectively. At high contents, water acts as a partial barrier and traps the solvent in the gangue, increasing the residual cyclohexane content. The liquid covers clusters of sand, forcing the solvent to diffuse through the water film.

Following Panda and Ejike's work, Khalkhali investigated the role of gangue composition on its drying at ambient conditions [69]. Reconstituted gangue samples were prepared with varying

bitumen, water, and fines content. Additionally, to further investigate the role of water, samples with 1 M NaCl and n-butanol were also studied. Increasing bitumen caused a decrease in initial drying rate. Doubling water content from 6 wt.% to 12 wt.% resulted in a 60% decrease in initial drying rate, but the complete elimination of water, i.e. 0 wt.%, also resulted in reduced initial evaporative flux. It is believed that high water contents inhibited the formation of cyclohexane films, while the removal of water reduced the average thickness of the films; both factors reduced the rate of cyclohexane removal. The addition of NaCl showed no effect on drying, while replacing water with n-butanol resulted in a slower initial drying rate. Unexpectedly, increasing the fraction of fine solids had no significant effect on the initial rate of drying

1.6. Objectives

The factors that affect solvent recovery in extracted gangue are not completely understood. Although variables such as temperature, bitumen, fines, and solid content have been examined, other effects such as the introduction of a convective current at the open boundary have not. The goal of this study is to determine the role of a convective current induced by a fan on the removal and recovery of cyclohexane in non-aqueous extracted gangue. Having a complete understanding of the drying process can lead not only to an accurate modelling of the system, but also can reduce or eliminate one of the largest problems associated with NAE and assist in its implementation on a commercial scale.

2. Methodology

2.1. Criteria for the Reconstituted Gangue

Composition of oil sands ore can vary depending on location and grade, and therefore the resulting solvent-extracted gangue will also have variation. The post extraction gangue consists of porous sand and clay solids with residue bitumen, water, and solvent; control over composition is difficult as each batch will vary with each extraction [58]. If experiments were performed using extracted gangue, the effects of various factors are difficult to isolate. To eliminate the variability associated with real gangue samples, a controlled or reconstituted gangue is prepared based on the parameters being investigated. Reconstituted gangue samples are prepared based on gangue obtained after solvent extraction with cyclohexane. Cyclohexane was chosen because its high bitumen recovery, low fines content in the recovered bitumen, and ease of removal post extraction [30]. In this study, the residual bitumen and water content will be varied.

Panda outlined the basis for the preparation of reconstituted gangue and compared their behaviour with real extracted gangues; drying results from both real and reconstituted gangue with comparable compositions were similar [66]. The goal was not to produce samples that perfectly reflected the characteristic of real gangue, but to create a material with controllable parameters that are to a certain degree reflective of the drying behaviour of real gangue and therefore able to provide insight on the effects of each parameter on the drying pattern.

The composition of the reconstituted gangue was prepared based on gangue obtained from NAE of rich-graded Athabasca oil sands. The cyclohexane content in extracted gangue varied between

8 and 18 wt.%, with an average of 11.8 + 2.1 wt.% [58]. The water content in the gangue post extraction was approximately the amount initially present as connate water in the ore, between 0 to 12 wt.% [68]. Residue bitumen content in the extracted gangue depended on the specific extraction process, but ideally should be above 96 wt.%.

Based on the composition of the extract gangue, the composition of the reconstituted gangue is prepared according to the following specifications:

- Bitumen associated carbon content at 0, 0.5, 1.0, 1.5 and 2.0 wt.%;
- Water content at 0, 3.7, 6 and 8 wt.%; and
- Cyclohexane content at 12 wt.%

Bitumen associated carbon or bitumen carbon (Bit. C) refers to the organic carbon that is sourced from bitumen. Sources of carbon in the gangue can be from bitumen or other inorganic material [66]. To determine the Bit. C content of a sample, the inorganic carbon weight needs to be subtracted from the total carbon weight. A sample with 0 to 2 wt.% Bit. C corresponds to 0 to 2.4 wt.% bitumen. The mass fraction of bitumen carbon in bitumen is 0.833 – i.e. there is 0.833 g of Bit. C in 1 g of bitumen, or 1 g of Bit. C per 1.2 g of bitumen.

2.2. Materials

The rich-grade oil sands utilized in this study was provided by Syncrude Canada Limited. Toluene and cyclohexane used during the Dean-Stark extraction and for the preparation of reconstituted gangue samples are both certified ACS grade and obtained from Fischer Scientific USA. The Soxhlet solids obtained from the Dean-Start extraction was coated with bitumen

courtesy of Syncrude. Demineralized water was also required for producing reconstituted gangue samples.

2.3. Dean Start Extraction

The Dean-Stark extraction is a procedure to determine the fluid saturation of a sample through vaporizing it with a boiling solvent, followed by condensation and collection of the fluid in a trap, as shown in Figure 9.

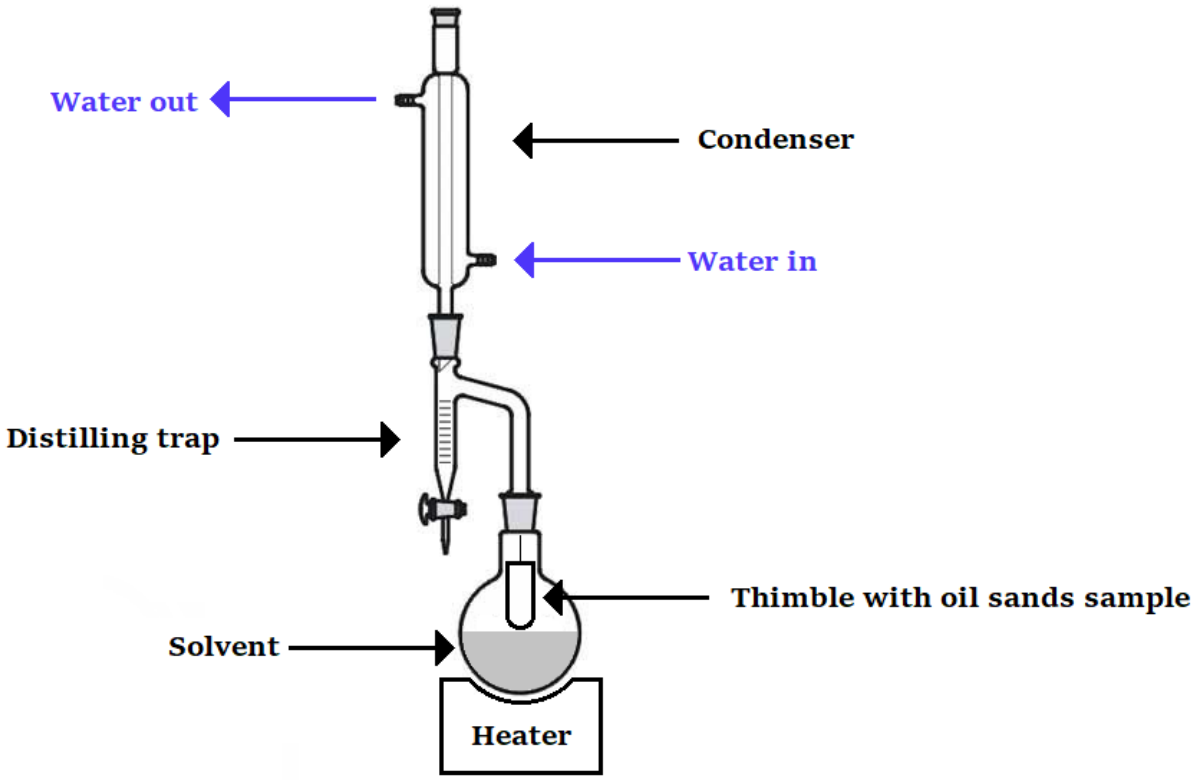

Figure 9. Schematic of Dean-Stark extraction apparatus.

For this study, the Dean-Stark extraction was used to determine the composition of the initial oil sand sample and to separate the individual components, such as bitumen, water, and mineral solids. Approximately 100 g of oil sands ore was placed into an extraction thimble and onto a wire holder suspended in the neck of a round bottom flask. Toluene, approximately 250 mL, was added to the flask. The solvent was heated using a round bottom flask heater, and it vaporized and refluxed through the system to dissolve the bitumen. Cold water flowed through the condenser to condense both the solvent and water. The connate water within the oil sand sample was first vaporized, and then was subsequently condensed and collected in the distilling trap. The Dean-Stark extraction process was left to run overnight to ensure all bitumen had been removed from the sample, and the solvent dripping from the thimble was clear.

At the end of the Dean-Stark extraction, all connate water was collected the distilling trap, bitumen was dissolved in toluene and resided at the bottom of the flask, and the mineral solids remained trapped in the thimble. The solids obtained post Dean-Stark extraction are called Soxhlet solids. The composition of the initial oil sand ore can be determined by weighing the individual components post extraction and comparing it to the weight of the original sample.

2.4. Preparation of Reconstituted Gangue

The composition of the Soxhlet gangue was assumed to be representative of the solids initially present in the oil sand ore. Although a small amount of fine solids migrated into the bitumen/toluene solution, the amount is less than 1% of the total solids originally in the sample. Bitumen is highly soluble in toluene, and therefore it is assumed all bitumen associated carbon has been removed, leaving behind only inorganic sources. Carbon content of the Soxhlet gangue, also known as the inorganic or toluene-insoluble carbon, was determined by CHNS analysis.

Soxhlet solids obtained immediately after the Dean-Stark extraction were wet with solvent. The solids were first dried at ambient conditions under the fume hood for 2 hours before being placed in the vacuum oven (80°C and 30 mbar) for 12 hours. These drying measures ensured the Soxhlet solids were completely free of solvent. To enable even mixing and distribution of bitumen, water and cyclohexane on the solid surface, particles > 500 μm were separated and removed from the bulk Soxhlet solids prior to preparation of the reconstituted gangue.

The protocol developed by Panda formed the basis for preparation of the reconstituted gangue, and the procedure is outlined in Figure 10 [66]. All steps were carried out at room temperature (20 ± 2 °C) and ambient pressures. It is assumed that bitumen, water, and cyclohexane will be evenly distributed in the real extracted gangue because of the vigorous mixing and sieving involved; the final product should be quite near homogeneity [30]. Detailed sample calculations can be found in Appendix A.

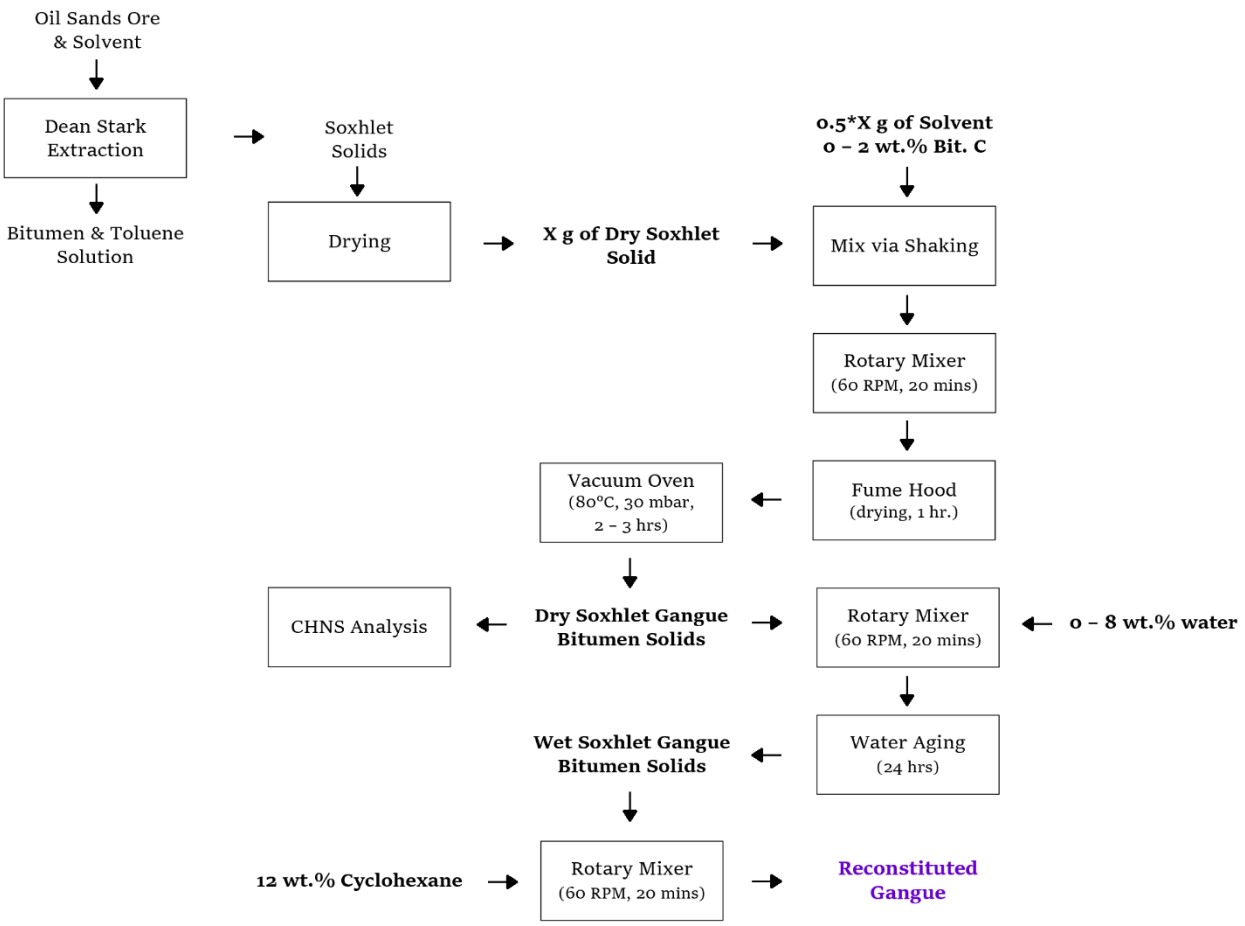

Figure 10. Flowchart for preparation of reconstituted gangue.

2.4.1. Addition of Bitumen

200 g of Soxhlet solids was used per batch of reconstituted gangue prepared. An amount of cyclohexane equal to half the weight of the Soxhlet gangue was added to a 500 mL Teflon bottle with the required amount of bitumen. The mass of bitumen added was calculated based on the specific Bit. C wt.% needed and was dependent on the amount of Soxhlet gangue used – see Appendix A for detailed calculations. Upon addition of the cyclohexane to bitumen, the bottle was capped and shaken until the bitumen was completely dissolved. The dry Soxhlet gangue was added to the solution in the Teflon bottom and placed on a rotary mixer at 60 rpm for 20 minutes.

Separating the mixing process helped ensure proper mixing and slurry formation. After 20 minutes on the rotary mixture, the slurry was poured into a large Pyrex glass dish and continually mixed manually for 1 hour to ensure even bitumen distribution. This step is crucial because if left unattended, bitumen would migrate with cyclohexane through the solid and deposit on the gangue surface. After 1 hour, the glass dish was placed into a vacuum oven at 80°C and 30 mbar for 2 to 3 hours to ensure complete removal of cyclohexane. The resulting solids are evenly coated with the desirable amount of bitumen and will be referred to as dry Soxhlet gangue bitumen solids or DSBS. A small amount of DSBS then underwent CHNS analysis to verify its bitumen content and to determine if bitumen was uniformly coated. Figure 11 shows DSBS with varying Bit. C content.

Figure 11. From left to right, DSBS with 2.0, 1.5, 1.0, 0.5 and 0 wt.% Bit. C.

2.4.2. Additional of Water

An amount of DSBS was weighed and transferred into a clean Teflon bottle and the target amount of water wad added based on the weight of DSBS. The bottle was capped and placed on a rotary mixer at 60 rpm for 20 minutes. After mixing, the bottle was sealed with Parafilm to prevent water loss via evaporation and left to age for 24 hours. Aging allows time for water to enter the pores of the DSBS; this aging process for the gangue is important in replicating the

dispersion of water in real gangue that occurs during the extraction process. The product at the end of this stage is termed wet Soxhlet gangue bitumen solids, or WSBS, and was stored at ambient conditions until the addition of cyclohexane.

2.4.3. Addition of Cyclohexane

The amount of cyclohexane required depended on the mass of the WSBS and was fixed at 12 wt.% for all samples. Sample calculations are in Appendix A. An amount of WSBS was transferred to a cup and the target cyclohexane quantity was added. The cup was capped and sealed using Parafilm and placed on a rotary mixer at 60 rpm for 20 minutes. The product at the end of this stage is termed reconstituted gangue.

2.4.4. Samples Prepared

Using the procedure outline previously, two groups of samples were prepared with specifications outlined in Table 2.

Table 2. Target composition of reconstituted bitumen for sample groups A and B.

Group	Bit. C Content (wt.%)	Water Content (wt.%)	Cyclohexane (wt.%)
A	0, 0.5, 1.0, 1.5, 2.0	3.7	12.0
B	1.0	0, 3.7, 6.0, 8.0	12.0

2.5. Sample Packing

A gangue sample, reconstituted or extracted, consists of Soxhlet solids with bitumen, cyclohexane and water trapped in its pores. Approximately 25.0 ± 0.5 g of reconstituted gangue was weighed onto a 5 cm (inner diameter), 1.5 cm deep Pyrex glass petri dish (CLS316060). The sample was spread out evenly to a 1.00 ± 0.05 cm bed height. By maintaining the same mass, bed height and bed radio, the bulk density (ρ_{bulk}) and average porosity of the sample was kept constant.

The bulk density of the packed bed can be calculated as

$$\rho_{bulk} = \frac{mass\ of\ solid\ in\ the\ packed\ bed}{volume\ of\ the\ packed\ bed} \tag{11}$$

The average porosity can be calculated as

$$\phi = 1 - \frac{\rho_{bulk}}{\rho_{particle}} \tag{12}$$

2.6. Drying Conditions

All drying experiments were performed under a fume hood, and the sash height was kept constant to maintain constant air flow. The petri dish was placed on a balance (Model XP203S, Mettler Toledo) and connected to a computer where the balance weight was recorded every 20 seconds using Mettler Toledo software. All sides of the balance were kept open during the duration of the experiment to enable flow through the sample. A fan (OPOLAR, 8 in was added

to one side of the balance and directly faced the drying gangue sample. All drying experiments were performed at room temperature (20 ± 2°C) and pressure, and samples were dried for 2 hours. The horizontal air current was measured by an anemometer (HoldPeak HP-866B-APP) with an operational range of 0.5 – 30 m/s, resolution to 0.1 and accuracy of ± 5%. Horizontal flow velocities corresponding to various fan settings are expressed in Table 3. The experimental setup is shown in Figure 12.

Table 3. Measured horizontal air current velocity.

Fan Setting	Ambient	Low	Medium	High
Flow (m/s)	0.9 ± 0.1	2.3 ± 0.1	3.0 ± 0.1	3.5 ± 0.1

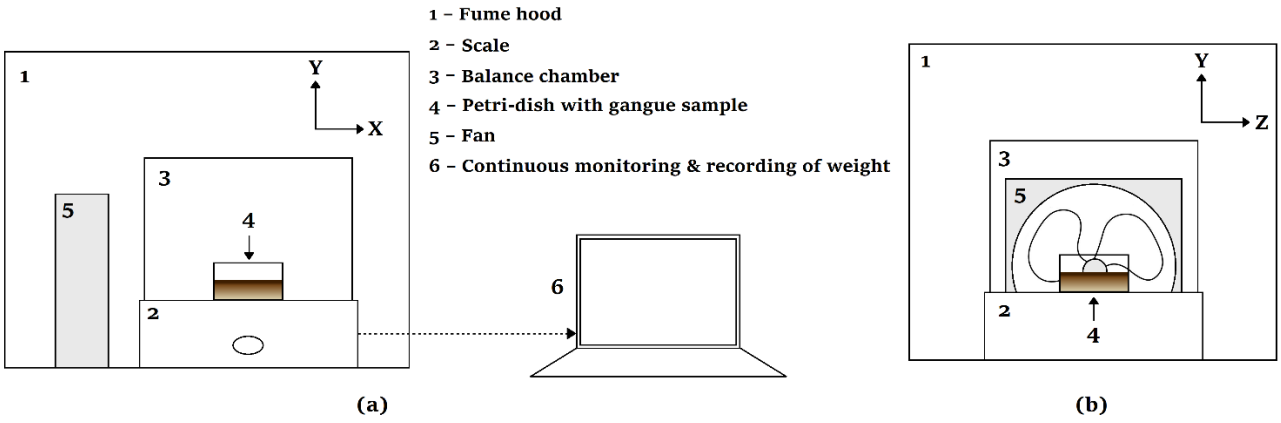

Figure 12. Experimental setup with (a) front view and (b) side view

2.7. CHNS Elemental Analysis

An elemental analyzer (Flash 2000 CHNS/0 Analyzer, Thermo Scientific) was used to determine the carbon, hydrogen, nitrogen, and sulfur content of the various gangue samples. Samples were first homogenized using a mortar and pestle before being placed into a tin capsule; 10 – 15 mg of sample was required per capsule. The capsules were loaded into the autosampler of the analyzer and sent to the quartz combustion reactor inside a furnace with a temperature of 900°C. Upon contact with oxygen in the reactor, a strong exothermic reaction was triggered due to the oxidizing environment; temperatures reached nearly 1800°C and the sample combusted instantaneously. The resulting combustion products were transported across the reactor and oxidation was finalized. Any nitrogen oxides and sulfur trioxides possibly formed would be reduced to nitrogen and sulfur gas. The gas mixture exiting the reactor consisting of CO_2, H_2O, N_2 and SO_2 was then fed into a chromatographic column and separated before being passed through a thermal conductivity detector (TCD). The TCD produces electrical signals which were then processed by the Eager Xperience software to provide the percentages of carbon, hydrogen, nitrogen and sulfur in the sample. The time required between dropping a sample into the reactor and obtaining the carbon, hydrogen, nitrogen, and sulfur fractions was approximately 12 minutes.

Inorganic or non-bitumen associated carbon can be determined via CHNS analysis of Soxhlet solids. The Bit. C content for a sample of DSBS can be determined by subtracting the inorganic content of Soxhlet solids from the carbon content obtained from CHNS analysis.

2.8. Pycnometry Measurements

Pycnometry measurements are used to determine the density and porosity of oil sand mineral solids. Approximately 4 g of Soxhlet gangue was weighted and placed into a pre-weighed 10 mL volumetric flask. The flask was subsequently filled to mark with cyclohexane and then shaken to release any trapped bubbles before being left overnight to allow invasion of all the pores by the solvent. The next day, the flask was re-filled to mark and weighed to obtain the weight of the mineral solid and solvent. Particle density (ρ_p) can be calculated by dividing the mass of the solid in the flask by the volume occupied by the solids.

3. Results and Discussions

3.1. Characteristics of Oil Sands Ore and Gangue

The bitumen, water and solids contents in the oil sands ore were determined using the Dean-Stark extraction and results are shown in Table 4. In this study, fine solids are those smaller than 45 μm.

Table 4. Composition of oil sands ore.

	Bitumen[1]	**Water[1]**	**Solids[1]**	**Fines[2] (< 45μm)**	**> 500 μm solids[2]**
Content (wt.%)	11.8 ± 0.9	3.2 ± 0.2	85.4 ± 0.7	6.9 ± 0.8	6.5 ± 0.5

[1] Calculated based on total oil sands ore weight
[2] Calculated based on solid weight

The bulk density, particle density, and porosity for Soxhlet solids are tabulated in Table 5.

Table 5. Bulk density, particle density, and porosity for Soxhlet solids with n=5.

Density (kg/m^3)		**Porosity (ϕ)**
Bulk (ρ_{bulk})	Particle ($\rho_{particle}$)	
1458 ± 22	2610 ± 68	0.44

The oil sand samples utilized in this study are identical to those used by Khalkhali and analyses showed nearly identical composition, density, and porosity values [69]. Table 6 shows the particle size distribution for Soxhlet samples (< 500μm) obtained from [69].

Table 6. Particle size distribution for Soxhlet gangue solids (> 500 μm particles removed).

	Particle Size (μm)				
	< 45	45 – 150	150 – 212	212 – 500	500 +
Weight Percent (wt.%)	7.33	27.05	53.99	10.90	0

Wettability of the gangue and therefore its affinity for cyclohexane or water are dependent on its composition. Methods to determine wettability include the sessile drop, Wilhelmy plate, and Washburn capillary rise technique [70]. Contact angle measurements for DSBS samples of varying fine solids fraction obtained from [69] are shown in Figure 13 and Table 7. The apparent contact angle refers to the angle observed on the composite surface (i.e. boric acid and the DSBS). The true contact angle between the DSBS and water can be calculated using the Cassie-Baxter equation if the contact angle between water and a boric acid pellet is known. Boric acid acted as a binding agent and was mixed with the DSBS in a 1:1 ratio to obtain pellets with smooth and homogenous surfaces.

Figure 13. Photographs of water on pellets of boric acid and DSBS with (a) 0% (b) 10% and (c) 20% fines content.

Table 7. Contact angle measurements for DSBS with various fines content.

Fines Content in DSBS Sample (%)	Apparent Contact Angle	DSBS and Water Contact Angle
0	56.3	59.70
10	58.1	64.16
20	69.3	91.06

Bitumen content of the Soxhlet solid and DSBS from groups A and B obtained through CHNS analysis are in Table 8. As previously mentioned, this was to verify the bitumen, and therefore Bit. C, content

Table 8. Bitumen and carbon content of Soxhlet solids and DSBS.

Group	Target Bit. C (wt.%)	Actual Bit. C (wt.%)
A[a]	0[c]	0
	0.5	0.471 ± 0.08
	1.0	0.970 ± 0.06
	1.5	1.47 ± 0.03
	2.0	1.93 ± 0.06
B[b]	1.0	1.08 ± 0.09

[a] n = 4
[b] n = 3
[c] 0 wt.% Bit. C corresponds to Soxhlet gangue solids.

3.2. Formation of Liquid Films

Liquid films are formed if the solid surface is wetted by the liquid and if capillary forces are dominant over viscous and gravitational effects [51] [57] [71].

The critical surface tension of Soxhlet solids obtained from rich-grade Athabasca oil sands and DSBS with 0.5 – 2 wt.% Bit. C was measured by Panda to be 34 ± 7 and 29 – 32 ± 5 mN/m, respectively [66]. Since the critical surface tension for Soxhlet gangue is higher than the surface tension of cyclohexane (23.8 – 24.5 mN/m for the temperature range of 30 – 25°C) but lower than that of water (72.8 – 71.2 mN/m for the temperature range of 20 – 23°C), it implies the reconstituted gangue will only be wetted by cyclohexane and not water [72], [73]. This was also

evident in that water forms droplets on the Soxhlet gangue surface while cyclohexane penetrates the porous media upon contact. During the drying of a cyclohexane and bitumen solution in a petri dish, a thick bitumen layer was observed to have formed on the glass wall over the solution. This bitumen deposition was due to cyclohexane liquid films that carried the bitumen upwards before evaporating and leaving the bitumen behind.

Khalkhali estimated the magnitude of the capillary and Bond number for samples with a mean pore size of 100 μm and 1 μm and found them to be on the order of $\sim 10^{-3}$ and $\sim 10^{-1}$, respectively [69]. Although the exact pore size distribution of a gangue sample is unknown, an assumed pore size of 1 μm is unrealistically small since roughly 93% of Soxhlet solids are larger than 45 μm, as specified in Section 3.1. As mentioned previously, for viscous effects to have a noticeable effect on the drying rate, Ca must be of *order 1* [51].

3.3. Drying Curve Analysis

The weight of the reconstituted gangue sample was recorded every 20 seconds over the duration of the drying experiment (2 hours) to determine cumulative weight loss of the sample at a given time. A typical cumulative weight loss vs time curve is shown in Figure 14.

The initial stage of drying is dominated by solvent removal and the evaporative flux will be at its highest [30], [68]. For the duration of the initial stage, liquid cyclohexane films are formed via capillarity that maintain hydraulic connectivity to the open surface. At the exposed surface, there is a large concentration gradient for cyclohexane that enables its rapid removal. These liquid films facilitate solvent removal by eliminating the need for transport via diffusion and the initial stage is drying is maintained if the liquid films remain connected to the exposed surface. The

liquid film flow rate was estimated to be on the order of 10^{-3} for samples with an average pore size of 1 μm, and on the order of 10^{-1} for pore size of 100 μm [69] .

During the second drying stage, the cyclohexane liquid films have detached from the open surface and receded into the porous matrix. Mass transfer during this stage is limited to diffusion through the media. Due to porosity and tortuosity, the effective molecular diffusivity is significantly less than the effective diffusivity in the mass boundary layer [61].

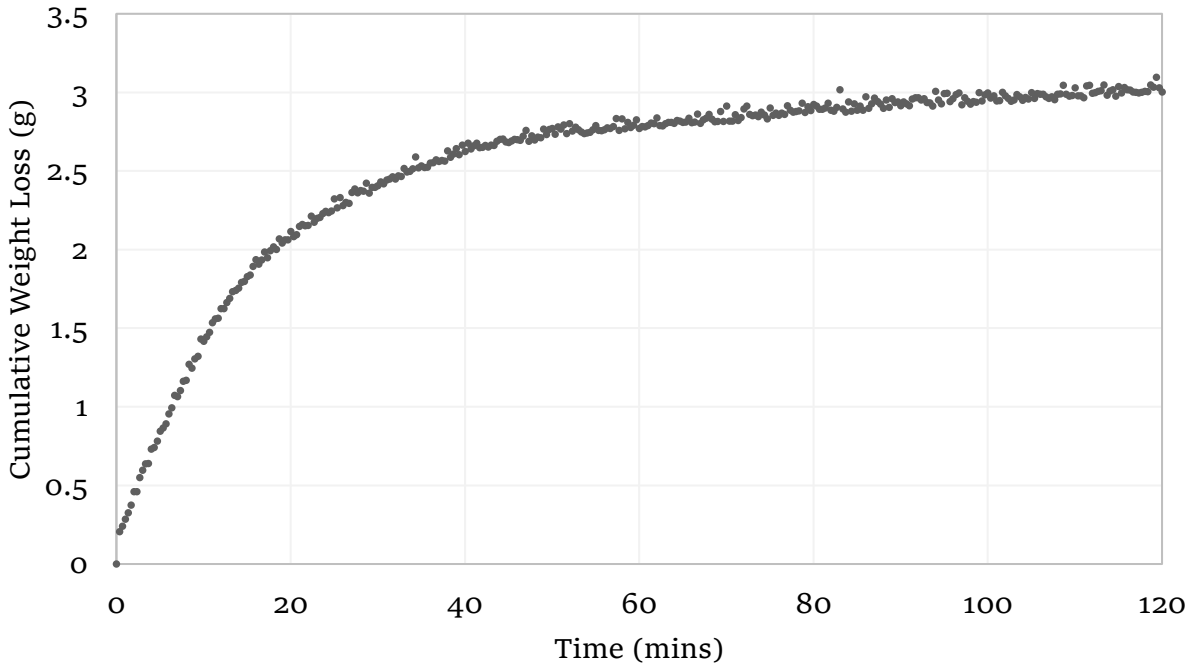

Figure 14. Cumulative weight loss at ambient conditions for reconstituted gangue sample with 0 wt.% Bit C, 3.7 wt.% water and 12 wt.% cyclohexane.

The initial flux, transition time, and final flux can be determined using the cumulative weight loss data by implementing a similar approach to the one proposed by Panda [66].

3.3.1. Initial Flux

The initial flux of a sample is the average evaporative flux over the first 10 minutes of drying. The slope of the drying curve for the first 10 minutes of drying was obtained through linear regression, as shown in Figure 15. Initial flux can be calculated by dividing the slope of the drying curve in the first 10 minutes by the evaporative surface area or the surface area of the petri dish.

$$Initial\ Flux = \frac{Slope\ of\ drying\ curve\ during\ first\ 10\ minutes}{Petri\ dish\ area\ (19.64\ cm^2)} \tag{13}$$

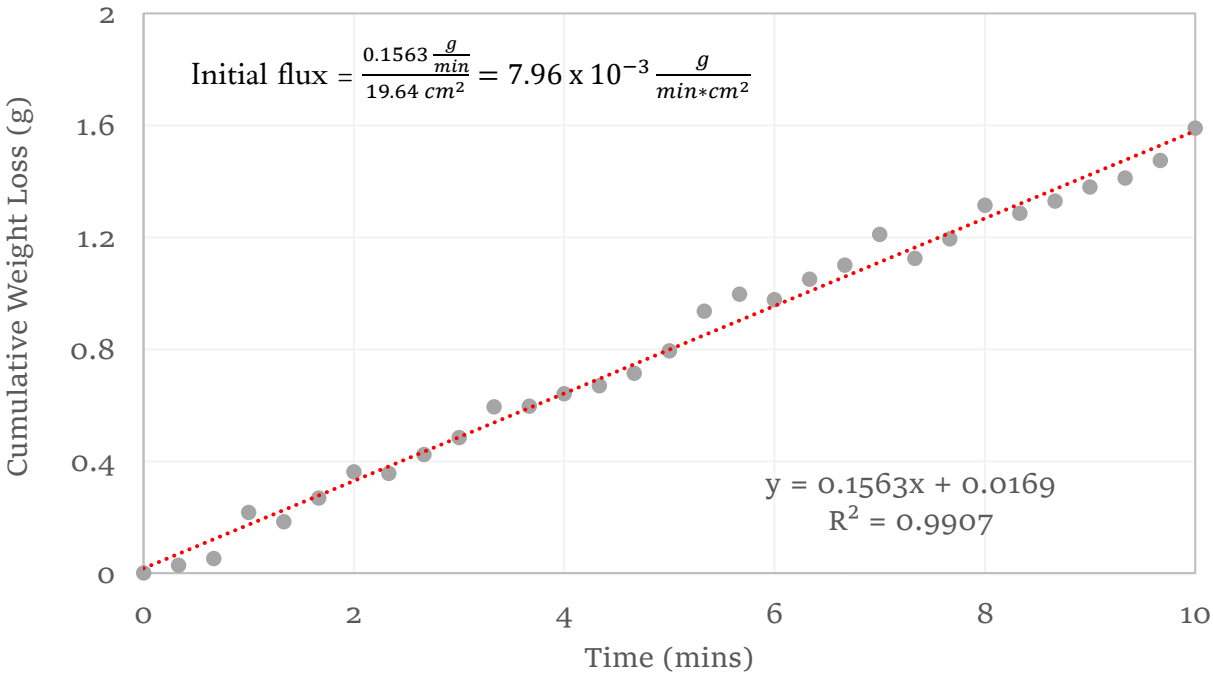

Figure 15. Average initial flux determination for reconstituted gangue sample at ambient conditions with 0 wt.% Bit C, 3.7 wt.% water and 12 wt.% cyclohexane.

3.3.2. Transition Time or Breakpoint

As evident in Figure 14, the drying curve for a reconstituted gangue sample can be roughly divided into two sections or intervals. The first interval corresponds to solvent-dominated loss while the second phase is water-dominated evaporation; these two stages are separated by a breakpoint, as shown in Figure 16. This breakpoint is also called the transition time because it denotes the point at which the faster initial drying stage transitions to the slower final drying stage.

The breakpoint or transition time is determined via piecewise linear regression and minimization of the mean square error (MSE). The piecewise model is continuous and consists of two straight lines for two different x domains separated by the breakpoint [74]. RMSE is the square root of MSE.

$$MSE = \frac{1}{n}\sum_{i=1}^{n}(y_i - \hat{y}_i)^2 \tag{14}$$

In the above equation, y_i is the observed value and $\hat{y}_i$ is the predicted value.

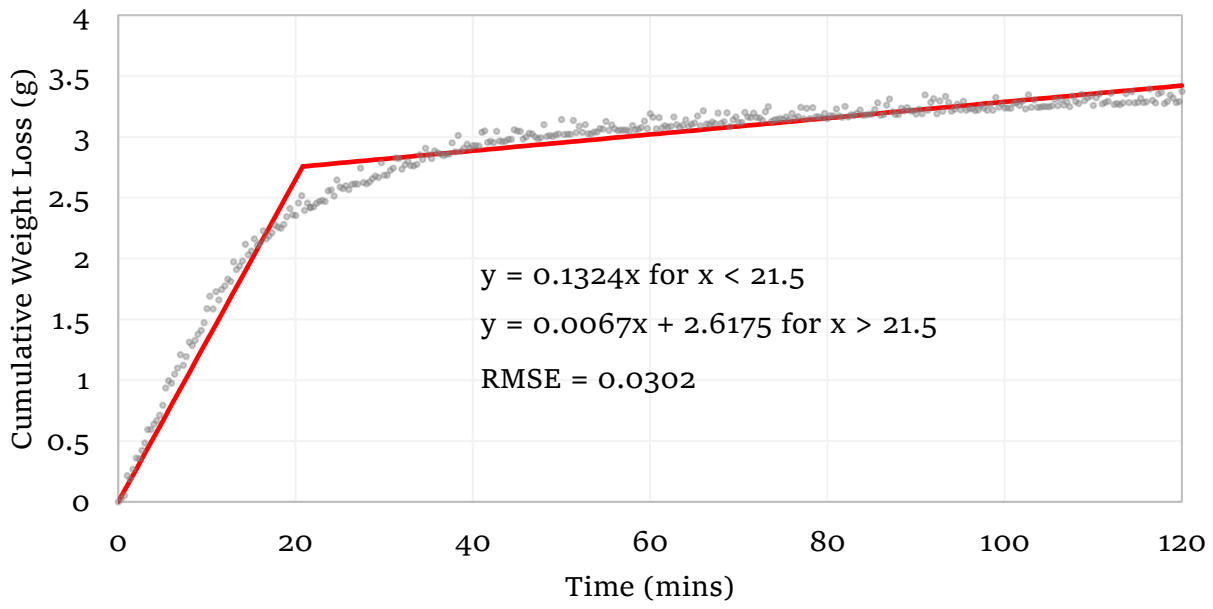

Figure 16. Determining transition time using piecewise liner regression.

3.3.3. Final Flux

The final flux is the average flux during the last 40 minutes of the drying experiment. Evaporative flux during this stage is limited by diffusion within the porous gangue. Like the initial flux, it is obtained through linear regression and can be calculated using Equation 15.

$$Final\ Flux = \frac{Slope\ of\ drying\ curve\ during\ last\ 40\ minutes}{Petri\ dish\ area\ (19.64\ cm^2)} \quad (15)$$

3.3.4. Data Variance from Fan

Figure 17 shows the effect of various fan settings on the weight measured by an otherwise empty scale. As evident in Figure 16, increasing the convective current also increases the variance of the data. However, the slopes obtained through linear regression were virtually zero for all flow rates. This means that although the fan increased the variability of the data and the value of individual data points, it did not affect the overall trend or drying pattern.

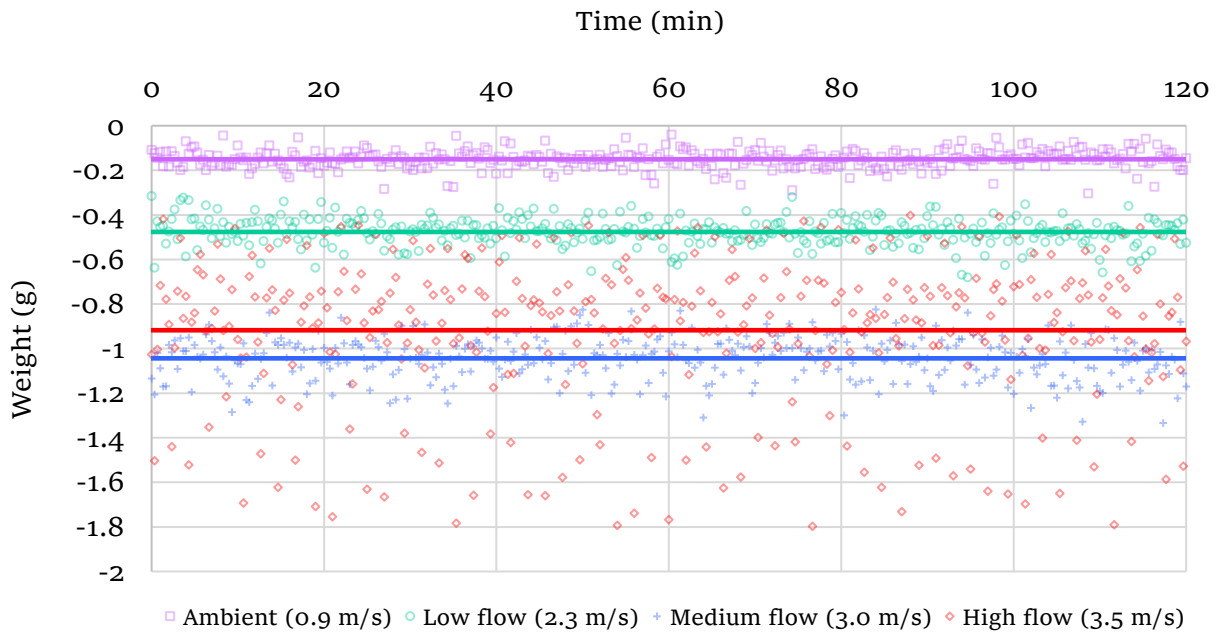

Figure 17. Weight of the otherwise empty scale in the presence of various flow rates.

3.4. Effect of Convective Flows

The effect of convective flows on reconstituted gangue samples of varying bitumen (Group A) and varying water (Group B) content were investigated. Drying experiments in Group A were performed in duplicates while experiments in group B were performed in triplicates. Select figures were plotted to illustrate the effect bitumen and water content on the drying curve and consequently the initial flux, transition time and final flux. Tabulated values shown in this section are the average values at each gangue composition and drying condition.

3.4.1. Effect of Bitumen

Figure 18 is the cumulative weight loss curve for reconstituted gangue samples with 0 wt.% Bit. C, 3.7 wt.% water and 12 wt.% cyclohexane and Figure 19 is a close-up of the drying curve during the first 10 minutes. The initial flux, final flux and transition time for the same samples are tabulated in Table 9. Although increasing flow velocity increased the variance of the data, the overall pattern of the drying curve was maintained. As evident in Figure 18, there are overlaps of the drying curves for all samples during the initial stages of drying. There was a 51.5% increase in initial flux when the current velocity increased from 0.9 m/s to 3.5 m/s; the average increase in initial flux per 1 m/s increase in flow velocity was 1.3 x 10^{-3} $\frac{g}{min*cm^2}$. The transition time decreased by 7 minutes, or 32.3%, for the same velocity change. Like results from previous studies, the final flux was at least one order of magnitude smaller than the initial flux [66]–[69]. The final flux showed no distinct relations with changing flow velocities.

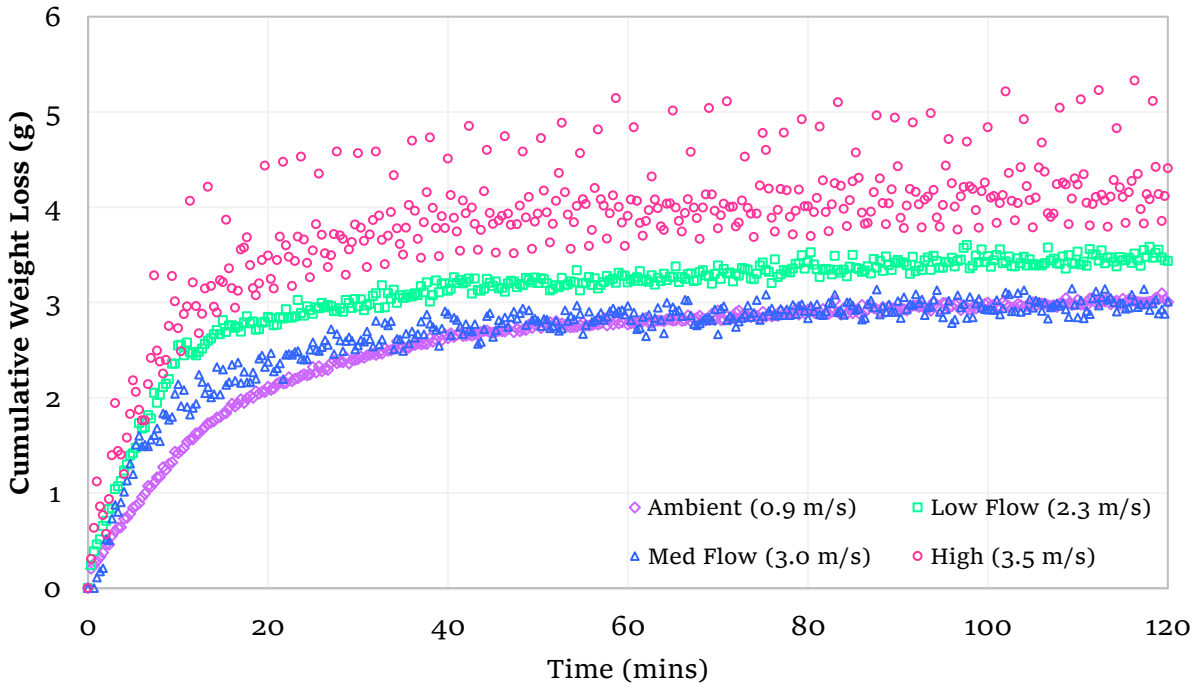

Figure 18. Cumulative weight loss for reconstituted gangue with 0 wt.% Bit. C, 3.7 wt.% water and 12 wt.% cyclohexane.

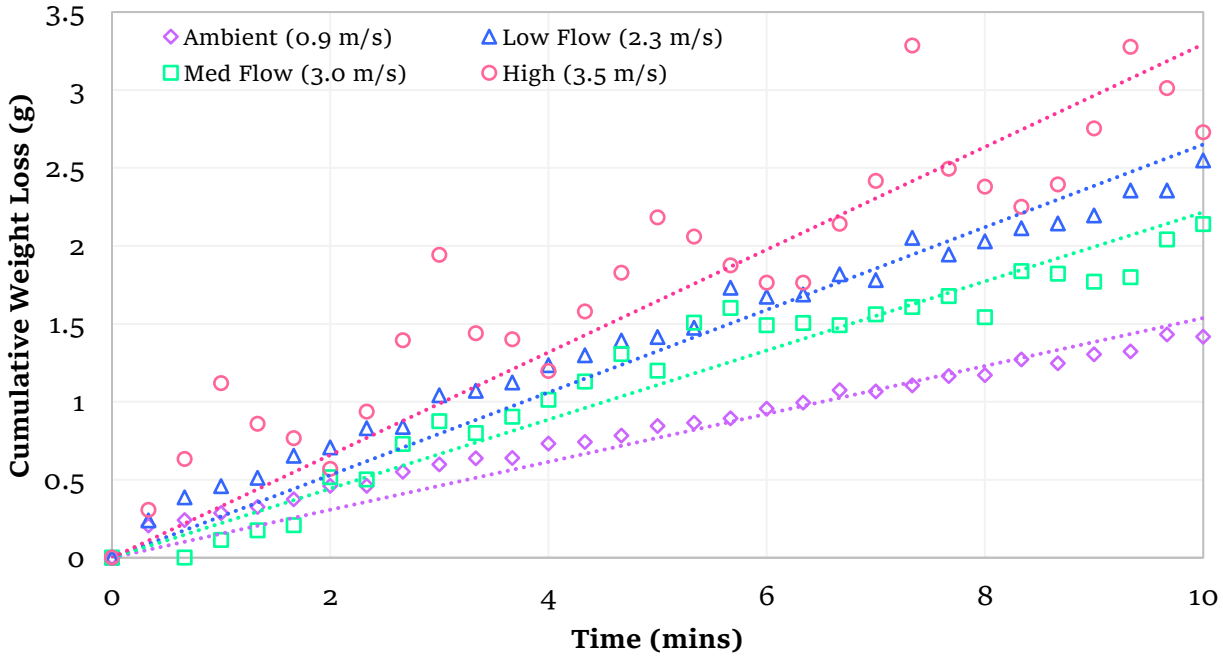

Figure 19. Cumulative weight loss for sample with 0 wt.% Bit. C, 3.7% water and 12 wt.% cyclohexane during first 10 minutes.

Table 9. Initial flux, final flux, and transition time of reconstituted gangue with 0 wt.% Bit. C, 3.7 wt.% water and 12 wt.% cyclohexane.

Flow velocity (m/s)	0.9	2.3	3	3.5
Initial flux ($\frac{g}{min*cm^2}$)	7.93 x 10^{-3}	1.10 x 10^{-2}	9.92 x 10^{-3}	1.20 x 10^{-2}
Transition time (mins)	21.7	15.2	15.8	14.7
Final flux ($\frac{g}{min*cm^2}$)	1.66 x 10^{-4}	1.58 x 10^{-4}	0.66 x 10^{-4}	1.86 x 10^{-4}

Figure 20 is the cumulative weight loss curve for reconstituted gangue samples with 0.5 wt.% Bit. C, 3.7 wt.% water and 12 wt.% cyclohexane, and Figure 21 is a closeup of the drying curve during the initial 10 minutes. The initial flux, final flux and transition time for the same samples are tabulated in Table 10. As evident in Figure 20, there are overlaps in the drying curve for flow rates of 2.3, 3.0 and 3.5 m/s during most of the drying process. Similar to samples with 0 wt.% bitumen, the initial flux increased with faster convective currents. The average increase in initial flux per 1 m/s increase in flow velocity was 1.0 x 10^{-3} $\frac{g}{min*cm^2}$, and the highest initial flux was reached when the flow velocity was 3.0 m/s. Increasing flow velocity resulted in an increase in the transition time. Transition time for samples at a flow velocity of 3.5 m/s was 8 minutes shorter than samples at 0.9 m/s. The final flux of all samples with 0.5 wt.% Bit. C were comparable with no observable patterns.

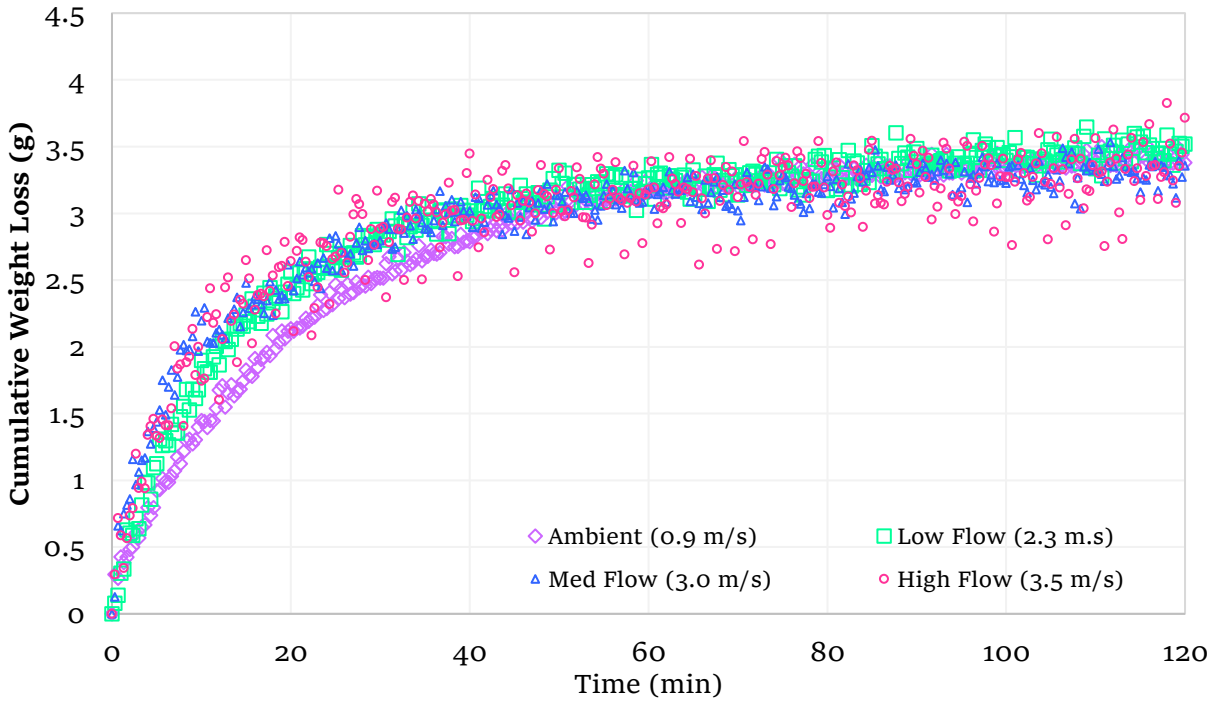

Figure 20. Cumulative weight loss for reconstituted gangue with 0.5 wt.% Bit. C, 3.7 wt.% water and 12 wt.% cyclohexane.

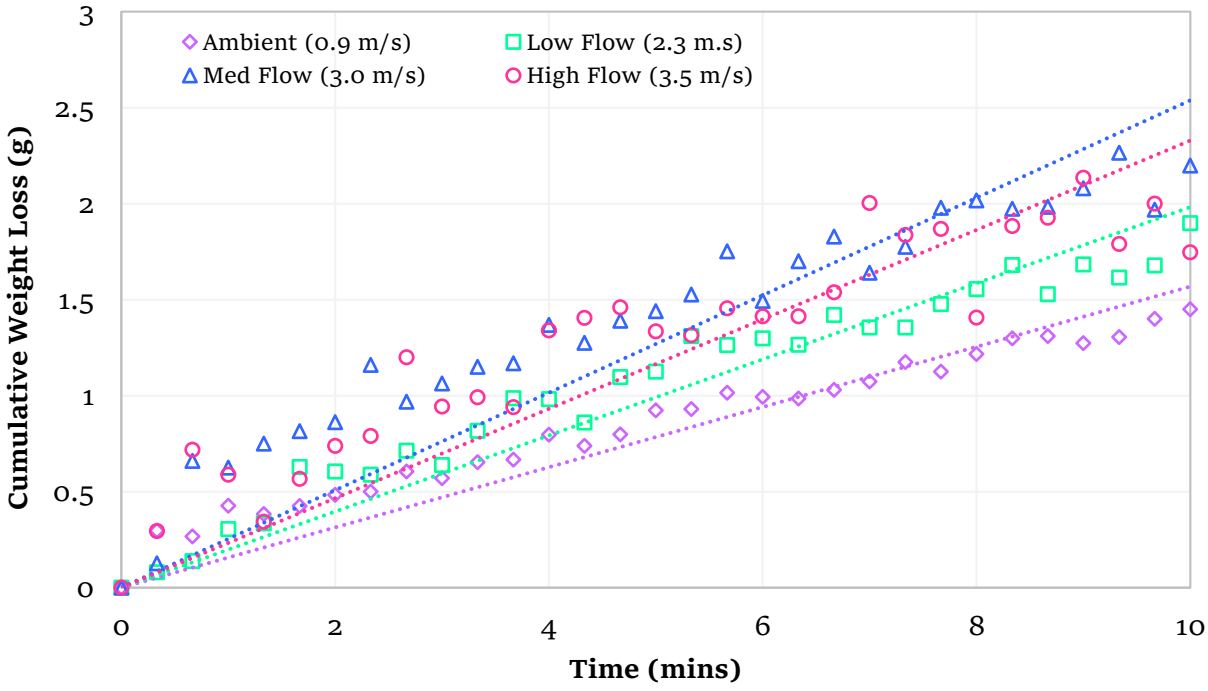

Figure 21. Cumulative weight loss for sample with 0.5 wt.% Bit. C, 3.7% water and 12 wt.% cyclohexane during first 10 minutes.

Table 10. Initial flux, final flux, and transition time of reconstituted gangue with 0.5 wt.% Bit. C, 3.7 wt.% water and 12 wt.% cyclohexane.

Flow velocity (m/s)	0.9	2.3	3	3.5
Initial flux ($\frac{g}{min*cm^2}$)	6.37 x 10^{-3}	7.86 x 10^{-3}	9.28 x 10^{-3}	8.70 x 10^{-3}
Transition time (mins)	26.9	23.9	18.2	18.9
Final flux ($\frac{g}{min*cm^2}$)	1.39 x 10^{-4}	1.65 x 10^{-4}	1.17 x 10^{-4}	2.14 x 10^{-4}

Figure 22 is the cumulative weight loss curve for reconstituted gangue samples with 1.0 wt.% Bit. C, 3.7 wt.% water and 12 wt.% cyclohexane, and Figure 23 is a closeup of the drying curve during the initial 10 minutes. The initial flux, final flux and transition time for the same samples are shown in Table 11. As seen in Figure 20, there seems to be overlap between all samples during the initial stages of drying. During the final stages of drying, there seems to be overlap between the drying curve at flow rates of 0.9 m/s and 3.5 m/s, and flow rates of 2.3 m/s and 3.0 m/s. There was only a slight increase in initial flux with increasing current velocities; the average increase in initial flux per 1 m/s increase in flow velocity was 2.0 x 10^{-4} $\frac{g}{min*cm^2}$. Like samples with 0.5 wt.% Bit. C, the maximum initial flux was reached at a flow velocity of 3 m/s. The transition time decreased by 10.7 seconds when flow velocity increased from 0.9 m/s to 3.0 m/s. The final flux of all samples with 1.0 wt.% Bit. C were at least one order of magnitude smaller than the initial flux and had no observable relations to the flow velocity.

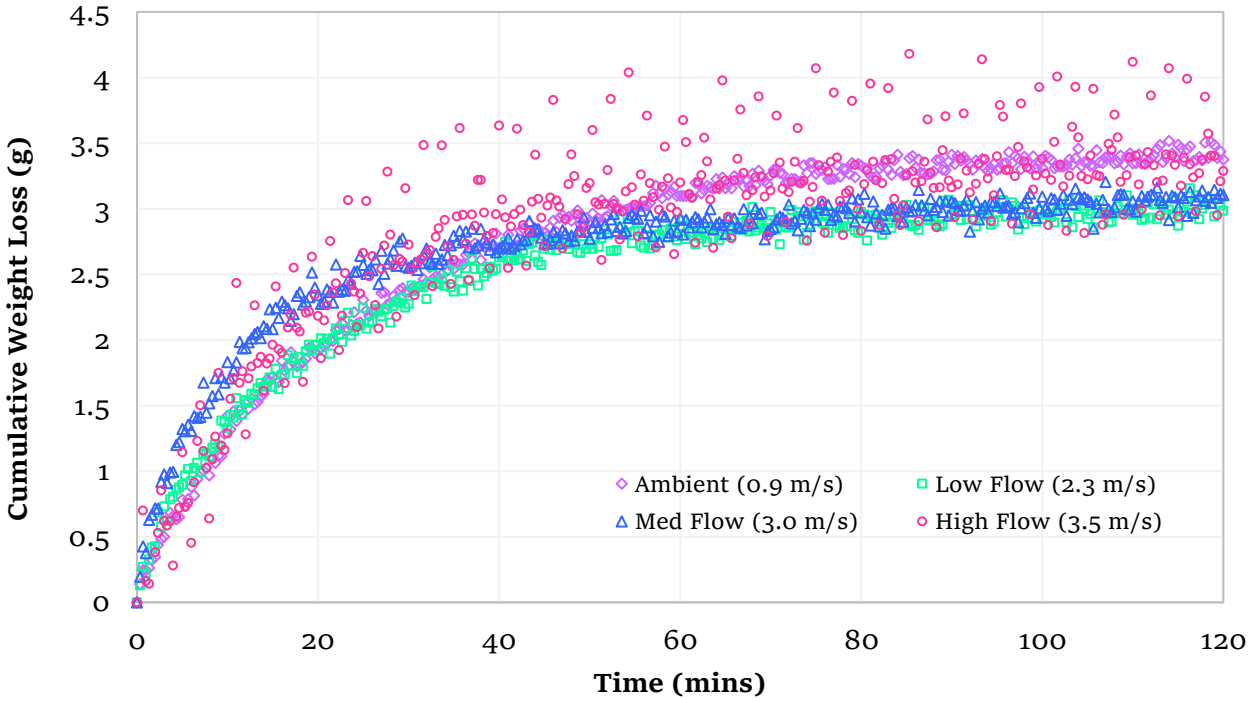

Figure 22. Cumulative weight loss for reconstituted gangue with 1.0 wt.% Bit. C, 3.7 wt.% water and 12 wt.% cyclohexane.

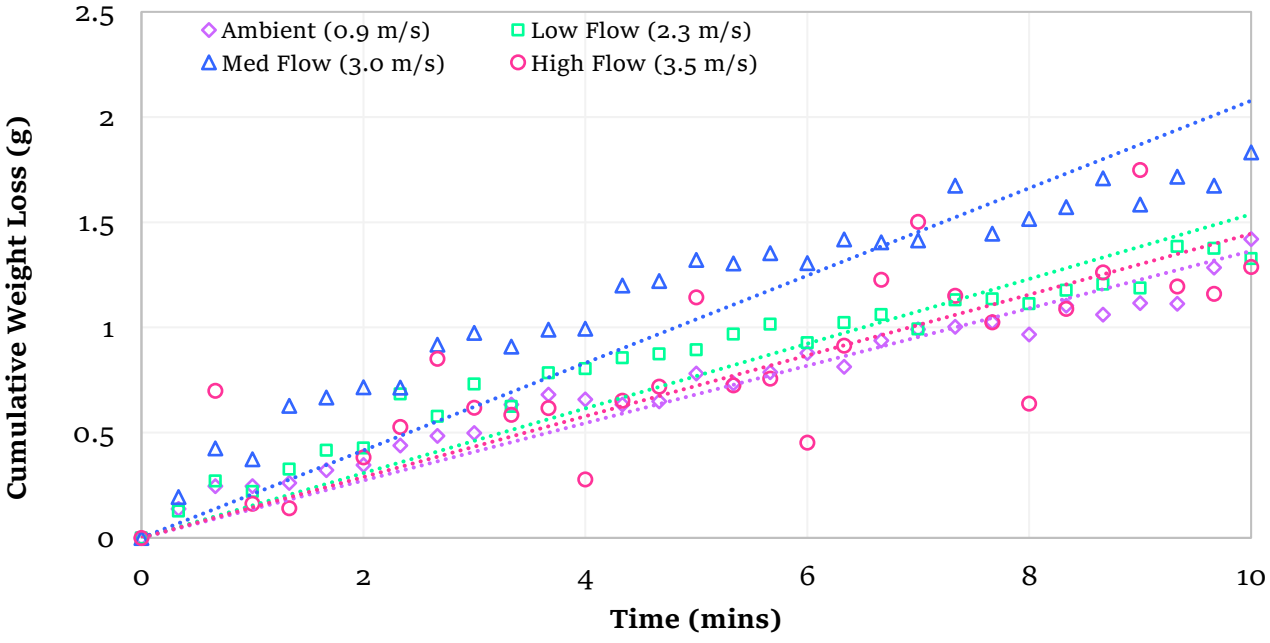

Figure 23. Cumulative weight loss for reconstituted gangue sample with 1 wt.% Bit. C, 3.7% water and 12 wt.% cyclohexane during first 10 minutes.

Table 11. Initial flux, final flux, and transition time of reconstituted gangue with 1.0 wt.% Bit. C, 3.7 wt.% water and 12 wt.% cyclohexane.

Flow velocity (m/s)	0.9	2.3	3	3.5
Initial flux ($\frac{g}{min*cm^2}$)	6.18 x 10^{-3}	6.40 x 10^{-3}	7.46 x 10^{-3}	6.26 x 10^{-3}
Transition time (mins)	35.5	31.0	24.8	31.3
Final flux ($\frac{g}{min*cm^2}$)	1.53 x 10^{-4}	1.43 x 10^{-4}	1.43 x 10^{-4}	1.35 x 10^{-4}

Figure 24 is the cumulative weight loss curve for reconstituted gangue samples with 1.5 wt.% Bit. C, 3.7 wt.% water and 12 wt.% cyclohexane and Figure 25 is a closeup during the first 10 minutes. The initial flux, final flux and transition time for the same samples are in Table 12. There are overlaps in the cumulative weight loss plot of samples dried at ambient, low flow and medium flow conditions. There appears to be a slight increase in initial flux with increasing flow velocity; the average increase in initial flux per 1 m/s increase in flow velocity was 1.0 x 10^{-6} $\frac{g}{min*cm^2}$. Like samples with 0.5 and 1.0 wt.% bitumen, the highest initial flux was reached at a flow rate of 3 m/s. The transition time decreased by 10.3 seconds when flow velocity increased from 0.9 m/s to 3.0 m/s, and by 7 seconds from 0.9 m/s to 3.5 m/s. There were no distinct relationships between final flux and flow conditions.

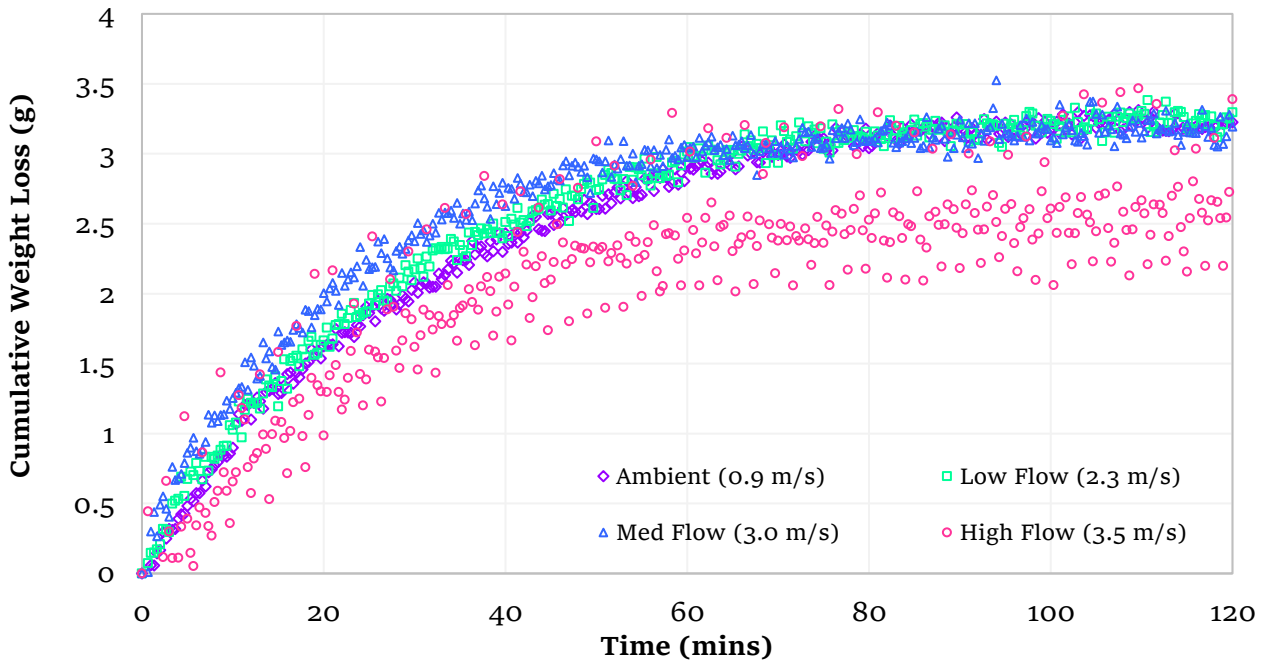

Figure 24. Cumulative weight loss for reconstituted gangue with 1.5 wt.% Bit. C, 3.7 wt.% water and 12 wt.% cyclohexane.

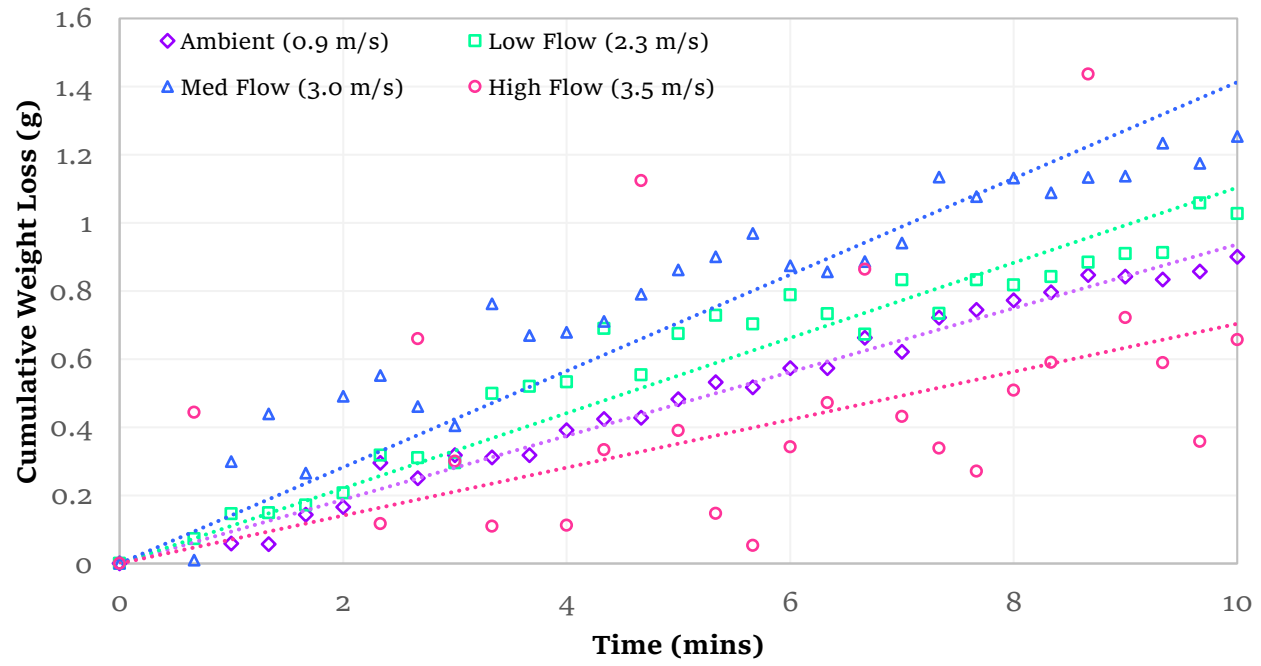

Figure 25. Cumulative weight loss for reconstituted gangue with 1.5 wt.% Bit. C, 3.7 wt.% water and 12 wt.% cyclohexane during first 10 minutes.

Table 12. Initial flux, final flux, and transition time of reconstituted gangue with 1.5 wt.% Bit. C, 3.7 wt.% water and 12 wt.% cyclohexane.

Flow velocity (m/s)	0.9	2.3	3	3.5
Initial flux ($\frac{g}{min*cm^2}$)	4.80 x 10^{-3}	5.26 x 10^{-3}	6.02 x 10^{-3}	4.21 x 10^{-3}
Transition time (mins)	44.5	38.8	34.2	37.5
Final flux ($\frac{g}{min*cm^2}$)	1.41 x 10^{-4}	1.63 x 10^{-4}	0.97 x 10^{-4}	1.45 x 10^{-4}

Figure 26 is the cumulative weight loss curve for reconstituted gangue samples with 2.0 wt.% Bit. C, 3.7 wt.% water and 12 wt.% cyclohexane and Figure 27 is a close-up of the drying curve during the initial 10 minutes. The initial flux, final flux and transition time for the samples are in Table 13. As evident in Figure 22, there were overlaps between the drying curves for flow velocities of 0.9 m/s and 2.3 m/s, and for flow velocities of 3.0 m/s and 3.5 m/s. Like samples with 1.5 wt.% Bit. C, there appeared to be a slight increase in initial flux with increasing flow velocity and the average increase in initial flux per 1 m/s increase in flow velocity was 5.0 x 10-4 $\frac{g}{min*cm^2}$. Increasing the flow rate from 0.9 m/s to 3.0 m/s and 3.5 m/s increased the initial flux by 26.7% and 29.0%, respectively. The transition time decreased by 13.1 seconds when flow velocity increased from 0.9 m/s to 3.0 m/s, and by 15.3 seconds from 0.9 m/s to 3.5 m/s. The final flux observed for all flow conditions were comparable and there were no distinct relationship with flow conditions.

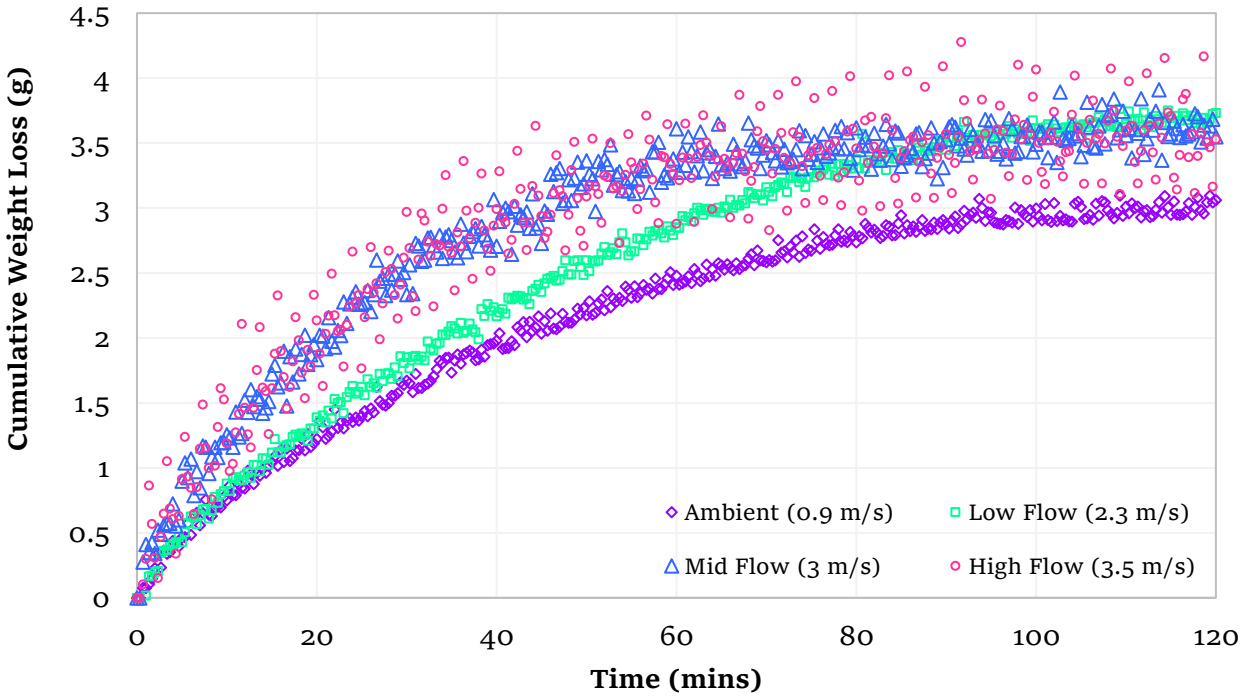

Figure 26. Cumulative weight loss for reconstituted gangue with 2.0 wt.% Bit. C, 3.7 wt.% water and 12 wt.% cyclohexane.

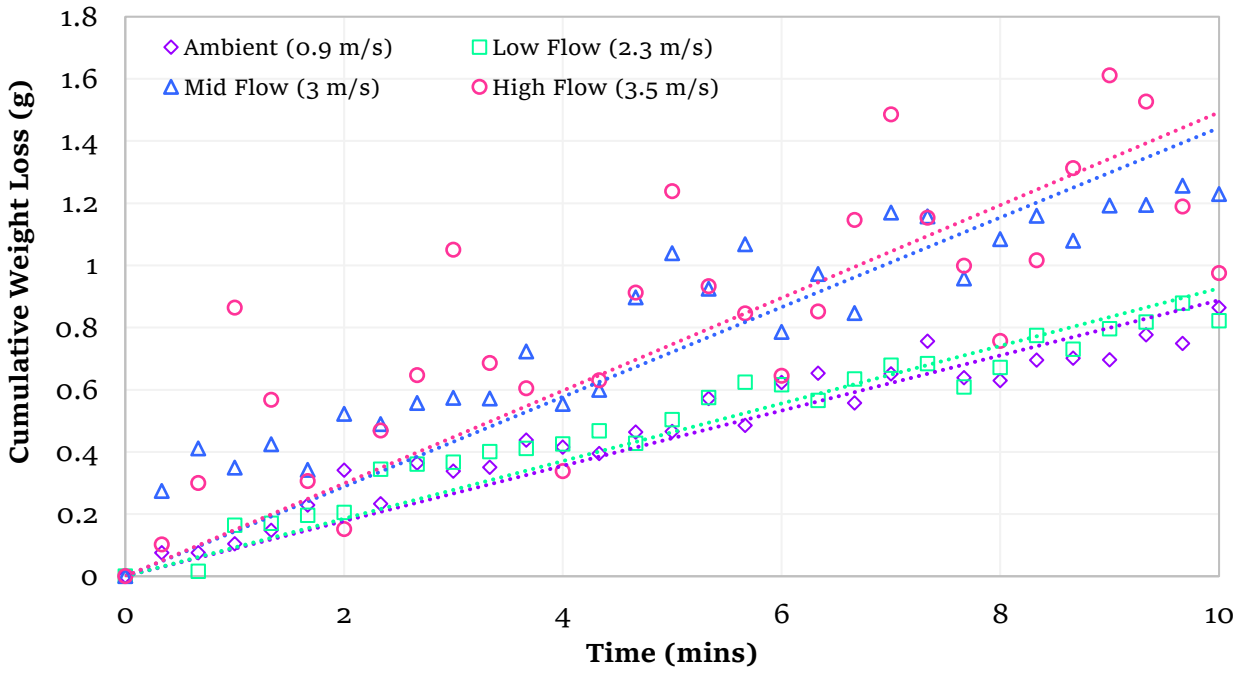

Figure 27. Cumulative weight loss for reconstituted gangue sample with 2.0 wt.% Bit. C, 3.7 wt.% water and 12 wt.% cyclohexane during first 10 minutes

Table 13. Initial flux, final flux, and transition time of reconstituted gangue with 2.0 wt.% Bit. C, 3.7 wt.% water and 12 wt.% cyclohexane.

Flow velocity (m/s)	0.9	2.3	3	3.5
Initial flux ($\frac{g}{min*cm^2}$)	4.30 x 10^{-3}	4.40 x 10^{-3}	5.45 x 10^{-3}	5.55 x 10^{-3}
Transition time (mins)	52.4	50.8	39.3	37.1
Final flux ($\frac{g}{min*cm^2}$)	2.38 x 10^{-4}	3.23 x 10^{-4}	2.44 x 10^{-4}	1.53 x 10^{-4}

Figure 28 summarizes the initial flux of reconstituted gangue samples of varying Bit. C content (3.7 wt.% water and 12% cyclohexane) at various flow velocities. At a given flow velocity, increasing the wt.% of Bit. C decreased the initial flux. This is consistent with results from Panda and Khalkhali [66], [69]. The reduced initial flux with increasing Bit. C content is due to a combination of three factors. First, increasing bitumen content increases the viscosity of the bulk solution and therefore reduces sorptivity of the gangue bed. The second factor is a zone of local flux reduction caused by bitumen deposits that form a thick bitumen-rich top layer. Pores within this top layer are largely saturated with bitumen which significantly increases viscosity and therefore reduces the ability to transfer fluids via capillarity. The third factor is solvent retention in bitumen. Noorjahan et al. found the rate of cyclohexane desorption was nearly four orders of magnitude lower than the absorption rate, and it took over a month to reach equilibrium [40].

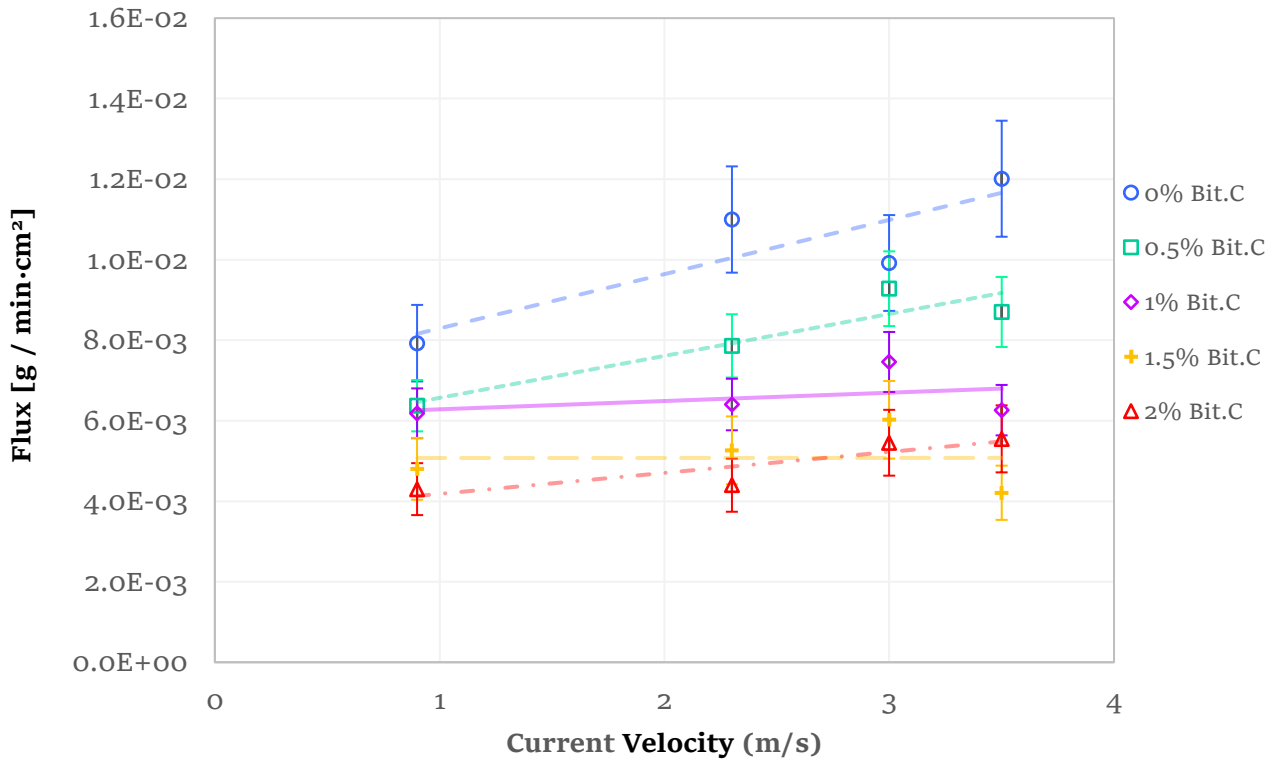

Figure 28. Initial flux of reconstituted gangue samples with varying Bit. C wt.% at various flow velocities.

As evident in Figure 28, increasing flow velocity over the sample surface appears to have a positive impact on the initial flux and subsequently the removal of cyclohexane, but this effect is reduced at higher bitumen contents. At its peak, initial flux increased by 51.3% for samples with 0 wt.% bitumen, 45.7% for samples with 0.5 wt.% Bit. C, 20.7% for samples with 1.0 wt.% Bit. C, 25.4% for samples of 1.5 wt.% Bit. C, and 29% for samples with 2.0 wt.% Bit. C. Increasing bitumen and increasing flow velocity have opposing effects – the first acts to hinders effective transport, while the latter accelerates transport.

Increasing the flow rate of air above the sample increases the initial flux by decreasing the concentration of cyclohexane directly above the sample. This continuous removal of existing cyclohexane gas allows newly escaping particles to take its place and thus increases the initial flux. Increasing the air flow velocity over a sample will also decrease the boundary layer thickness, leading to a decrease in the diffusive distance required for gaseous cyclohexane.

For simplicity, the flow characteristics of air over a flat plate, as shown in Figure 29, will be used to explain the relationship between flow velocity and the boundary layer thickness [75]. In reality, there are many other factors that can affect boundary layer conditions, such as surface roughness and location from the edge [76].

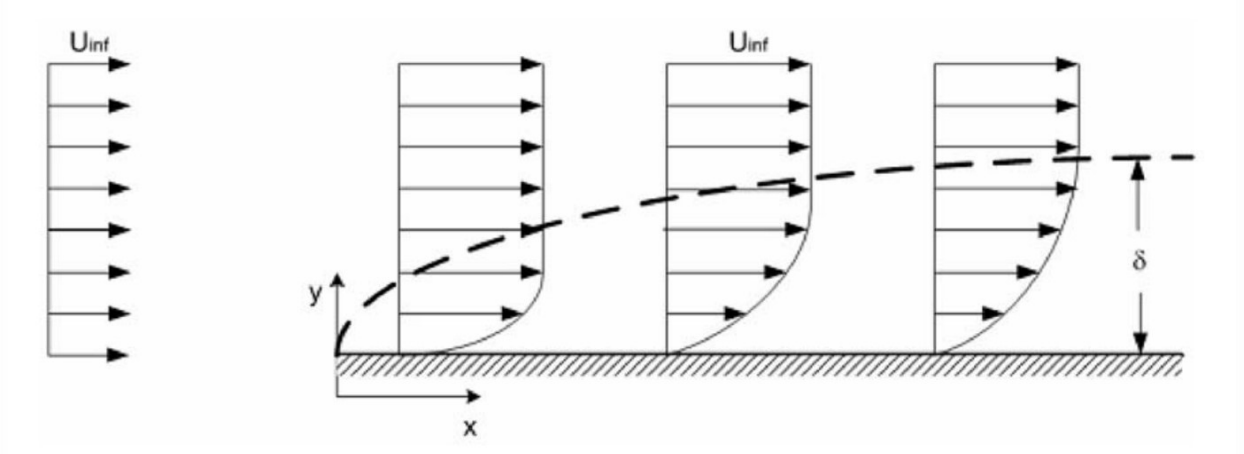

Figure 29. Flow over a flat plate [75].

Reynold's number (Re) is defined as the ratio of inertial forces to viscous forces, and can be calculated as [75], [76]

$$Re = \frac{\rho UL}{\mu} = \frac{UL}{\nu} \tag{16}$$

where ρ is air density, U is the stream velocity, L is the length measured from the leading edge of the flat plate, μ is the dynamic viscosity and v is the kinematic viscosity.

For laminar flow ($Re < 5 \times 10^5$), the boundary layer thickness (δ_L) can be calculated as

$$\delta_L = \frac{5 * L}{Re^{0.5}} \tag{17}$$

For turbulent flow ($Re > 5 \times 10^5$) the boundary layer thickness (δ_L) can be calculated as

$$\delta_L = \frac{5 * L}{Re^{0.5}} \tag{18}$$

As evident in Equations (17) and (18), the thickness of the boundary layer is proportional to the Reynold's number, which is inversely proportional to the flow velocity. The boundary layer is a thin, viscous layer close to the surface of the flat plate where the flow velocity varies from 0 m/s at the surface to the plate to U m/s at the boundary [77]. An increase in flow velocity will result in a larger Re, and subsequently reduce the boundary layer thickness.

Re for air velocities of 0.9, 2.3, 3.0 and 3.5 m/s over a flat plate are estimated to be 2,968, 7,586, 9,894 and 11,544, respectively, and because these values are less than 5×10^5, the flow regime is likely laminar. Increasing flow velocity from 0.9 m/s to 3.5 m/s decreases the boundary layer thickness from 0.46 cm to 0.23 cm, a 50% reduction. Sample calculations for Reynolds number and boundary layer thickness are in Appendix B.

Nikakhtari et al. found the initial drying rate of gangue (0.5 wt.% bitumen, 18 wt.% cyclohexane and 3.4 wt.% water was 2.7 times higher in an environmental chamber than in a fume hood

because of strong convective currents in the chamber generated by a fan [68]. The horizontal flow velocity measured across a sample in the fume hood and in the environmental chamber were < 0.2 m/s and 0.83 m/s, respectively. Despite a similar framework, there are several differences between the study by Nikakhtari et al. and this current one. First, the gangue samples were dried at 24°C rather than 20°C, and higher temperatures cause higher rates of evaporation. Secondly, the sample packing was different in that 15 g of gangue was spread out with a sample depth (i.e. bed height) of 0.5 cm and exposed surface area of 23 cm^2, as opposed to 25 g of reconstituted gangue spread out to a bed height of 1 cm with an exposed area of 19.64 cm^2. Increased surface area increases the number of surface molecules per unit of volume that can escape the liquid phase.

For samples between 0.5 and 1.5 wt.% Bit. C, the maximum initial flow rate is reached when the flow velocity is ~3 m/s, after which the initial flux decreases or remains roughly unchanged. The drying process for gangue samples occurs in two distinct stages separated by the breakpoint or transition time. The first stage involves the cyclohexane and bitumen solution travelling upwards through the pores via capillary action. When the solution reaches the top of the gangue, cyclohexane evaporates and the bitumen is deposited on the top surface. The receding of cyclohexane liquid films signifies the beginning of the second stage, where cyclohexane must now diffuse through the pores to escape the gangue; this stage is significantly shower than its predecessor. Given that the initial flux peaks at roughly 3 m/s for these samples, this suggests that there is an optimal convective velocity for maximum solvent removal. For samples containing 2.0 wt.% Bit. C, the highest initial flux was achieved at a flow velocity of 3.5 m/s, as compared to 3 m/s for samples with 0.5 – 1.5 wt.% Bit. C. This shows the optimal velocity is expected to increase for gangue samples with more Bit. C, as to overcome the hinderance caused

by bitumen. For samples with 0.5 – 1.5 wt.% Bit. C, there appears to be a decrease in initial flux after the maximum initial flux was reached. This would signify liquid film disruption at high flow rates that reduces the initial flux. After reaching the optimal velocity, any subsequent increases will not induce any further increases in the initial flux and is not only a waste of energy but may even be detrimental in overall removal of cyclohexane.

Figure 30 shows the transition time for reconstituted gangue samples with varying Bit. C wt.% at various flow velocities. At a given flow velocity, the transition time is higher for samples with more Bit. C, and this is consistent with previous studies [66], [67]. An increase in the wt.% of Bit. C decreases the rate of drying during the initial stage. Since this stage is slowed, its duration is longer and thus the breakpoint or transition time occurs later. At a given wt.% of Bit. C, increasing the flow velocity decreased the transition time. As previously discussed, increasing flow rate will increase the initial flux, and therefore reducing the duration where liquid films remain hydraulically connected to the open surface.

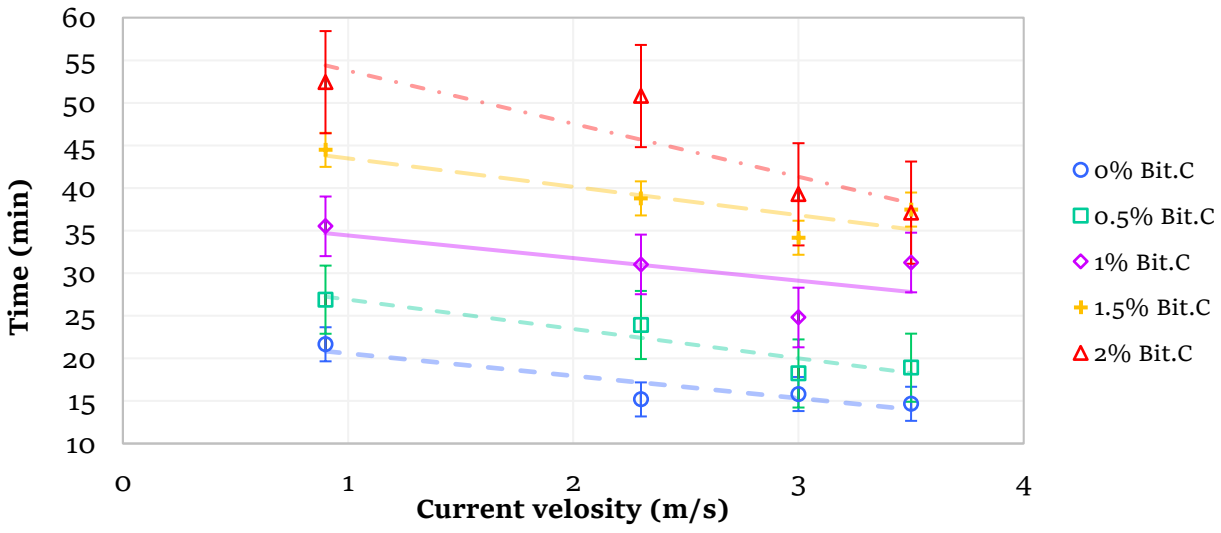

Figure 30. Transition time for reconstituted gangue samples with varying Bit. C wt.% at various flow velocities.

Figure 31 shows the final flux of reconstituted gangue samples with varying Bit. C wt.% at various flow rates. The final flux is dominated by water evaporation and is significantly slower than the initial flux. Mass transfer during this stage occurs exclusively through diffusion through the porous matrix. Due to porosity and tortuosity, the effective molecular diffusivity within the gangue is significantly less than the effective diffusivity in the mass boundary layer [61]. As evident in Figure 26, neither the wt.% of Bit. C or the current velocity appears to have an effect on the final flux. Since the second phase of drying (i.e., the final stage), is controlled by water evaporation, it has little impact on the removal of cyclohexane and thus holds little significance for this study.

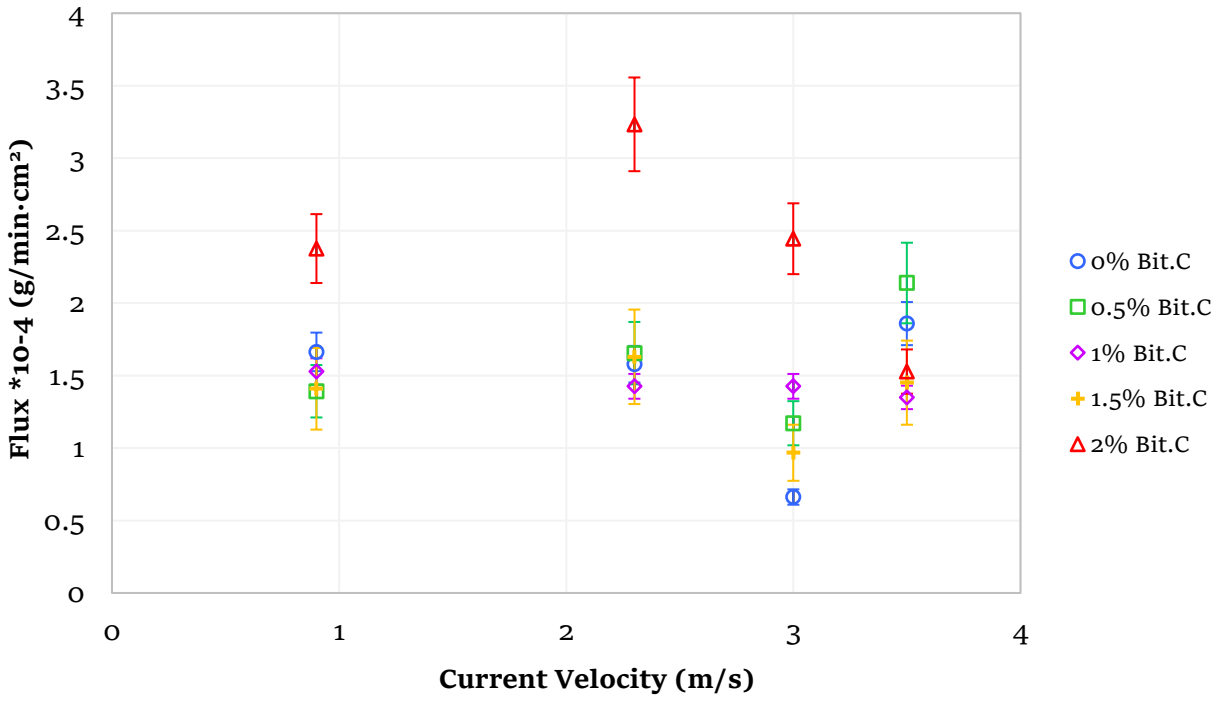

Figure 31. Final flux of reconstituted gangue samples with varying Bit. C wt.% at various flow rates.

A comparison can be made between the drying of oil sands gangue and the drying of soil as both involve the removal of a liquid (or solution) in a porous media. Davarzani et al. studied the effect of wind speed on evaporation from soil samples with a dry bulk density of 1770 kg/m^3, porosity of 0.335, and 2.8 wt.% water [78]. As shown in Figure 32, increasing the wind speed increases the first stage evaporation rate and decreases the transition time between the faster initial stage and the slower final stage, but only at low velocity values [78]. At high wind speeds, the evaporation rate became less dependent and finally independent on wind speed. As evident in the experimental results, a critical velocity from which evaporation is no longer dependent on wind speed can be identified. At the critical wind speed, the vapour concentration reduces to the wind vapour concentration above the soil surface and therefore higher wind speeds cannot change the evaporation process. The second stage of drying was not significantly affected by wind velocity.

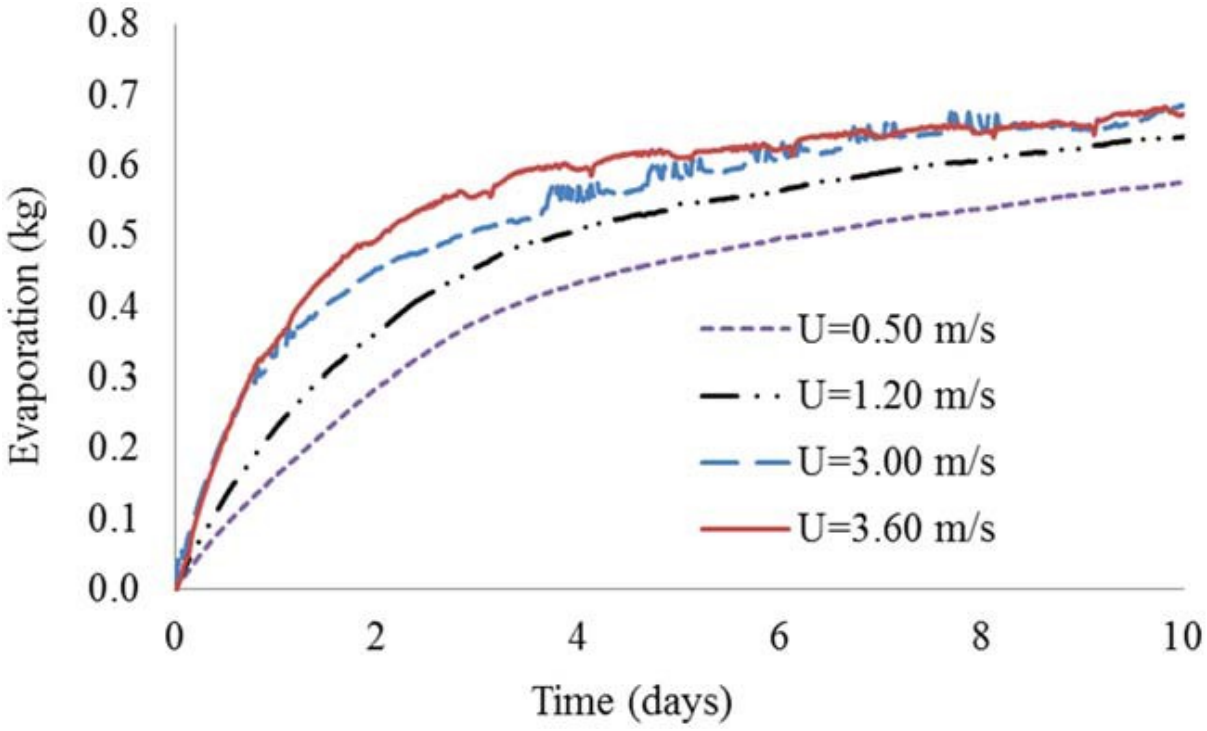

Figure 32. Kinetics of cumulative evaporation for different wind speeds (U = maximum wind speed in the free medium) [78].

3.4.2. Effect of Water

Figure 33 is the cumulative weight loss curves for reconstituted gangue sample with 1 wt.% Bit. C, 0 wt.% water and 12 wt.% cyclohexane at various current velocity values, Figure 34 is a close-up of the drying curve during the initial 10 minutes, and Table 14 are the corresponding initial flux, final flux, and transition time values. The initial flux peaked when flow velocity was 2.3 m/s, a 9.5% increase from the initial flux when flow velocity was 0.9 m/s. After reaching the maximum initial flux, any further increases in velocity had negligible effects. The effect of an induced air current on initial flux appears to be small for gangue samples without any water. As expected, the transition time for all samples were similar at ~50 minutes because the initial flux values were comparable. Values of the final flux are an order of magnitude smaller than the initial flux and seems independent of flow velocity.

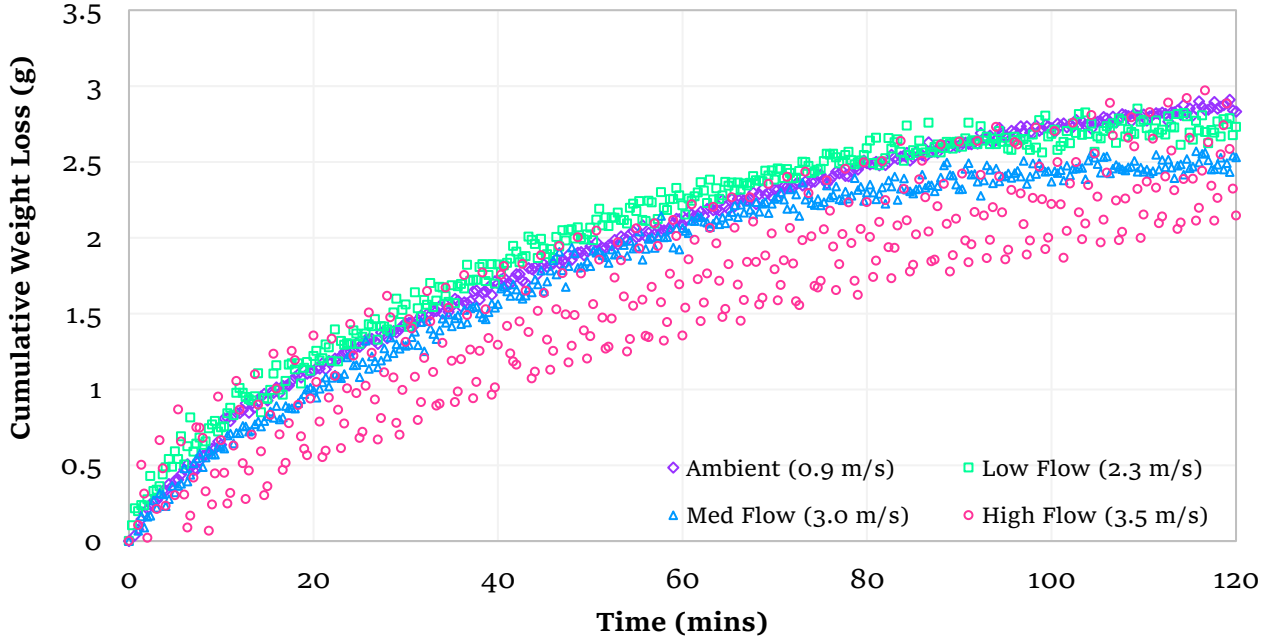

Figure 33. Cumulative weight loss for reconstituted gangue with 1.0 wt.% Bit. C, 0 wt.% water and 12 wt.% cyclohexane.

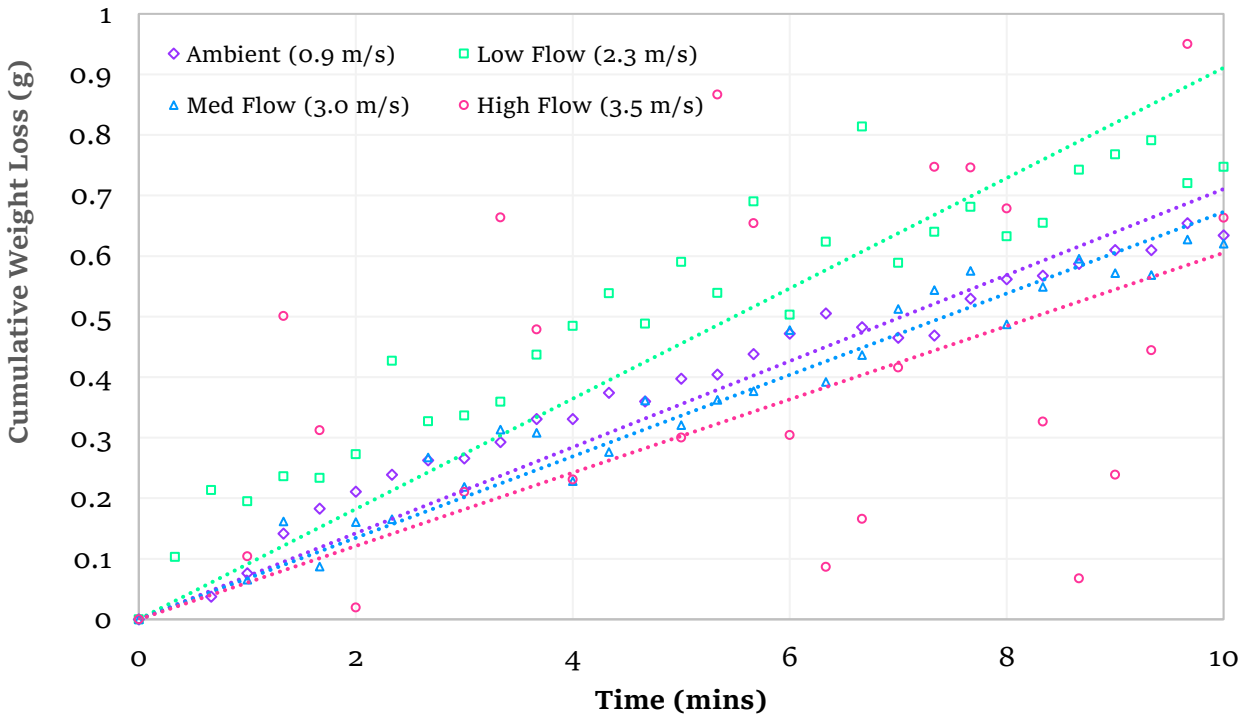

Figure 34. Cumulative weight loss for reconstituted gangue with 1.0 wt.% Bit. C, 0 wt.% water and 12 wt.% cyclohexane during initial 10 minutes.

Table 14. Initial flux, final flux, and transition time of reconstituted gangue with 1.0 wt.% Bit. C, 0 wt.% water and 12 wt.% cyclohexane.

Flow velocity (m/s)	0.9	2.3	3	3.5
Initial flux ($\frac{g}{min*cm^2}$)	3.27 x 10^{-3}	3.58 x 10^{-3}	3.26 x 10^{-3}	3.16 x 10^{-3}
Transition time (mins)	48.2	50.4	50.7	50.4
Final flux ($\frac{g}{min*cm^2}$)	4.94 x 10^{-4}	2.22 x 10^{-4}	2.65 x 10^{-4}	3.47 x 10^{-4}

Figure 35 is the cumulative weight loss curves for gangue sample with 1 wt.% Bit. C, 3.7 wt.% water and 12 wt.% cyclohexane at various current velocity values and Figure 36 is a close-up of the drying curve during the first 10 minutes. Table 15 are the corresponding initial flux, final flux, and transition time values. There appears be good overlap between all samples during the initial drying process, and divergences during the final drying stage. Increasing the flow velocity from 0.9 m/s to 3.0 m/s increased the initial flux by 18.7%, and the optimal flow velocity to maximize solvent removal appears to be around 3 m/s. For the same velocity increase, the transition time decreased by 9.3 minutes from 36.5 minutes to 27.2 minutes. Transition time will decrease as initial flux increases because the duration of the fast-drying stage shortens. The final flux of the reconstituted gangue samples appear independent of flow velocity.

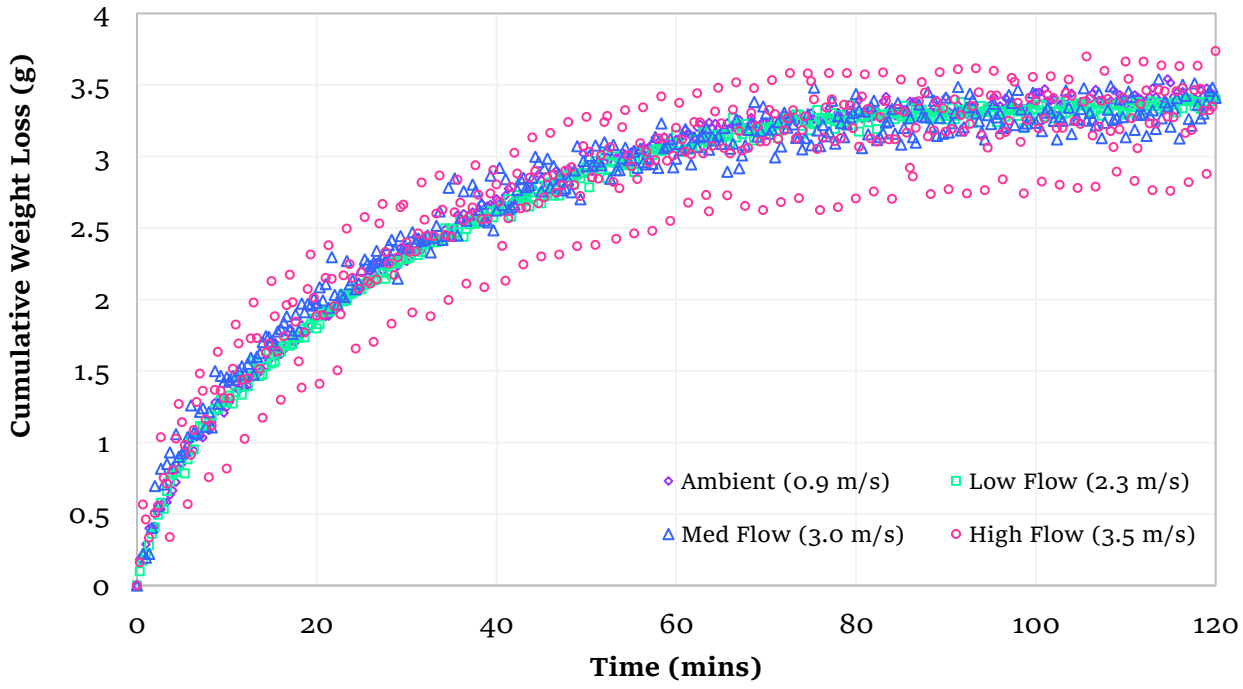

Figure 35. Cumulative weight loss for reconstituted gangue with 1.0 wt.% Bit. C, 3.7 wt.% water and 12 wt.% cyclohexane.

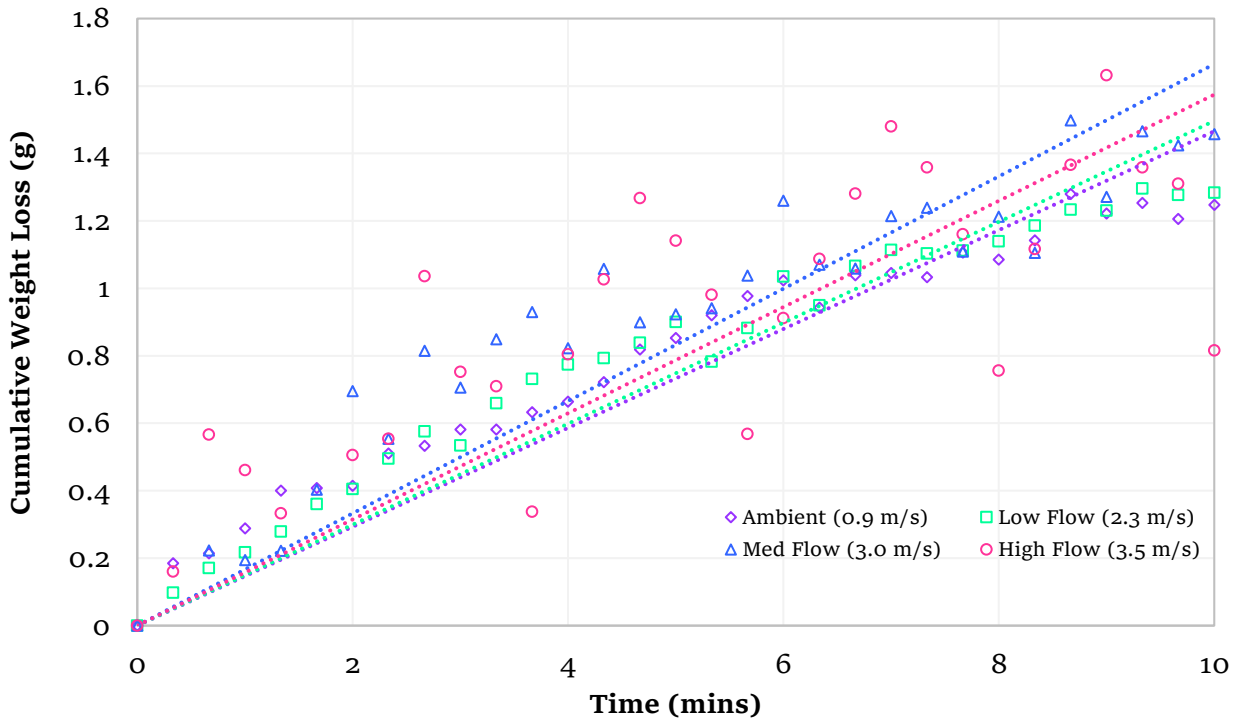

Figure 36. Cumulative weight loss for reconstituted gangue with 1.0 wt.% Bit. C, 3.7 wt.% water and 12 wt.% cyclohexane during initial 10 minutes

Table 15. Initial flux, final flux, and transition time of reconstituted gangue with 1.0 wt.% Bit. C, 3.7 wt.% water and 12 wt.% cyclohexane.

Flow velocity (m/s)	0.9	2.3	3	3.5
Initial flux ($\frac{g}{min*cm^2}$)	5.98 x 10^{-3}	6.58 x 10^{-3}	7.10 x 10^{-3}	6.67 x 10^{-2}
Transition time (mins)	36.5	32.2	27.2	30.8
Final flux ($\frac{g}{min*cm^2}$)	1.61 x 10^{-4}	1.34 x 10^{-4}	2.38 x 10^{-4}	1.61 x 10^{-4}

Figure 37 shows the cumulative weight loss curves for gangue sample with 1 wt.% Bit. C, 6 wt.% water and 12 wt.% cyclohexane at various current velocity values, Figure 38 is a close-up during the initial 10 minutes, and Table 16 are the corresponding initial flux, final flux, and transition time values. The drying curve obtained from flow velocities of 0.9 m/s and 2.3 m/s appear to have the most overlap. The initial flux is increased by 10% when the flow velocity is increased from 0.9 m/s to 3.0 m/s. Like samples with 3.7 wt.% water, the optimal flow velocity appears to be ~ 3 m/s. The transition time remained relatively constant for flow rates of 0.9 – 3 m/s, and only decreased by 1.7 minutes when flow velocity was 3.5 m/s. The final fluxes of the gangue samples were all similar and appear independent of flow velocity.

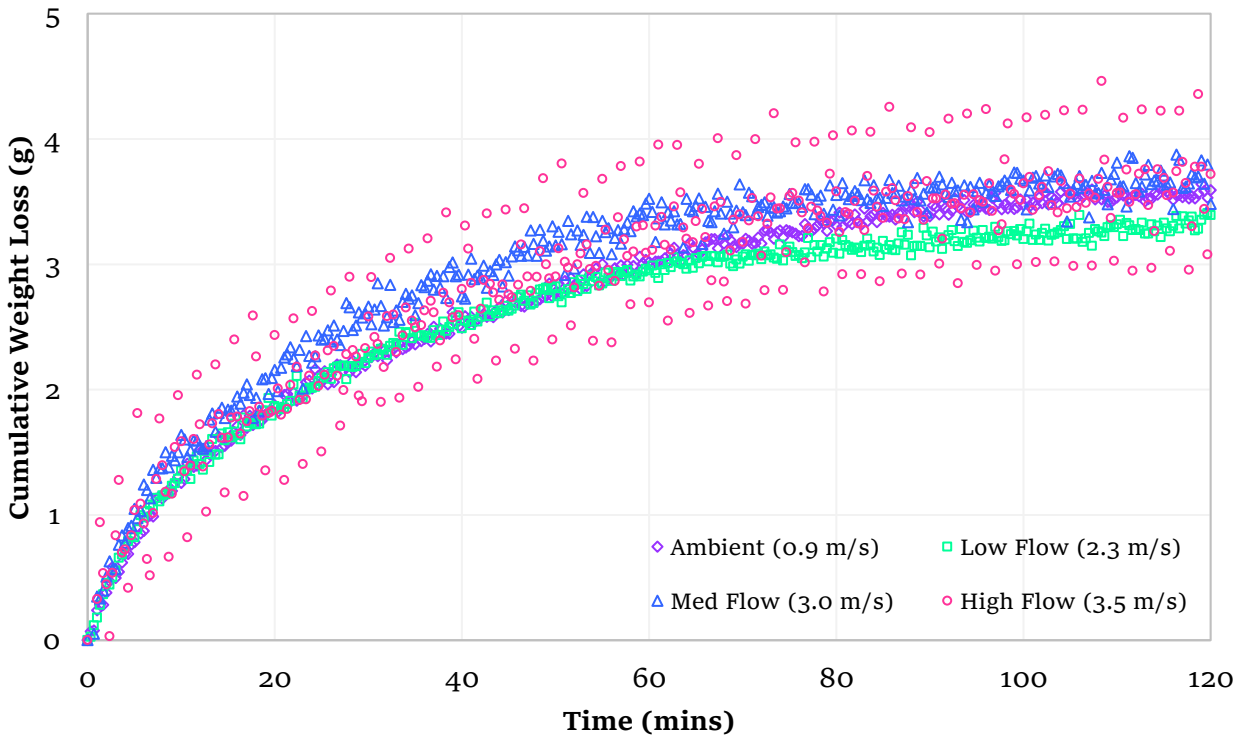

Figure 37. Cumulative weight loss for reconstituted gangue with 1.0 wt.% Bit. C, 6 wt.% water and 12 wt.% cyclohexane.

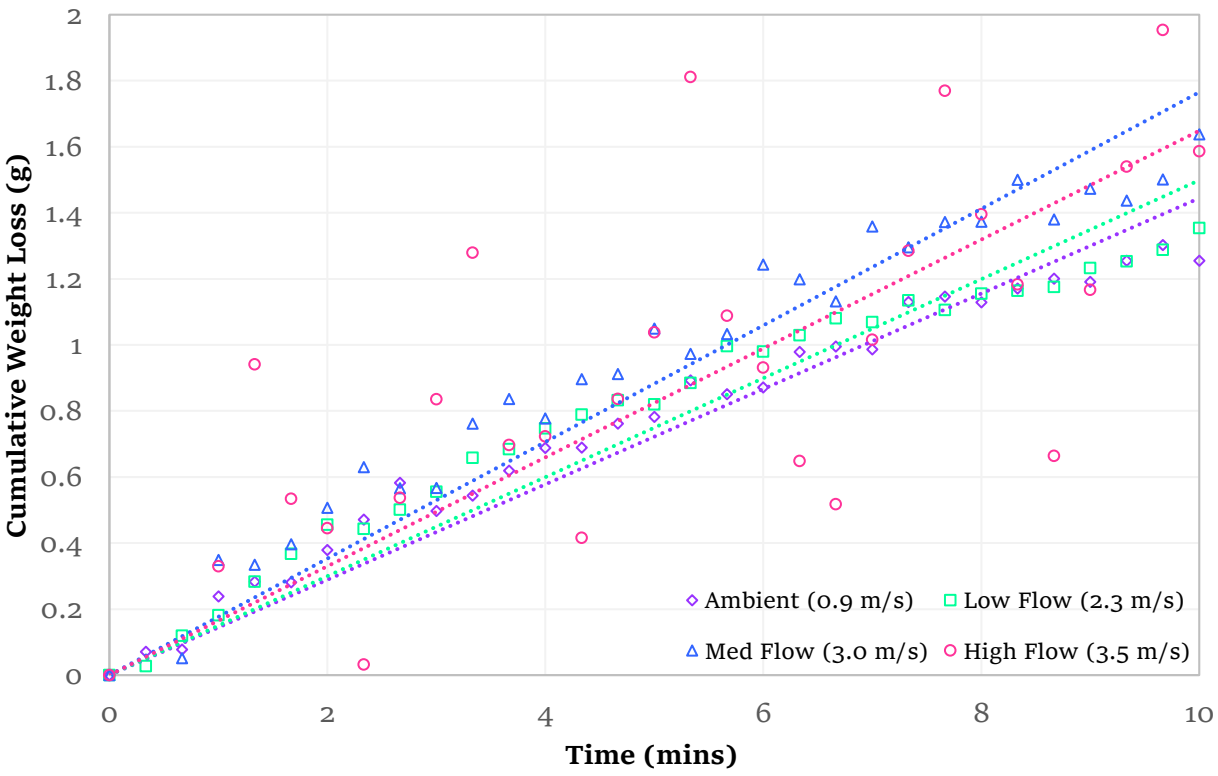

Figure 38. Cumulative weight loss for reconstituted gangue with 1.0 wt.% Bit. C, 6 wt.% water and 12 wt.% cyclohexane during initial 10 minutes.

Table 16. Initial flux, final flux, and transition time of reconstituted gangue with 1.0 wt.% Bit. C, 6 wt.% water and 12 wt.% cyclohexane.

Flow velocity (m/s)	0.9	2.3	3	3.5
Initial flux ($\frac{g}{min*cm^2}$)	6.57×10^{-3}	6.80×10^{-3}	7.21×10^{-3}	7.05×10^{-2}
Transition time (mins)	34.6	34.7	33.4	32.9
Final flux ($\frac{g}{min*cm^2}$)	2.83×10^{-4}	2.53×10^{-4}	2.51×10^{-4}	2.39×10^{-4}

Figure 39 shows the cumulative weight loss curve for reconstituted gangue samples with 1 wt.% Bit. C, 8 wt.% water and 12 wt.% cyclohexane at various current velocity values, and Figure 40 is a close-up during the first 10 minutes. Corresponding values of initial flux, final flux and transition time are in Table 17. There appears to be a fair amount of overlap between the drying curves obtained at all flow rates. The initial flux reaches its maximum at a flow velocity of 3.5 m/s, a 11% increase from the value at 0.9 m/s. Like all samples previously discussed, increasing flow velocity had a positive effect on the removal of cyclohexane by increasing the initial flux. Based on the results, the optimal flow velocity for these gangue samples appear to be roughly 3.5 m/s. Similar to results for samples with 6 wt.% water, the change in transition time was not large and only decreased by 3.9 minutes when flow velocity increased from 0.9 to 3.5 m/s. Values of the final flux were all similar and showed no dependence on flow velocity.

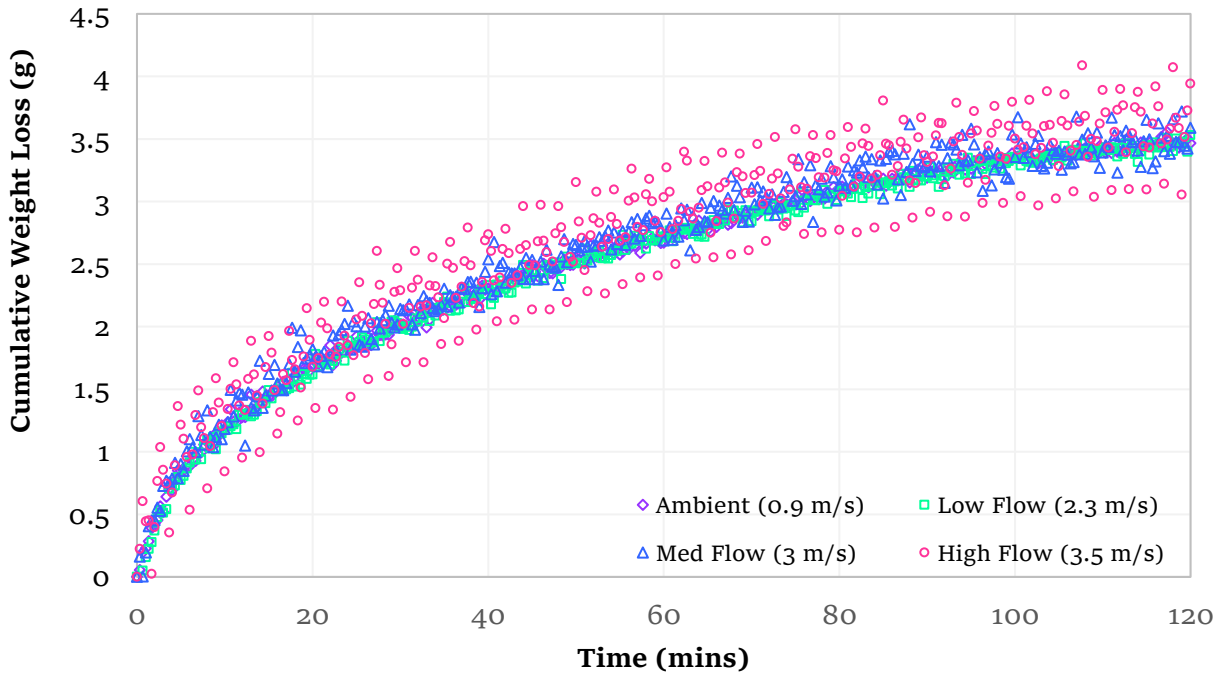

Figure 39. Cumulative weight loss for reconstituted gangue with 1.0 wt.% Bit. C, 8 wt.% water and 12 wt.% cyclohexane.

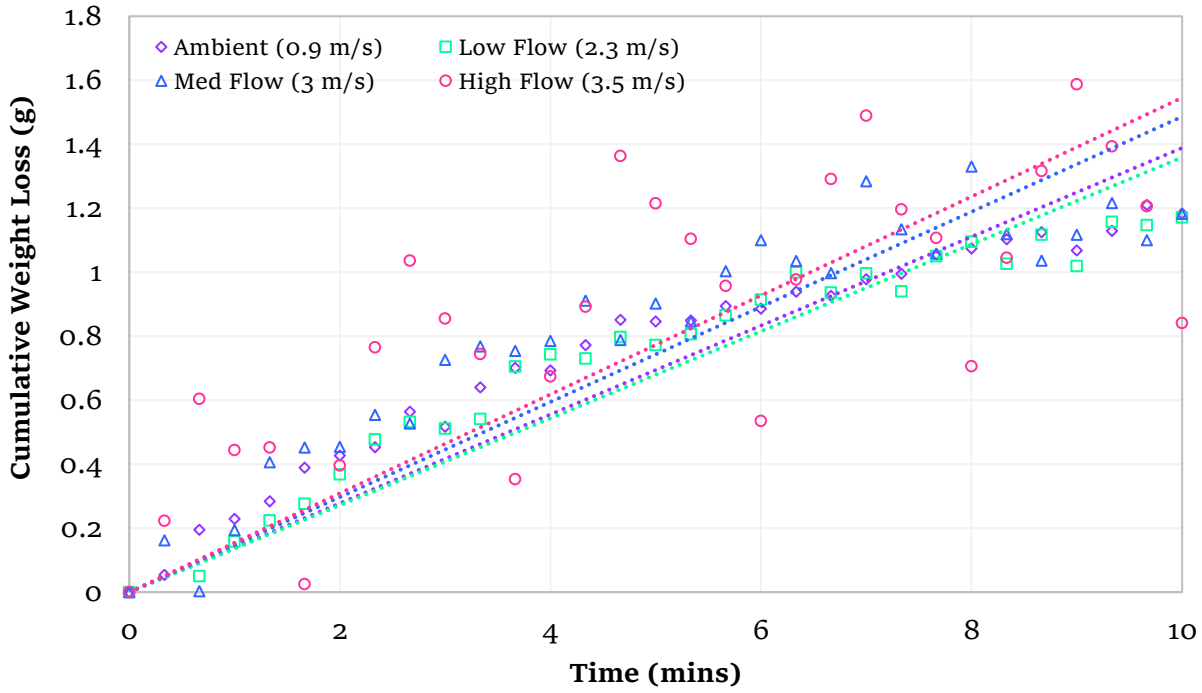

Figure 40. Cumulative weight loss for reconstituted gangue with 1.0 wt.% Bit. C, 8 wt.% water and 12 wt.% cyclohexane during initial 10 minutes.

Table 17. Initial flux, final flux, and transition time of reconstituted gangue with 1.0 wt.% Bit. C, 8 wt.% water and 12 wt.% cyclohexane.

Flow velocity (m/s)	0.9	2.3	3	3.5
Initial flux ($\frac{g}{min*cm^2}$)	6.11×10^{-3}	6.00×10^{-3}	6.46×10^{-3}	6.76×10^{-2}
Transition time (mins)	31.6	29.8	30.9	27.7
Final flux ($\frac{g}{min*cm^2}$)	4.79×10^{-4}	5.11×10^{-4}	4.09×10^{-4}	5.79×10^{-4}

Figure 41 shows the initial flux of reconstituted gangue samples of varying water content (Bit. C and cyclohexane kept constant at 1.0 and 12 wt.%, respectively) at various flow velocities. At a given flow velocity, the initial flux is lowest for samples without water (i.e., 0 wt.% water). This result can be explained by the hydrophobic/hydrophilic nature of the gangue. Gangue samples are not homogeneously hydrophobic, as surface hydrophobicity/hydrophilicity is dependent on surface roughness and other chemical interactions. Within the same gangue sample, there will be areas that more hydrophilic or hydrophobic. When water is present, it will prefer to wet the hydrophilic surfaces and reduce the surface area that will be wetted by cyclohexane. The average hydrophobicity of the surfaces wetted by cyclohexane will be higher because water has occupied the surfaces of hydrophilic particles. Since cyclohexane now wets a smaller surface area than if there was no water, the liquid films formed are thicker and more stable. In addition, water with its high surface tension, tends to condensate in smaller pores, and smaller pores from smaller particles will supress vapor pressure due to the Kelvin effect [58], [69]. Together, these factors help explain why initial drying flux is reduced in the absence of water.

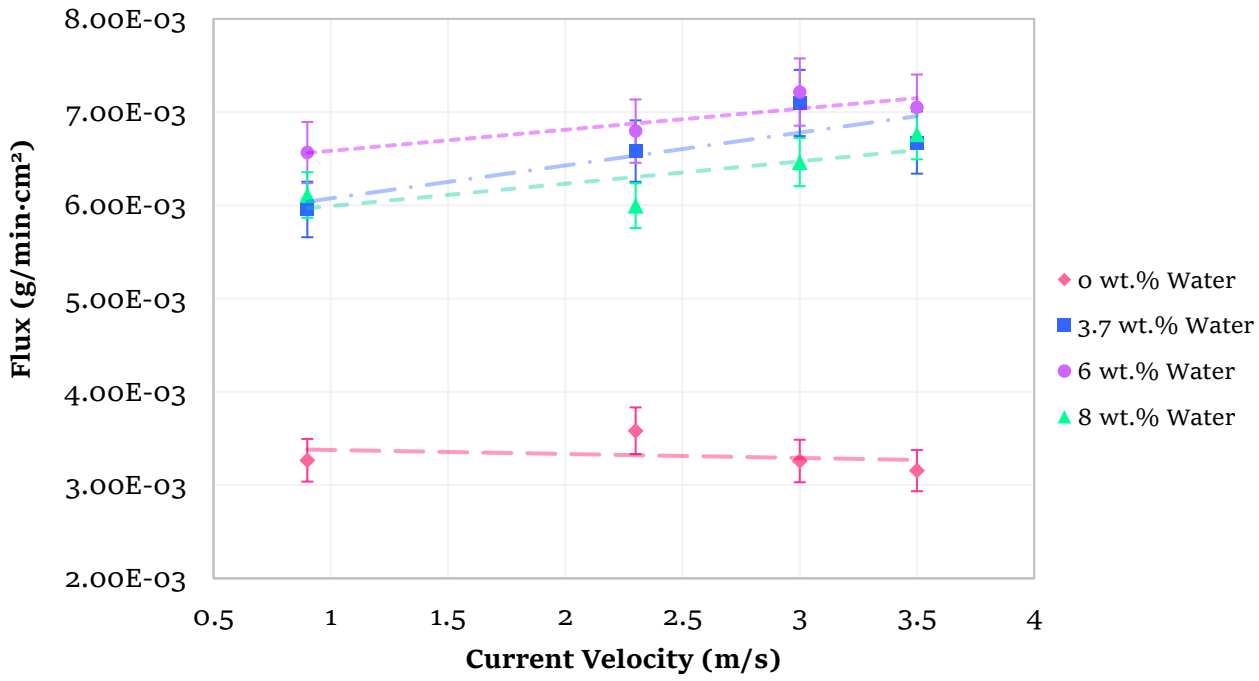

Figure 41. Initial flux of reconstituted gangue samples with varying water wt.% at various flow velocities.

Although the initial flux for samples with 3.7, 6.0 and 8.0 wt.% water were all similar (~ 6 – 7 x 10^{-3} $\frac{g}{min*cm^2}$), samples with 6 wt.% water exhibited the highest initial flux at any given flow velocity. As discussed earlier, water is required to facilitate the formation of thicker and more stable liquid films. For a square pore, increasing the content of water from 0 wt.% to 3.7, 6 and 8 wt.% will increase the liquid film thickness to pore size ratio to 0.15, 0.19 and 0.20, respectively [69]. This increased film thickness will induce a stronger liquid film flow and increase the initial flux. However, in excess, water can block pores, limit access to hydrophobic surfaces by cyclohexane, entrap cyclohexane clusters, and disrupt cyclohexane liquid film formation and stability [69]. These reasons are possible why the initial flux of samples with 8 wt.% water is less

than that of 3.7 and 6 wt.%. The optimal amount of water for reconstituted gangue samples with 1 wt.% Bit. C and 12 wt.% cyclohexane appears to be approximately 6 wt.%.

As evident in Figure 41, it appears that increasing the content of water does not diminish the effect of increased flow velocity on the rate of cyclohexane removal during the initial drying stage, as long as water content remains in an acceptable range. At 0 wt.% water, the initial drying stage seems independent of current velocity. In the absence of water, cyclohexane liquid film formation is supressed and the films that do form are thin and delicate. Without water, the rate of cyclohexane removal is governed internally by film characteristics. For samples with water, the initial drying flux is dependent on the conditions at the exposed gangue surface (i.e. boundary layer conditions). Based on these experimental results, the optimal acceptable water content ranges from 4 – 7 wt.%. This value may be different than the amount of connate water initially present in the ore.

Figure 42 illustrates the transition time for reconstituted gangue samples with varying water content at various flow velocities. At any given flow velocity, the transition time for 0 wt.% water is the highest, because it exhibited the lowest initial flux and therefore the initial stage of drying was prolonged. Since the initial flux for samples with 0 wt.% water showed little change with current velocity increases, the transition time also remained relatively constant. Samples containing water will have a faster transition time because their initial cyclohexane removal rates are higher. An interesting observation from Figure 42 is that for samples containing 6 wt.% water, despite a 10 % increase in the initial flux when flow velocity increased from 0.9 m/s to 3 m/s, the transition time only decreased by 1.7 minutes. This may be due to increased liquid film

thickness, as discussed prior, that contributes to the stability and resilience of the films to maintain hydraulic connectivity to the open boundary.

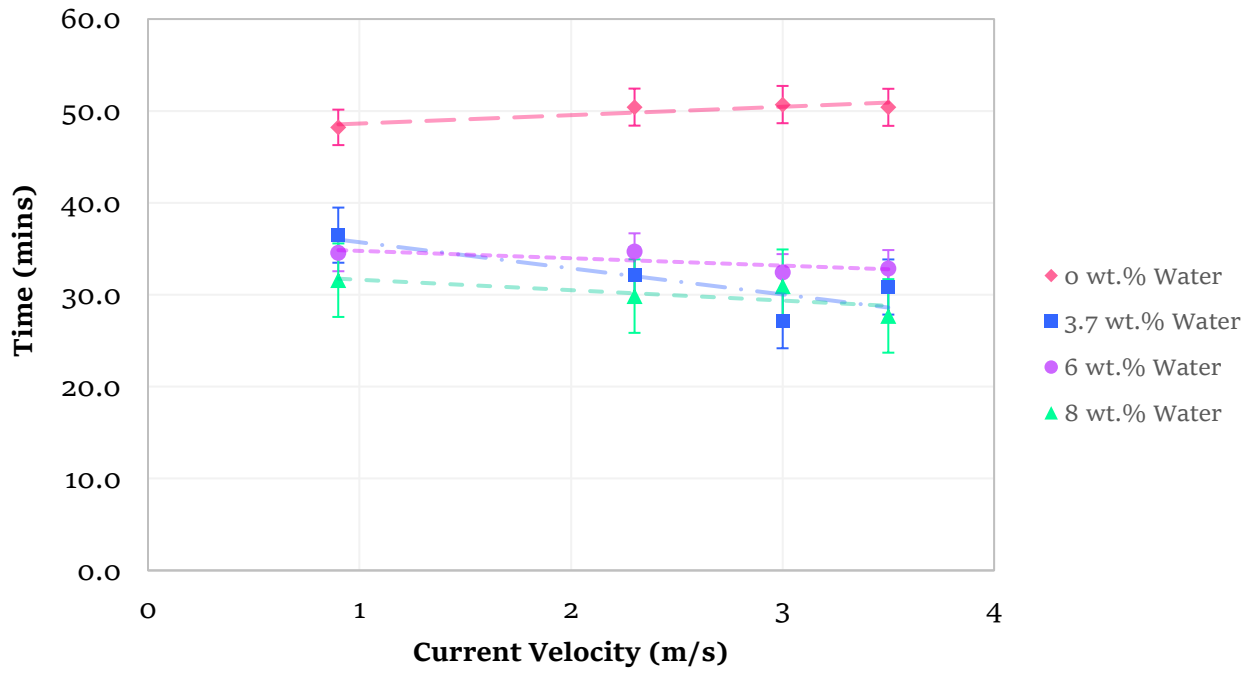

Figure 42. Transition times for reconstituted gangue samples with varying water wt.% at various flow velocities.

Figure 43 illustrates the final flux for samples of reconstituted gangue with varying water content at various flow rates. For all samples, the final flux was an order of magnitude lower than the initial flux. The final flux is dominated by water evaporation (for samples containing water). Without liquid films, the only way for vapour to escape the porous matrix is through diffusion. As previously mentioned, effective diffusion within the gangue is slow and negligibly affected by external boundary surface conditions. The final flux for samples with more water will higher because with more bulk liquid in the gangue leads to a shorter diffusive distance, as shown in Figure 44. In the absence of water, cyclohexane may be trapped in small pores of fine particles,

were the vapor pressure is suppressed by the Kelvin effect [58]. No distinguishable relationships can be established between final flux and current velocity.

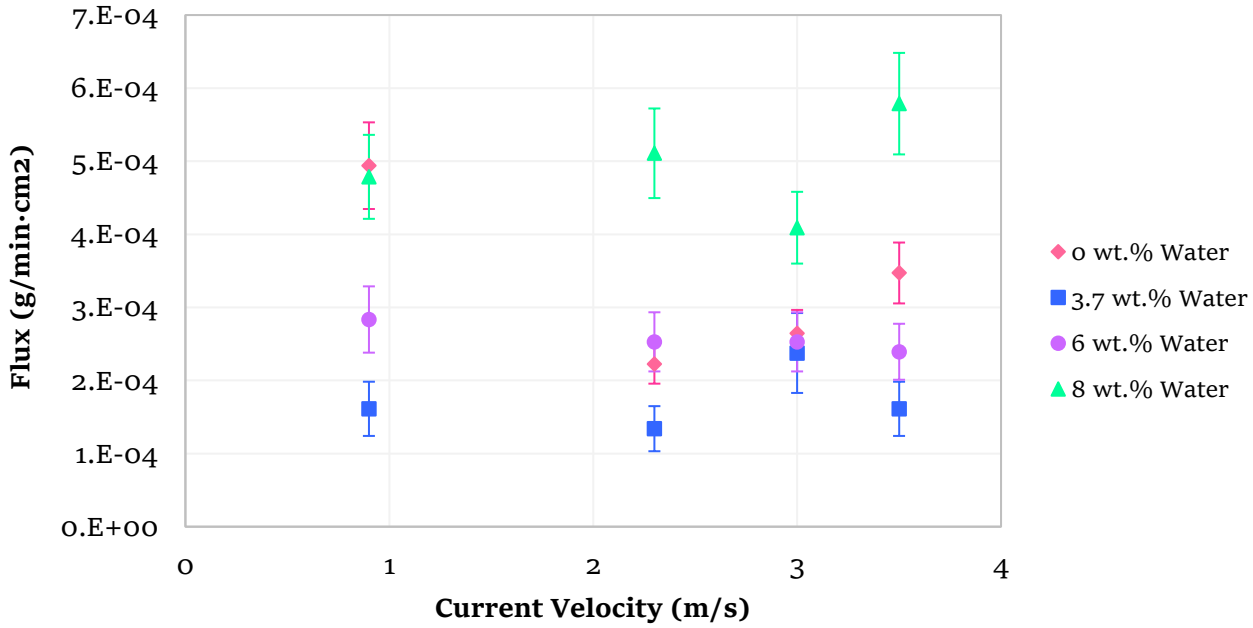

Figure 43. Final fluxes of reconstituted gangue samples with varying water wt.% at various flow velocities.

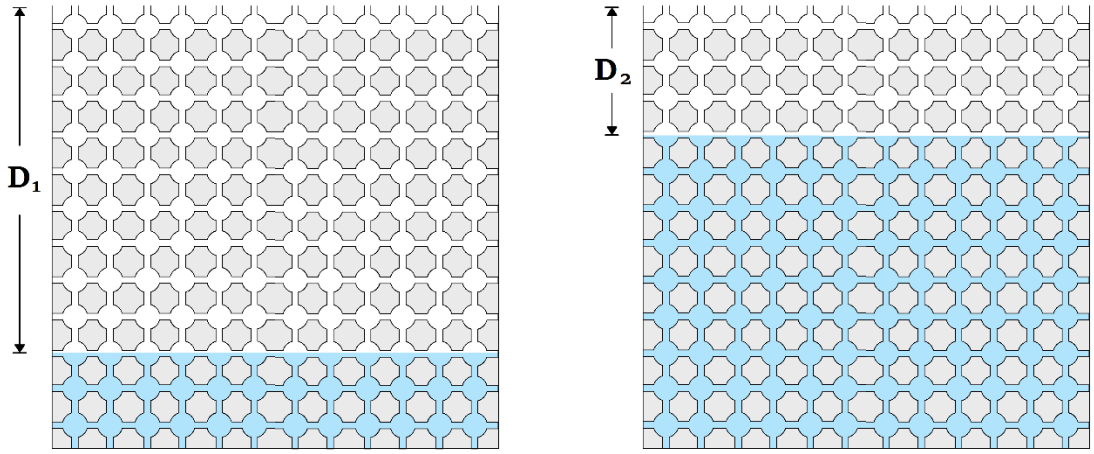

Figure 44. Diffusive distance, D_1 and D_2, for samples of varying water amounts.

4. Conclusion

This study investigated the effects of flow velocity on the removal of cyclohexane from gangue samples. The Dean-Stark extraction was used to separate the components of rich-grade Athabasca oil sands and determine its composition. Reconstituted gangue samples were prepared with known amounts of water, bitumen, and cyclohexane to eliminate variability associated with real gangue. Samples were dried under a fume hood for 2 hours at four air flow velocities (0.9, 2.3, 3.0, and 3.5 m/s) and the sample weight was continuously recorded.

The cumulative weight loss or drying curves of all samples exhibited two distinct stages, a faster initial stage, and a slower final stage. The initial stage is characterized by the formation of cyclohexane liquid films that maintain hydraulic connectivity between the bulk solution and the exposed open surface. The transition time denotes the point when hydraulic connectivity is lost and the liquid film tips recede into the porous matrix due to viscous and gravitational effects; this signifies the beginning of the slower drying stage. Evaporative flux in the final drying stage is at least one order of magnitude smaller than the initial stage because in the absence of liquid films, mass transfer within the gangue is governed by diffusion.

To determine the effect of flow velocity on samples of varying bitumen contents, reconstituted gangue samples with 0 – 2 wt.% Bit. C, 3.7 wt.% water and 12 wt.% cyclohexane were prepared. At any given flow velocity, increasing the amount of Bit. C decreased the initial flux due to an increase in the viscosity of the bulk solution that reduces sorptivity of the gangue bed; the formation of a zone of local flux reduction caused by bitumen deposits at the surface; and an increased cyclohexane retention in bitumen. For all samples, increasing the flow velocity

increased the initial flux by decreasing the concentration of cyclohexane directly above the sample and decreasing the diffusive distance required for gaseous cyclohexane. Although increasing flow velocity increased the initial flux, this positive effect was less prominent at higher bitumen contents. At its peak, initial flux increased by 46% for samples with 0.5 wt.% Bit. C as compared to 29% for samples with 2.0 wt.% Bit. C. The peak initial flux for samples with 0.5 – 1.5 wt.% Bit. C was observed at a flow rate of 3 m/s, while it was at 3.5 m/s for samples with 2.0 wt. % Bit. C. This suggests that there exists an optimal velocity corresponding to the maximum initial flux, after which any further increases will not yield improvements and may even be detrimental. Transition time was observed to decrease if there was an increase in the initial flux. The lowest transition time seems to be a consequence of the highest initial flux. The final flux is dominated by water evaporation and appeared to be independent of flow velocity for the samples examined.

To investigate the effect of flow velocity on samples of varying water contents, reconstituted gangue samples with 0 – 8 wt.% water, 1 wt.% Bit. C, and 12 wt.% cyclohexane were prepared. At any given flow velocity, the initial flux is the lowest for samples without water. The presence of water increases cyclohexane removal by occupying smaller pores and more hydrophilic surfaces, and increasing the liquid film thickness. In excess, water will cause pore blockages, limit cyclohexane's access to hydrophobic surfaces, entrap cyclohexane clusters and disrupt liquid film formation and stability. Although the initial flux for samples with 3.7, 6 and 8 wt.% water were comparable, the highest values were exhibited by samples with 6 wt.% water at any given flow rate. This may be the optimal amount of water that maximizes cyclohexane liquid film thickness and stability, and any further addition of water will introduce adverse effects. For

all samples containing water, increasing the flow velocity increases the initial flux. Increasing the fraction of water does not diminish the positive effect of increased flow velocity on the rate of cyclohexane removal, as long as water content remains in an acceptable range (likely 4 – 7 wt.%). Transition time is dependent on the initial flux and all samples containing water showed comparable transition times. A later transition may also be indicative of stronger, more stable liquid films if the initial flux values are comparable. No distinguishable relationships can be established between final flux and current velocity.

4.1. Future Directions

This study provides new insights into the factors affecting cyclohexane removal from extraction gangue, but before non-aqueous extraction methods can be implemented on a commercial scale, a comprehensive understanding of all underlying factors for solvent removal is required. This task is extremely challenging as the process is influenced by many variables.

As demonstrated in this study, solvent removal is dependent on gangue characteristics. There is much variation in real extracted gangue due to the variance in ore sample and extraction procedure. Experiments have shown conclusive evidence that cyclohexane removal is more difficult with increased residue bitumen. Improvements to the extraction process can reduce the burden on improving solvent removal. Although there have been studies on the effect of gangue composition on solvent removal, some parameters are still not entirely understood, such as pore shape and size distribution. Knowledge on pore shapes within the gangue will grant a greater insight into liquid film characteristics.

This study, and others before it, only investigated gangue samples in small amounts, e.g., 25 g of gangue with a sample thickness of 1 cm. If commercialized, the resulting volume of gangue will be significantly greater. Any scale-up from the current bench-scale may change the effects of individual factors, and an accurate solvent recovery model should account for such differences.

In this study, the air flow was parallel to the surface of the gangue sample. Modifications to the angle of air flow (e.g. perpendicular or at 45°) may alter its effect on the initial flux and should be investigated. To recover the cyclohexane and prevent its discharge into the environment, the drying process should be in a closed environment. Air should be recycled until a saturation point after which it is sent for processing to separate and recover cyclohexane. Design and optimization of this process should be considered in the future.

Solvent recovery from gangue can be increased through aeration by perforating the gangue with small holes, introducing physical agitation via a drum mixer, or through the additional of heat in combination with induced air currents. These are possible methods to enhance solvent removal and should be investigated separately.

Other possible drying techniques for solvent removal from gangue should be investigated, including microwave and electrohydrodynamic drying. Microwaves can provide rapid and uniform drying of porous media, which results from volumetric heating and internal evaporation [79]. Microwaves can also be combined with other drying processes, such as microwave-convective drying [80] [81]. In electrohydrodynamic drying, heat and mass transfer may be enhanced by electrical fields [82].

It is evident that despite substantial progress made by recent studies, there remain many other mechanisms and factors to consider before the solvent removal from extracted gangue can be optimized and utilized on a commercial scale.

References

[1] “Oil Resources”, Government of Canada, Dec. 16, 2019. [Online]. Available: https://www.nrcan.gc.ca/energy/energy-sources-distribution/crude-oil/oil-resources/18085 [Accessed: Apr. 4, 2020].

[2] "What are the Oil Sands", Canadian Association of Petroleum Producers. [Online]. Available: https://www.capp.ca/oil/what-are-the-oil-sands [Accessed: Apr. 4, 2020].

[3] F. Lin, S.R. Stoyanov and Y. Xu, "Recent Advances in Nonaqueous Extraction of Bitumen from Mineable Oil Sands: A Review," Org. Process Res. Dev., vol. 21, no. 4, pp. 492-510, Mar. 2017.

[4] "Oil Sands Geology and the Properties of Bitumen", Oil Sands Magazine, Feb. 28, 2020. [Online]. Available: https://www.oilsandsmagazine.com/technical/properties [Accessed: Apr. 4, 2020].

[5] J. Masliyah, Z. J. Zhou, Z. Xu, J. Czarnecki, and H. Hamza, “Understanding Water-Based Bitumen Extraction from Athabasca Oil Sands,” Can. J. Chem. Eng., vol. 82, no. 4, pp. 628–654, 2004.

[6] "Refinery Economics", Government of Canada, Aug 24, 2018. [Online]. Available: https://www.nrcan.gc.ca/energy/energy-sources-distribution/refinery-economics/4561 [Accessed: Apr. 4, 2020].

[7] “Alberta Energy Statistics", Oil Sands Magazine, Mar 5, 2020. [Online]. Available: https://www.oilsandsmagazine.com/energy-statistics/alberta [Accessed: Apr. 4, 2020].

[8] "Canadian Economic Contribution", Canadian Association of Petroleum Producers, 2019. [Online] Available: https://www.capp.ca/economy/canadian-economic-contribution/ [Accessed April 4, 2020].

[9] "Crude Oil Facts", National Resources Canada, Jan 25, 2010. [Online]. Available: https://www.nrcan.gc.ca/science-data/data-analysis/energy-data-analysis/energy-facts/crude-oil-facts/20064 [Accessed Apr. 4, 2020].

[10] "Froth Treatment Explained", Oil Sands Magazine. [Online]. Available: https://www.oilsandsmagazine.com/technical/mining/froth-treatment [Accessed Apr. 6, 2020].

[11] "Industry Landmark: The Great Canadian Oil Sands Plant", Government of Alberta. [Online]. Available: http://www.history.alberta.ca/energyheritage/sands/mega-projects/experimentation-and-commercial-development/industry-landmark-the-great-canadian-oil-sands-plant.aspx [Accessed Apr. 7, 2020].

[12] "Mining for Bitumen", Oil Sands Magazine, Nov 7, 2017. [Online]. Available: https://www.oilsandsmagazine.com/technical/mining [Accessed Apr. 7, 2020].

[13] "In Situ Bitumen Extraction", Oil Sands Magazine, Jun 3, 2019. [Online]. Available: https://www.oilsandsmagazine.com/technical/in-situ [Accessed Apr. 7, 2020].

[14] "Water", Alberta Energy Regulator. [Online]. Available: https://www.aer.ca/providing-information/by-topic/water [Accessed Apr. 9, 2020].

[15] "Water Use Performance", Alberta Energy Regulator, Aug 2019. [Online]. Available: https://www.aer.ca/protecting-what-matters/holding-industry-accountable/industry-performance/water-use-performance/about-water-use [Accessed Apr. 9, 2020]

[16] J. McNeill and N. Lothian, "Review of Directive 085 Tailings Management Plans," Pembina Institute, Mar 13, 2017. [Online]. Available: https://www.pembina.org/reports/tailings-whitepaper-d85.pdf [Accessed Apr. 9, 2020]

[17] E. N. Kelly, J. W. Short, D. W. Schindler, P. V. Hodson, M. Ma, A. K. Kwan and B. L. Fortin, "Oil sands development contributes polycyclic aromatic compounds to the Athabasca River and its tributaries," Proc. Natl. Acad. Sci., vol. 106, no. 52, pp. 22346-22351, Sept 21, 2009.

[18] J. Kurek, J. L. Kirk, D. Muir, X. Wang, M. S. Evans and J. P. Smol, "Legacy of a half century of Athabasca oil sands development recorded by lake ecosystems," Proc. Natl. Acad. Sci, vol. 110, no. 5, pp. 1761-1766, Jan 20, 2013.

[19] K. Orland, "The battle over when and how to clean up oilsands tailing ponds is escalating," Calgary Herald, Jan 16, 2018.

[20] R. A. Frank, J. W. Roy, G. Bickerton, S. J. Rowland, J. V. Headley, A. G. Scarlett, C. E. West, K. M. Peru, J. L. Parrott, F. M. Conly and L. M. Hewitt, "Profiling Oil Sands Mixtures from Industrial Developments and Natural Groundwaters for Source Identification," Environ. Sci. Technol, vol. 48, no. 5, pp. 2660–2670, Jan 21, 2014.

[21] "Tailings Management", Suncor, [Online]. Available: https://www.suncor.com/en-ca/sustainability/environment/tailings-management [Accessed: Apr. 9, 2020].

[22] "Managing Tailings", Canadian Natural Resources Limited, [Online]. Available: https://www.cnrl.com/corporate-responsibility/advancements-in-technology/managing-tailings [Accessed Apr. 9, 2020].

[23] M. Gray, "Notes: Fundamentals of Oil Sands Upgrading", 2015. University of Alberta

[24] "Climate change in Alberta", Government of Alberta. [Online]. Available: https://www.alberta.ca/climate-change-alberta.aspx [Accessed: Apr. 9, 2020].

[25] “Greenhouse gas sources and sinks in Canada: executive summary 2020”, Environment and Climate Change Canada. [Online]. Available: https://www.canada.ca/en/environment-climate-change/services/climate-change/greenhouse-gas-emissions/sources-sinks-executive-summary-2020.html [Accessed Apr. 9, 2020].

[26]. B. Israel, "Measuring oilsands carbon emissions intensity", Pembina Institute, Aug. 2016. [Online]. Available: https://www.pembina.org/reports/measuring-carbon-emission-intensity.pdf [Accessed Apr. 9, 2020].

[27]. B. Israel, J. Gorski, N. Lothian, C. Sevenson-Baker and N. Way, "The oilsands in a carbon-constrained Canada", Pembina Institute, Feb 2020. [Online]. Available: https://www.pembina.org/reports/the-oilsands-in-a-carbon-constrained-canada-march-2020.pdf [Accessed Apr. 10].

[28]. "Alberta Oil Sands Royalty Guidelines: Appendix", Government of Alberta, Jun 2018. [Online]. Available: https://open.alberta.ca/dataset/faf9a465-eeb1-4af0-845a-a79898b6e208/resource/0b8c0eaf-0688-470a-af47-714550a0214a/download/osrglossaryappendix.pdf [Accessed Apr. 10, 2020].

[29]. "Petroteq's patented oil sands extraction technology is a breakthrough for the oil sands industry", Petroteq Energy Inc., [Online]. Available: https://petroteq.energy/technology/oil-sands-extraction [Accessed Apr. 10, 2020].

[30]. Nikakhtari, L. Vagi, P. Choi, Q. Liu, and M. R. Gray, “Solvent screening for non-aqueous extraction of Alberta oil sands,” Can. J. Chem. Eng., vol. 91, no. 6, pp. 1153–1160, Jun. 2013.

[31]. G. R. Coulson, “Process for separating oil from bituminous sands, shales, etc.,” US 2825677 A, Mar 4, 1958.

[32]. N. F. Blaine and B. Geneva, “Solvent extraction of oil from tar sands utilizing a trichloroethylene solvent,” US 4046669 A, Sept 6, 1977.

[33]. D.E. Cormack, J.M. Kenchington, C.R. Phillips and P.J. Leblanc, "Parameters and mechanisms in the solvent extraction of mined athabasca oil sand," Can. J. Chem. Eng., vol. 55, no. 5, pp. 572-580, Oct 1977.

[34] F.W. Meadus, P.J. Chevrier and B.D. Sparks, "Solvent extraction of athabasca oil-sand in a rotating mill Part 1. Dissolution of bitumen," Fuel Process. Technol., vol. 6, no. 3, pp. 277-287, Sept 1982.

[35] H. Leung and C.R. Phillips, “Solvent Extraction of Mined Athabasca Oil Sands,” Ind. Eng. Chem. Fundamen., vol. 24, no. 4, pp. 373–379, Aug 1,1985.

[36] P. Painter, P. Williams and E. Mannebach, "Recovery of Bitumen from Oil or Tar Sands Using Ionic Liquids," Energy & Fuels, vol. 24, no. 2, pp. 1094-1098, Oct 7, 2010.

[37] T. Wang, C. Zhang, R. Zhao, C. Zhu, C. Yang and C. Liu, "Solvent Extraction of Bitumen from Oil Sands," Energy & Fuels, vol. 28, no. 4, pp. 2297-2304, Mar 21, 2014.

[38] A. Hooshiar, P. Uhlik, D. G. Ivey, Q. Liu and T. H. Etsell, "Clay minerals in nonaqueous extraction of bitumen from Alberta oil sands," Fuel Process. Technol., vol. 96, pp. 183-194, 2012.

[39] J. Wu and T. Dabros, "Process for Solvent Extraction of Bitumen from Oil Sand," Energy & Fuels, vol. 26, no. 2, pp. 1002-1008, 2012.

[40] A. Noorjahan, X. Tan, Q. Liu, M.R. Gray and P. Choi, "Study of Cyclohexane Diffusion in Athabasca Asphaltenes," Energy & fuels, vol. 28, no. 2, pp. 1004–1011, 2014.

[41] J. H. Hildebrand, Solubility of Non-Electrolytes. New York: Reinhold Pub. Corp, 1936.

[42] J. H. Hildebrand and R. L. Scott, The Solubility of Non-Electrolytes, 3rd Ed. New York, Reinhold Pub. Corp, 1950.

[43] K. Pal, Nogueira Branco, Lucas da Paz, A. Heintz, P. Choi, Q. Liu, P.R. Seidl and M.R. Gray, "Performance of Solvent Mixtures for Non-aqueous Extraction of Alberta Oil Sands," Energy & Fuels, vol. 29, no. 4, pp. 2261-2267, 2015.

[44]. I. Rahimian and G. Zenke, “Zum verhalten organischer loesemittel gegenueber bitumen,” Bitumen, vol. 48, no. 1, 1986.

[45] C. M. Hansen, Hansen Solubility Parameter: a user’s handbook. CRC Press, 2002.

[46] P.G. Redelius, "Solubility parameters and bitumen," Fuel, vol. 79, no. 1, pp. 27-35, 2000.

[47] D. Wilkinson and J.F. Willemsen, "Invasion percolation: a new form of percolation theory," J. Phys. A Math. Theor., vol. 16, no. 14, pp. 3365-3376, 1983.

[48] R. Chandler, J. Koplik, K. Lerman and J. F. Willemsen, "Capillary displacement and percolation in porous media," J. Fluid Mech., vol. 119, pp. 249-267, 1982.

[49] Y. C. Yortsos and A. K. Stubos, "Phase change in porous media," Curr. Opin. Colloid Interface Sci., vol. 6, no. 3, pp. 208-216, 2001.

[50] A. G. Yiotis, A. G. Boudouvis, A. K. Stubos, I. N. Tsimpanogiannis and Y.C. Yortsos, "Effect of liquid films on the isothermal drying of porous media," Phys. Rev. E., vol. 68, no. 3, pp. 037303, 2003.

[51] A. G. Yiotis, A. G. Boudouvis, A. K. Stubos, I. N. Tsimpanogiannis and Y.C. Yortsos, "Effect of liquid films on the drying of porous media," AIChE J., vol. 50, no. 11, pp. 2721-2737, 2004.

[52] M. Prat and F. Bouleux, "Drying of capillary porous media with a stabilized front in two dimensions," Phys. Rev. E., vol. 60, no. 5, pp. 5647-5656, 1999.

[53] J. B. Laurindo and M. Prat, "Numerical and experimental network study of evaporation in capillary porous media. Drying rates," Chem. Eng. Sci., vol. 53, no. 12, pp. 2257-2269, 1998.

[54] F. Plourde and M. Prat, "Pore network simulations of drying of capillary porous media. Influence of thermal gradients," Int. J. Heat Mass Transf., vol. 46, no. 7, pp. 1293-1307, 2003.

[55] A. G. Yiotis, D. Salin, E. S. Tajer and Y. C. Yortsos, "Drying in porous media with gravity-stabilized fronts: Experimental results," Phys. Rev. E., vol. 86, no. 2, pp. 026310, Aug 2012.

[56] A.G. Yiotis, A.K. Stubos, A.G. Boudouvis and Y.C. Yortsos, "A 2-D pore-network model of the drying of single-component liquids in porous media," Adv. Water Resour., vol. 24, no. 3, pp. 439-460, 2001.

[57] M. Prat, "On the influence of pore shape, contact angle and film flows on drying of capillary porous media," Int. J. Heat Mass Transf., vol. 50, no. 7-8, pp. 1455-1468, April 2007.

[58] R. Renaud, "Study on the Effect of Temperature and Pressure on the Removal of Cyclohexane from Non-Aqueous Extraction Gangue," M.Sc. thesis, Dept. Chem Eng., University of Alberta, Canada, 2014.

[59] A. G. Yiotis, D. Salin, E. S. Tajer and Y. C. Yortsos, "Analytical solutions of drying in porous media for gravity-stabilized fronts," Phys. Rev. E., vol. 85, no. 4, pp. 046308, 2012.

[60] M. Suzuki and S. Maeda, "On the mechanism of drying of granular beds," J. Chem. Eng. Japan, vol. 1, no. 1, pp. 26-31, 1968.

[61] A. Yiotis, D. Salin and Y. Yortsos, "Pore Network Modeling of Drying Processes in Macroporous Materials: Effects of Gravity, Mass Boundary Layer and Pore Microstructure," Transp. Porous Med, vol. 110, no. 2, pp. 175-196, 2015.

[62] P. Lehmann, S. Assouline and D. Or, "Characteristic lengths affecting evaporative drying of porous media," Phys. Rev. E., vol. 77, no. 5, pp. 056309, 2008.

[63] N. Shokri and D. Or, "Drying patterns of porous media containing wettability contrasts," J. Colloid Interface Sci., vol. 391, pp. 135-141, 2013.

[64] N. Shokri, P. Lehmann and D. Or, "Characteristics of evaporation from partially wettable porous media," Water Resour. Res., vol. 45, no. 2, 2009.

[65] N. Shokri, P. Lehmann and D. Or, "Effects of hydrophobic layers on evaporation from porous media," Geophys. Res. Lett., vol. 35, no. 19, CiteID. L19407, 2008

[66] S. Panda, "Role of Residual Bitumen on the Solvent Removal from Alberta Oil Sands Gangue," M.Sc. thesis, Dept. Chem Eng., University of Alberta, Canada, 2015.

[67] L.I. Ejike, "Role of Fine Solids in Solvent Recovery from Reconstituted Alberta Oil Sands Gangue," M.Sc. thesis, Dept. Chem Eng., University of Alberta, Canada, 2016.

[68] H. Nikakhtari, K. Pal, S. Wolf, P. Choi, Q. Liu and M.R. Gray, "Solvent removal from cyclohexane-extracted oil sands gangue," Can. J. Chem. Eng., vol. 94, no. 3, pp. 408-414, 2015.

[69] R. Khalkhali, "'Role of the Composition of Cyclohexane-extracted gangue on its drying at ambient conditions," M.Sc. thesis, Dept. Chem Eng., University of Alberta, Canada, 2019.

[70] A. Alghunaim, S. Kirdponpattara and B. Z. Newby, "Techniques for determining contact angle and wettability of powders," Powder Technol., vol. 287, pp. 201-215, 2016.

[71] B. Camassel, N. Sghaier, M. Prat and S. Ben Nasrallah, "Evaporation in a capillary tube of square cross-section: application to ion transport," Chem Eng. Sci., vol. 60, no. 3, pp. 815-826, 2005.

[72] “Surface Tension of Cyclohexane from Dortmund Data Bank.” [Online]. Available: http://www.ddbst.com/en/EED/PCP/SFT_C50.php. [Accessed: Jun 23, 2020].

[73] "Surface Tension," Engineering Toolbox. [Online]. Available: https://www.engineeringtoolbox.com/surface-tension-d_962.html [Accessed June 23, 2020].

[74] S. E. Ryan and L. S. Porth, “A tutorial on the piecewise regression approach applied to bedload transport data.” Fort Collins, CO: U.S. Dept. of Agriculture, Forest Service, Rocky Mountain Research Station, 2007.

[75] K. Gemba, "'Measurement of Boundary Layer on a Flat Plate," California State University, Long Beach, 2007.

[76] P. J. LaNasa and E. L. Upp, Fluid Flow Measurement, 3rd Ed., Gulf Professional Publishing, 2014.

[77] V.M. Epifanov, "Boundary Layer," Thermopedia. [Online]. Available: http://thermopedia.com/content/595/ [Accessed July 22, 2020]

[78] H. Davarzani, K. Smits, R.M. Tolene and T. Illangasekare, "Study of the effect of wind speed on evaporation from soil through integrated modeling of the atmospheric boundary layer and shallow subsurface," Water Resour. Res., vol. 50, no. 1, pp. 661-680, 2013.

[79] J. Zhou, X. Yang, H. Zhu, J. Yuan and K. Huang, "Microwave drying process of corns based on double-porous model," Dry. Technol., vol. 37, no. 1, pp. 92-104, 2018.

[80] S. J. Kowalski, G. Musielak and J. Banaszak, "Heat and mass transfer during microwave-convective drying," AIChE Journal, vol. 56, no. 1, pp. 24-25, 2009.

[81] I. W. Turner and P. C. Jolly, "Combined microwave and convective drying of a porous material," Dry. Technol., vol. 9, no. 5, pp. 1209-1269, 2010.

[82] P. Xu, A. P. Sasmito and A. S. Mujumdar, Heat and Mass Transfer in Drying of Porous Media. Boca Raton, FL: CRC Press, 2020.

Appendix A – Reconstituted Gangue Composition Calculations

1) Addition of Bitumen

Begin with X grams of Soxhlet gangue and 0.5*X grams of cyclohexane.

Bitumen by weight is 83.3 wt.% carbon. This means 1.2 g of bitumen contains 1 g of carbon (Bit. C). Reconstituted gangue samples prepared for this study has Bit. C ranging from 0 to 2 wt.%. Amount of bitumen required can be calculated with the following equation:

$$\frac{x_1}{(1.2 * x_1) + X} = \frac{a}{100}$$

Where: x_1 – mass of Bit. C

X_1 – mass of Soxhlet gangue

a – mass percent of Bit. C (0.5 – 2%)

Since some bitumen is lost during sample preparation (e.g. sticking to container walls), an additional 0.5 – 0.6 wt.% is added to obtain the right fraction.

The mass of bitumen required is calculated as:

$$x_{Bit} = 1.2 * x_1$$

The resulting DSBS (X_2) will have the following weight:

$$X_2 = X_1 + 1.2 * x_1$$

2) Addition of Water

Reconstituted gangue samples were prepared with 0, 3.7, 6 a d 8 wt.% water. This fraction is based on the DSBS weight. Amount of water required can be calculated as

$$\frac{x_2}{x_2 + X_2} = \frac{b}{100}$$

Where: x_2 – mass of demineralized water to be added to DSBS
X_2 – mass of DSBS from step (1)
b – mass percent of water (0 – 8 %)

The resulting WSBS (X_3) will have the following weight:

$$X_3 = X_2 + x_2$$

3) Addition of Cyclohexane

Experimentally, cyclohexane is very volatile and concentration is difficult to control. Gangue samples with 12 wt.% cyclohexane were prepared, and amount of cyclohexane required can be calculated as

$$\frac{x_3}{x_3 + X_3} = \frac{c}{100}$$

Where: x_3 – mass of cyclohexane be added to WSBS
X_3 – mass of WSBS from step (2)
c – mass percent of cyclohexane (12%)

The resulting reconstituted gangue (X_4) will have the following weight:

$$X_4 = X_3 + x_3$$

Since cyclohexane is so volatile, an additional 1% is added to account for losses during sample preparation.

Example: 100 g of Soxhlet solids to prepare reconstituted gangue with 1 wt.% Bit. C, 3.7 wt.% water, and 12 wt.% cyclohexane.

Given: $X_1 = 100$, a = 1, b = 3.7, c = 12

Amount of Bit. C required:

$$\frac{x_1}{(1.2 * x_1) + 100} = \frac{1}{100} \rightarrow x_1 = 1.01215\ g$$

Amount of bitumen required:

$$x_{Bit} = 1.2 * x_1 = 1.2 * 1.01215 = 1.21458\ g$$

Weight of DSBS:

$$X_2 = X_1 + 1.2 * x_1 = 100 + 1.21458 = 101.21458\ g$$

Amount of water required:

$$\frac{x_2}{x_2 + 101.21458} = \frac{3.7}{100} \rightarrow x_2 = 3.88883\ g$$

Weight of WSBS:

$$X_3 = X_2 + x_2 = 101.21458 + 3.88883 = 105.10341\ g$$

Amount of cyclohexane required:

$$\frac{x_3}{x_3 + 105.10341} = \frac{12}{100} \rightarrow x_3 = 14.3323\ g$$

Reconstituted gangue sample weight:

$$X_4 = 105.10341 + 14.3323 = 119.43571\ g$$

Appendix B – Calculation of Reynolds Number & Boundary Layer Thickness

Reynolds number (Re) can be calculated as:

$$Re = \frac{\rho UL}{\mu} = \frac{UL}{\nu}$$

Where ρ is air density, U is the stream velocity, L is the length measured from the leading edge of the flat plate, μ is the dynamic viscosity and ν is the kinematic viscosity.

For air at 20°C and 1 atm, the kinematic viscosity, ν, is 1.516×10^{-5} m^2/s.

The diameter of the petri-dish is 0.05 cm, therefore the length, L, is 0.05 m.

The Re for an air flow velocity, U, of 0.9 m/s can be calculated as:

$$Re = \frac{UL}{\nu} = \frac{0.9\ \frac{m}{s} * 0.05\ m}{1.516 \times 10^{-5}\ \frac{m^2}{s}} = 2968$$

Similarly, the Re for flow velocities of 2.3, 3.0 and 3.5 m/s can be calculated – results are tabulated below.

Velocity	0.9	2.3	3.0	3.5
Re	2968	7586	9894	11544

For laminar flow, the boundary layer thickness, δ_L, can be estimated as:

$$\delta_L = \frac{5 * L}{Re^{0.5}}$$

For Re = 2968 and L = 0.05, δ_L is calculated as

$$\delta_L = \frac{5 * 0.05\ m}{2968^{\ 0.5}} = 0.0046\ m = 0.46\ cm$$

Results for the remaining Re are tabulated below:

Velocity	0.9	2.3	3.0	3.5
$\boldsymbol{\delta_L}$ **(cm)**	0.46	0.29	0.25	0.23